U.PORTO

PROGRAMA DOUTORAL
BIOLOGIA BÁSICA E APLICADA

Defining the role of tumor-derived exosomes in brain metastasis

Gonçalo Rodrigues

D 2020

U.PORTO

Gonçalo Rodrigues. Defining the role of tumor-derived exosomes in brain metastasis

D.ICBAS **2020**

Defining the role of tumor-derived exosomes in brain metastasis

Gonçalo Rodrigues

SEDE ADMINISTRATIVA INSTITUTO DE CIÊNCIAS BIOMÉDICAS ABEL SALAZAR
FACULDADE DE CIÊNCIAS
FACULDADE DE MEDICINA

GONÇALO MARTINS DA COSTA PEREIRA RODRIGUES

DEFINING THE ROLE OF TUMOR-DERIVED EXOSOMES IN BRAIN METASTASIS

Tese de Candidatura ao grau de Doutor em Biologia Básica e Aplicada submetida ao Instituto de Ciências Biomédicas Abel Salazar da Universidade do Porto.

Orientador – Doutor David Lyden

Categoria – Professor of Pediatrics, and of Cell and Developmental Biology

Afiliação – Weill Cornell Medical College, Cornell University

Co-orientador – Doutora Maria de Sousa

Categoria – Professora Catedrática

Afiliação – Instituto de Ciências Biomédicas Abel Salazar da Universidade do Porto.

Os artigos científicos publicados no âmbito desta tese, e que serviram para a escrita da mesma, foram:

Tumour exosomal CEMIP protein promotes cancer cell colonization in brain metastasis.
Rodrigues G*, Hoshino A*, Kenific CM*, Matei I*, Steiner L, Freitas D, Kim HS, Oxley PR, Scandariato I, Casanova-Salas I, Dai J, Badwe CR, Gril B, Mark MT, Dill BD, Molina H, Zhang H, Benito-Martin A, Bojmar L, Ararso Y, Offer K, LaPlant Q, Buehring W, Wang H, Jiang X, Lu TM, Liu Y, Sabari JK, Shin SJ, Narula N, Ginter PS, Rajasekhar VK, Healey JH, Meylan E, Costa-Silva B, Wang SE, Rafii S, Altorki NK, Rudin CM, Jones DR, Steeg PS, Peinado H, Ghajar CM, Bromberg J, De Sousa M#, Pisapia D#, Lyden D#.
Nat Cell Biol. 2019 Nov;21(11):1403-1412. doi: 10.1038/s41556-019-0404-4. Epub 2019 Nov 4. PMID: 31685984

Tumour vesicular micromachinery uncovered.
Rodrigues G, Zhang H, Lyden D.
Nat Cell Biol. 2019 Jul;21(7):795-797. doi: 10.1038/s41556-019-0351-0.
PMID: 31235937

Pre-metastatic niches: organ-specific homes for metastases.
Peinado H*, Zhang H*, Matei IR*, Costa-Silva B, Hoshino A, **Rodrigues G**, Psaila B, Kaplan RN, Bromberg JF, Kang Y, Bissell MJ, Cox TR, Giaccia AJ, Erler JT, Hiratsuka S, Ghajar CM, Lyden D.
Nat Rev Cancer. 2017 May;17(5):302-317. doi: 10.1038/nrc.2017.6. Epub 2017 Mar 17. Review. PMID: 28303905

Tumour exosome integrins determine organotropic metastasis.
Hoshino A*, Costa-Silva B*, Shen TL*, **Rodrigues G**, Hashimoto A, Tesic Mark M, Molina H, Kohsaka S, Di Giannatale A, Ceder S, Singh S, Williams C, Soplop N, Uryu K, Pharmer L, King T, Bojmar L, Davies AE, Ararso Y, Zhang T, Zhang H, Hernandez J, Weiss JM, Dumont-Cole VD, Kramer K, Wexler LH, Narendran A, Schwartz GK, Healey JH, Sandstrom P, Labori KJ, Kure EH, Grandgenett PM, Hollingsworth MA, de Sousa M, Kaur S, Jain M, Mallya K, Batra SK, Jarnagin WR, Brady MS, Fodstad O, Muller V, Pantel K, Minn AJ, Bissell MJ, Garcia BA, Kang Y, Rajasekhar VK, Ghajar CM, Matei I, Peinado H, Bromberg J, Lyden D.
Nature. 2015 Nov 19;527(7578):329-35. doi: 10.1038/nature15756. Epub 2015 Oct 28. PMID: 26524530

Pancreatic cancer exosomes initiate pre-metastatic niche formation in the liver.
Costa-Silva B, Aiello NM, Ocean AJ, Singh S, Zhang H, Thakur BK, Becker A, Hoshino A, Mark MT, Molina H, Xiang J, Zhang T, Theilen TM, García-Santos G, Williams C, Ararso Y, Huang Y, **Rodrigues G**, Shen TL, Labori KJ, Lothe IM, Kure EH, Hernandez J, Doussot A, Ebbesen SH, Grandgenett PM, Hollingsworth MA, Jain M, Mallya K, Batra SK, Jarnagin WR, Schwartz RE, Matei I, Peinado H, Stanger BZ, Bromberg J, Lyden D.
Nat Cell Biol. 2015 Jun;17(6):816-26. doi: 10.1038/ncb3169. Epub 2015 May 18. PMID: 25985394

Dedicado à minha mãe e em memória do meu pai,

The saddest aspect of life right now is that science gathers knowledge faster than society gathers wisdom

Isaac Asimov

ACKNOWLEDGEMENTS

My experience as a PhD student ended up cementing the idyllic idea I had when I started doing research, that the uncharted and challenging paths are indeed the ones worth pursuing in science. However, one should not disregard lightly the risks and setbacks that accompany it. In these paths, mistakes and wrong turns easily remove you from the right track and as time goes by they become increasingly costly, sometimes leading to dismal scenarios of frustration. Luckily, during this same path I also had the privilege to encounter amazing people, from scientific colleagues to friends, who helped me to steer my boat in the right direction so I could reach my scientific destination and the conclusion of the thesis work presented here. To all of you, I whole-heartedly dedicate the following paragraphs.

"If I have seen further it is by standing on the shoulders of Giants." – Isaac Newton

To begin with, this experience would have never been possible without the amazing work of David Lyden, whose ideas captivated me so much that they made me move one ocean apart from the place I called home, so I could learn in first-hand more about them. For that alone, and for giving me the opportunity of integrating his lab, I owe an enormous thank you to David. Besides being a brilliant scientist and dedicated doctor, David mentored me in my scientific approach, and thought me how to sharpen my scientific mind, go after my objectives, and not be afraid of aiming high at challenging new ideas. Thank you for giving me the liberty to pursue my own path and believing in my capabilities.

A colossal thank you to Professor Maria de Sousa, for accepting me as her student, and more importantly, for keeping me as so throughout this time and not giving up on me, although the though must have occurred more than a handful of times. Jokes aside, without the guidance and help of Professor Maria de Sousa I would have been lost in this journey from the start. She wasn't always the supporter that I wanted, but she always was the mentor that I needed. In addition to the extremely important contributions in shaping my thesis work, Professor Maria always provided me with an insightful, honest and direct perspective on matters of science and life. I will forever cherish the coffee place scientific discussions we shared about different and intriguing scientific questions, especially the one surrounding that weirdly named molecule – KIAA1199, of which there was very little known about, and that would eventually become the center piece of this thesis work.

A huge thank you to Irina Matei, one that words cannot really describe. Besides her crucial and direct contributions for this thesis work, Irina was one of the best persons I had the privilege to cross paths with. Irina helped me in every single obstacle I encountered, even the ones not related to my work. Irina was a lighthouse for me in critical periods and I know for sure that I would have not been able to carry out this project without her. In addition to her friendliness and helping nature, Irina's extended scientific knowledge, common interest in brain metastasis, and exquisite scientific writing skills, helped me to grow as a scientist and provided me with the precious tools needed to finish my thesis and for use my future.

There are many more wonderful people who supported me greatly and were key in materializing this thesis, such as Ayuko Hoshino, who was by my side since the first time I stepped into the lab and that thought me everything about science on a day-to-day basis. I thank Ayuko not only for all the teachings and skills I learned from her but above all, for so openly sharing her scientific journey with me and believing in myself when I wouldn't. Hector Peinado, who pioneered the study of exosomes in our lab and received me with open arms when I first arrived, mentoring me during my initial forming years. Hector's door was always open, regardless of the issue. Besides teaching me a lot of what I know today, he also thought me that you can deal with anything in life with a positive attitude. Bruno Costa-Silva, with who I had the pleasure to share the bench, and the language, and who thought me the importance of perseverance and determination to become

successful in science. Candia Kenific and my other fellow lab members who were extremely involved in this project, giving critical contributions for the accomplishment of this work. Namely, my student Loic Steiner, who will become in his own right a great PhD student, for all the maturity shown and the hard work he had in helping me with experiments and putting up with me. I would also like to further extend my sincere thank you to everyone else not mentioned here that was involved in this project. The work presented here results from the effort of many more people, and without each of them this project would have been even harder, and very likely, not as good.

Obviously an enormous thanks to the GABBA program, which was the catalyst for all of this. Specially for allowing me to pursue what I was truly interested in and giving me the privilege to do a PhD in such a wonderful lab abroad. I thank the current and former directors, as well as Catarina and the office members of ICBAS for all their help and support throughout my thesis.
My PhD experience would have not been the same if I would have not met and been with my fellow GABBAs 15th, in special Joao, Joana, Mafalda and Diana. I became great friends with them and knew I could always count on tem if in need of friendly support or to spend a great time just being silly all around. Thank you for all the beautiful moments and memories I so fondly remember while writing this section.

To Porto and the friends I made there for accepting me how I am and embracing me as one of their own, and to New York for opening me the doors to the world and forcing me to become a better person by so bluntly exposing my flaws and weak points. Thanks to my friends of always from home, Alex, Angelo, Miguel and Nuno, for always supporting me and remaining close in spite of the distance. And, Yonathan, of course, who cannot go unmentioned, for being the truest of friends during my stay in the US, and an inspiration on hard work and dedication.

Obrigado a minha mae e avo, pelo apoio constante e amor incondicional que me deram, e por me deixarem seguir os meus sonhos, independentemente dos seus desejos proprios. Obrigado tambem pelos bons conselhos que me dao todos os dias, as qualidades que tenho e a razao de estar hoje aqui, a fechar com sucesso mais um capitulo da minha vida, sao resultado da vossa boa influencia em mim.

Finally, a very loving and special thanks to Irene, my partner, who joined me in this ride during a tormented time and was a ray of sunshine that helped me see life in brighter colors, not only on rainy days but every day we have shared together. Thank you for balancing me, reminding me of what is important in life and continuously contributing in my strive to become a better person. That the completion of this thesis marks not only a new chapter in my life, but in ours.

ABSTRACT

Abstract

Despite advances in our knowledge of the molecular determinants that drive the overall process of metastasis, metastatic entry and adaptation to specific organs remain poorly understood. This is particularly true for brain metastasis, as evidenced by its growing incidence, now ten times higher than that of all primary brain tumors combined. Brain metastases most commonly arise from cancers of the lung and breast and constitute one of the most pernicious outcomes of cancer, characterized by neurological complications, poor prognosis and high mortality, with no effective therapies available. Hence, discovery of new drivers of brain metastasis with potential to become therapeutic and preventive targets is required to advance the care of brain metastasis patients as well as cancer patients at risk of metastatic spread to the brain. The major challenges facing brain metastasis research stem not only from our incomplete understanding of the molecular mechanisms regulating metastasis to this organ, but also from the limited number of pre-clinical models available that mimic human disease and enable the study of the complex interactions between tumor cells and the brain microenvironment. Brain metastatic colonization underlies acquisition of key adaptations by metastatic tumor cells and is determined by both tumor-intrinsic properties and the crosstalk between tumor cells and stromal cells in the brain. The low metastatic efficiency observed for this organ results from its particular microenvironment and resident cells, which constitute a hostile “soil” for seeding tumor cells to colonize. Ultimately, it is the ability of tumor cells to remodel the brain microenvironment and create a supportive niche for metastatic tumor cell survival and outgrowth that determines successful metastatic colonization. Among tumor-secreted factors, which are recognized as major contributors to the formation of pre-metastatic and metastatic niches, tumor-derived exosomes have recently arisen as crucial players in cell-to-cell communication and in the remodeling of distant microenvironments that favor organ-specific metastasis. Therefore, we sought to determine the role of tumor-derived exosomes in the modulation of the brain microenvironment and their specific contribution to supporting metastatic colonization of the brain. For that, we used *in vivo* pre-clinical models of brain metastasis and adapted an organotypic brain slice *ex vivo* model for the study of tumor-derived exosomes in brain metastasis, allowing us to assess their role in metastatic colonization and tumor outgrowth.

Our characterization of the organ distribution of tumor exosomes revealed that circulating exosomes of brain metastatic cell origin preferentially localize to the brain, where they interact predominantly with endothelial cells. Interestingly, exosome-positive vessels in the brain showed indication of vascular dysfunction, suggesting that their interaction with the brain microenvironment, and the vascular niche in particular, can lead to pro-metastatic effects of relevance for brain metastasis. Using our optimized *ex vivo* brain slice model we observed that pre-conditioning the brain microenvironment with exosomes from brain metastatic cells enhances cancer cell colonization of the brain. We then set to investigate which factor present in brain metastatic exosomes could be responsible for their pro-metastatic. Given the relevance of the exosome protein content in previously documented pro-metastatic functions of tumor exosomes we decided to pursue the characterization of the specific exosomal protein composition of exosomes from brain metastatic models. Our unbiased proteomic analysis of exosomes isolated from tumor cell models of common origin but different metastatic organotropisms identified cell migration-inducing and hyaluronan-binding protein (CEMIP, KIAA1199) as a protein distinctively enriched in exosomes from brain metastatic breast and lung tumor cell models. We now show that CEMIP, a Wnt-related protein involved in cancer and inflammation, mediates brain metastasis and promotes a pro-metastatic environment conducive to tumor cell-vascular association. Mechanistically, exosomal CEMIP stimulated a pro-inflammatory state in the brain vascular niche, namely through its effect on brain endothelial cells and microglia, characterized by the upregulation of diverse cytokines and chemokines known to promote brain tissue colonization (e.g. *Ptgs2*, *Tnf*, and *Ccl/Cxcl* family genes). Importantly, CEMIP was identified in exosomes secreted from surgically resected live human brain metastatic tissue samples obtained from breast and lung cancer patients. Moreover, high CEMIP expression in human primary and metastatic tumor tissue samples significantly associated with faster brain metastasis progression and poor survival.

Our work defining the contribution of CEMIP to brain metastasis brings new insight into the molecular mechanisms through which tumor-secreted exosomes promote metastasis to the brain and highlights the importance of the trophic properties of the brain vascular niche in this process.

RESUMO

Apesar de avanços no nosso conhecimento relativamente aos determinantes moleculares que governam o processo geral de metastização, a entrada e a adaptação de células metastáticas em órgãos específicos permanece pouco compreendida. Esta afirmação é particularmente verdadeira para o caso das metástases cerebrais, como é evidenciado pela sua crescente incidência, agora dez vezes maior que a de todos os tumores cerebrais primários combinados. As metástases cerebrais surgem normalmente de cancros do pulmão e de mama e são umas das consequencias mais perniciosas da metastização do cancro, sendo caracterizadas por complicações neurológicas, mau prognóstico e alta mortalidade, padecendo actualmente de terapias eficazes disponíveis para o seu tratamento. Por este motivo, é necessário compreender melhor os processos que estão na origem da formação de metástases cerebrais e descobrir novos mecanismos envolvidos nestes processos que tenham potencial para se tornarem alvos terapêuticos e preventivos. Desta forma, poderemos avançar o tratamento de pacientes com metástases cerebrais e pacientes oncológicos em risco de disseminação metastática para o cérebro. Os principais desafios enfrentados pela pesquisa em metástases cerebrais não são apenas fruto da nossa compreensão incompleta dos mecanismos moleculares que o regulam este processo, mas também do número limitado de modelos pré-clínicos disponíveis capazes de mimetizar a progressão doença em humanos e que também permitam o estudo das complexas interações entre as células tumorais e as células do microambiente cerebral. A colonização metastática do cérebro está subjacente à aquisição de adaptações cruciais pelas células tumorais metastáticas e é determinada pelas propriedades intrínsecas do tumor e pela comunicação entre as células tumorais e as células estromais do cérebro. A baixa eficiência metastática observada para este órgão resulta do seu microambiente e células residentes, que constituem um "solo" hostil para a colonização das células tumorais, que o semeiam. Como resultado, é a capacidade que as células tumorais têm de remodelar o microambiente cerebral e criar um nicho que promova a sobrevivência e crescimento das mesmas que determina uma colonização metastática bem-sucedida no cérebro. Entre os factores secretados por tumores, reconhecidos como os principais contribuintes na formação de nichos pré-metastáticos e metastáticos, os exossomas surgiram recentemente como actores críticos para a comunicação célula-a-célula e para a

remodelação de microambientes distantes que favoreçam a metastização específica para distintos órgãos. Por estes motivos, procurámos determinar o papel dos exossomas derivados de tumores na modulação do microambiente cerebral e sua contribuição específica no suporte da colonização metastática do cérebro. Para isso, usámos modelos pré-clinicos de metástases cerebrais *in vivo* e adaptámos um modelo organotípico de secções cerebrais *ex vivo* para o estudo de exossomas derivados de tumores metastáticos cerebrais, permitindo desta forma avaliar seu papel específico na colonização metastática e no crescimento tumoral.

A nossa caracterização da distribuição de exossomas tumorais em diferentes órgãos revelou que os exossomas circulantes de origem celular metastática cerebral localizam-se preferencialmente no cérebro, onde interagem predominantemente com células endoteliais. Curiosamente, os vasos sanguíneos encontrados no cérebro que interagiram com exosomas tumorais demonstraram indicações de disfunção vascular, sugerindo que a interação de exossomas com o microambiente cerebral, e o nicho vascular em particular, pode levar a efeitos pró-metastáticos relevantes para a formação metástases cerebrais. Utilizando o nosso modelo optimizado de secções cerebrais *ex vivo*, observamos que o pré-condicionamento do microambiente cerebral com exossomas de células metastáticas cerebrais promove a colonização de células cancerígenas no cérebro. Em seguida, decidimos investigar a identidade do fator presente em exossomas metastáticos cerebrais que poderia ser responsável pelos efeitos pró-metastáticos observados. Dada a relevância do conteúdo proteico de exossomas tumorais em funções pró-metastáticas previamente documentadas, decidimos prosseguir com a caracterização da composição proteica específica dos exossomas derivados de modelos metastáticos cerebrais. Utilizando uma abordagem exploratória imparcial, a análise proteómica de exossomas isolados de modelos tumorais celulares com origem comum mas predilecção metastática para diferentes orgãos, identificou a *cell migration-inducing and hyaluronan-binding protein*, ou proteína inductora de migração celular e de ligação ao ácido hialurónico (CEMIP, KIAA1199), como sendo uma proteína enriquecida distintamente em exossomas derivadas de células metastáticas cerebrais de cancro de da mama e de pulmão. Neste trabalho, demonstramos que a CEMIP, uma proteína relacionada com a sinalização Wnt, e previamente envolvida na progressão de diferentes

cancros e em processos de inflamação, medeia a formação de metástases cerebrais e promove um ambiente pró-metastático, propício à associação de células tumorais com a vasculatura cerebral. Mecanisticamente, a CEMIP exossomal estimulou um estado pró-inflamatório no nicho vascular do cérebro, através do seu efeito em células endoteliais do cérebro e micróglia, que é caracterizado pela promoção da expressão génica de diversas citocinas conhecidas por promover a colonização do tecido cerebral (ex.: *Ptgs2*, *Tnf*, e genes da família Ccl/Cxcl). É importante salientar que o CEMIP também foi identificado em exossomas secretados a partir de amostras de tecido metastático cerebral humano, obtidas a partir da resecção cirúrgica de pacientes com cancro da mama e do pulmão. Além disso, a expressão elevada de CEMIP em amostras de tecidos tumorais primários e metastáticos humanos associou-se significativamente a uma progressão mais rápida da formação de metástases cerebrais e a baixas taxas de sobrevivência.

O nosso trabalho, define desta forma a contribuição do CEMIP para metástases cerebrais, trazendo uma nova visão dos mecanismos moleculares através dos quais os exossomas secretados por tumores promovem metástases para o cérebro, destacando também a importância das propriedades tróficas do nicho vascular cerebral neste processo.

LIST OF ABBREVIATIONS

α	Alpha
β	Beta
3D	Tri-dimensional
ACA	Anterior cerebral artery
ACTB	Beta-actin
BA	Basilar artery
BBB	Blood brain barrier
BCA	Bicinchoninic acid
BMDC	Bone-marrow derived cell
BoT	Bone tropic
BrEC	Brain endothelial cell
BrM	Brain metastasis
BrT	Brain tropic
c	Cells
CC	Cell compartment
CCR7	C-C chemokine receptor type 7
CEMIP	Cell migration-inducing and hyaluronan-binding protein
Cm	Conditioned media
CNS	Central nervous system
COX2	Cyclooxygenase 2
Cp	Cytoplasm
Cs	Cytoskeleton
CSF	Cerebrospinal fluid
CTC	Circulating tumor cell
CXCR4	C-X-C chemokine receptor type 4
DTC	Disseminated tumor cell
e	Exosomes
exo	Exosomes
EC	Endothelial cell
ECM	Extracellular matrix
EGFR	Epidermal growth factor

ER	Estrogen receptor
ESCRT	Endosomal sorting complex required for transport
ETF	Endothelial tube formation
EV	Extracellular vesicle
FACS	Fluorescence-activated cell sorting
FBS	Fetal bovine serum
FDR	False discovery rate
Fig	Figure
FOV	Field of view
GFP	Green fluorescent protein
gRNA	Guide RNA
h	Hours
HA	Hyaluronic acid
H&E	Hematoxylin and eosin
IA	Intussusceptive angiogenesis
IC	Internal carotid
IHC	Immunohistochemistry
ITG	Integrin
ILV	Intra-luminal vesicle
IPA	Ingenuity Pathway analysis
KO	Knock-out
LFQ	Label-free quantification
LFU	Last follow-up
LuT	Lung tropic
m	Molecular marker
Mb	Membrane
Met	Metastasis
MG	Microglia
MMP	Metalloproteinase
MT	Metastatic tumor
MVB	Multivesicular bodies

Nc	Nuclear
NSLC	Non-small cell lung cancer
OE	Overexpression
PC	Polycarbonate
PCA	Principal component analysis
PCR	Polymerase chain reaction
PMN	Pre-metastatic niche
PR	Progesterone receptor
p/s	Photons per second
PT	Primary tumor
RNA	Ribonucleic acid
SCA	Superior cerebellar artery
SEM	Standard error of mean
SPC	Surfactant protein C
Sup	Supplementary
TEM	Transmission electron microscope
VA	Ventral artery
VEGF	Vascular endothelial growth factor
WC	Whole cell
WT	Wild type

TABLE OF CONTENTS

Section Page

ACKNOWLEDGEMENTS vii

ABSTRACT xi

RESUMO xv

LIST OF ABBREVIATIONS xx

TABLE OF CONTENTS xxv

CHAPTER I: INTRODUCTION 1

Section 1: Mechanisms of Cancer Metastasis 3

Section 2: Brain Metastasis Biology 11

Section 3: Exosomes in Cancer progression and Metastasis 18

Section 4: Background and Research Aims 23

CHAPTER II: MATERIALS AND METHODS 26

- Cancer cell lines and cell culture 28
- Exosome purification, labelling, characterization and analysis 28
- Brain slice assay 29
- Proteomics methods and data analysis 32
- Western blot analysis 33
- OptiPrep™ density gradient (ODG) exosome isolation 34
- Mouse studies 34
- Tissue processing and immunostaining 37
- Generation of CEMIP knockout and overexpression cell lines 38
- Proliferation and invasion in vitro assays 40
- Brain endothelial cell isolation, culture and assays 40
- FACS analysis 42
- RNA preparation, sequencing and data analysis 43
- Human studies 44
- Data presentation and statistical analysis 46

CHAPTER III: BIODISTRIBUTION AND VASCULAR INTERACTION OF METASTATIC TUMOR EXOSOMES IN THE BRAIN 48

CHAPTER IV: EX VIVO MODELING OF BRAIN METASTATIC COLONIZATION FOR TUMOR EXOSOME STUDIES 59

CHAPTER V: CEMIP, A TUMOR EXOSOME PROTEIN WITH FUNCTIONS IN BRAIN METASTASIS 69

CHAPTER VI: EXOSOMAL CEMIP-DEPENDENT MECHANISMS UNDERLYING BRAIN VASCULAR NICHE RESHAPING 84

CHAPTER VII: CEMIP AS A BIOMARKER OF BRAIN METASTASIS 97

CHAPTER VIII: DISCUSSION 106

REFERENCES 124

CHAPTER I

Introduction

Section 1

Mechanisms of Cancer Metastasis

Section 1 – Mechanisms of Cancer Metastasis

Despite continuous research efforts to understand the molecular drivers of cancer for the past 70 years, metastasis remains a mystery and the primary cause of cancer-related death. Metastasis encompasses the spread of cancer from its primary organ site to other organs. Development of secondary malignant tumor lesions in distant organs disturbs physiological homeostasis and can provoke physical alterations in tissue architecture which can lead to loss of organ function and death. It is now well established that organs of future metastasis are not passive receivers of circulating tumor cells, but are instead selectively and actively modified by the primary tumor before metastatic spread has even occurred. Sowing the 'seeds' of metastasis requires the action of tumor-secreted factors and tumor-shed extracellular vesicles that enable the 'soil' at distant metastatic sites to encourage the outgrowth of incoming cancer cells [1].

1.1 – Tumor progression and evolution

Primary tumors were initially viewed as homogeneous masses of cancer cells; however, work in the past 30 years has shown that primary tumors are composed of a heterogeneous mixture of cancer cells, with diverse genetic profiles, as well as stromal cells and infiltrating immune cells [2]. Recent work has demonstrated that clonal evolution occurs in primary tumors, driving the emergence of distinct cancer cell clones with different characteristics and contributions at the tumor cell population level. Genetic tumor heterogeneity, either intrinsic or developed as a result of selection due to environmental stress, may confer tumor cells properties that allow them to become more malignant. Genetic alterations and epigenetic regulation of genes impacting biological pathways such as cell migration and remodeling of surrounding extracellular matrixes, are likely to impact the ability of tumor cells to disseminate and conquer new territories, one of the hallmarks of metastasis.

Alterations in key pro-metastatic drivers synergize, rendering tumor cells metastatic and (e.g. EMT) allowing them to escape the primary tumor and generate secondary lesions in distinct organs [3]. Metastasis is a multi-step process, and rather inefficient, as tumor cells encounter challenges at every step [4]. Tumor cells first need to escape the primary tumor

mass by intravasating into the vasculature that supplies the primary tumor and this way spread into circulation to reach distant organs. Depending on the type of vasculature present in the tumor, metastatic spread can occur through the haematogenous or lymphatic systems, via the blood vessels or lymphatic vessels, respectively. After exiting the primary tumor, tumor cells have to survive in circulation, avoiding destruction by the immune system and eventually arresting in capillaries of distant organs where they could give rise to secondary tumor lesions [2]. Due to all these requirements, the metastatic process is extremely inefficient and only a very small percentage of disseminated tumor cells ever becomes a metastatic lesion [4]. Tumor cell arrest within the vasculature is a complex process which depends on vascular architecture and the physical properties of the blood/lymph flow, contributions from the clotting system, and expression of cell membrane adhesion molecules by tumor cells. After intravascular arrest tumor cells extravasate into the tissues of the new organ. For extravasation, tumor cells need to overcome the vascular barrier, usually by disrupting it, so they can access the parenchyma of the target organ. Interaction with endothelial cells of distinct organs is a common feature of all metastasis [5]. Cancer cells closely interact with endothelium during initial arrest and seeding, subsequent extravasation, and then later during angiogenic remodeling that occurs in metastatic growth phase. Extravasation is a critical step which can severely limit tumor cell entry and subsequent metastases formation. Once this barrier is surpassed, the ability of tumor cells to survive within their new environment and remodel it in support of their growth fully determines their true potential to generate metastases.

In addition to the intrinsic properties of tumor cells that confer them motility and metastatic potential, it is their unique ability to remodel their surrounding microenvironment that determines successful metastatic colonization [3].

1.2 – Metastatic tumor colonization

The first mechanisms proposed to explain organ-specific metastasis focused mainly on tumor cell intrinsic properties, such as metabolic or extracellular matrix (ECM)-interacting/remodeling adaptations, which lead to increased cancer cell survival at

metastatic sites and successful metastatic colonization. During the initial phase of metastatic colonization, tumor cells rely on ligand/receptor interactions between cancer cell membrane proteins and ECM components of the vasculature and microenvironment of distinct organs during metastatic seeding (e.g. tumor integrin interactions with vascular adhesion and ECM molecules). These and other observations underscore the importance and contribution of the colonizing organ microenvironment to metastasis as a major driver of tumor malignancy and progression [6, 7].

The understanding that the microenvironment is a critical determinant of tumor growth as well as metastatic outcome, led to a shift towards a new, non-tumor centric perspective, leading to the identification of tumor cell extrinsic drivers of metastasis. Thus, it was established that receptor/ligand interactions, paracrine signaling and secreted factors mediate the crosstalk between tumor and stromal cells in the metastatic organ microenvironment. The tumor and surrounding environment (blood vessels, stromal cells, immune cells, ECM and signaling molecules) constantly interact and co-evolve [2].

Interestingly, tumor-secreted factors, such as cytokines, chemokines, metabolites, and extracellular vesicles/particles can not only mediate crosstalk in the local tumor microenvironment, but can also have systemic effects, influencing the behavior of stromal and immune cells at distant sites [8]. This discovery brought tumor secreted factors into the spotlight, and they became a major focus of metastasis research in the past decade. More importantly, tumor-secreted factors can affect several distinct steps of the metastatic cascade by: a) inducing thrombotic events and adhesive properties in the endothelium during cancer cell arrest phase that allow cancer cell attachment ; b) altering the permeability of vessels during extravasation phase to facilitate cell entry ; c) promoting cancer cell invasion and tissue colonization through basement membrane processing and ECM deposition by stromal cells via inflammatory signaling ; d) promoting stromal cell recruitment and induction of pro-survival signaling in stroma by release of chemotactic signals during metastatic growth ; and e) inhibiting immune cell function [3].

1.3 – Tumor-type specific organ metastatic patterns

A pivotal discovery by Stephen Paget in 1889 [9] postulated that metastasis is dependent on the interactions between ‘seeds’ (or the cancer cells) and the ‘soil’ (or the host microenvironment). Paget’s theory was challenged in the 1930s by James Ewing [10], who advocated that metastatic dissemination could be explained solely by the dynamics of haematogenous flow. Ewing’s perspective became the prevalent viewpoint until Isaiah Fidler’s research in the 1970s [11] demonstrated that, although the mechanical properties of blood flow were important, successful metastatic colonization could occur only at certain organ sites and that distinct tumor-types displayed specific metastatic organ patterns that could not solely be explained by the mechanic flow properties.

In experimental metastasis assays, Fidler et al. demonstrated that cancer cells derived from a certain metastatic site displayed enhanced abilities to metastasize to that specific organ, providing support for Paget’s organ-specific metastasis theory [12].

In addition to strengthening Paget’s theory, Fidler’s findings reignited interest in the question that first captivated Paget: why do tumor cells emerge only as disseminated tumor cells (DTCs) within specific organs? Is metastatic seeding monoclonal or polyclonal in nature? Moreover, does metastatic seeding occur only directly from the primary tumor or is secondary seeding from one metastatic organ to another also a biologically relevant event? This organ specificity observed in metastasis is known as organotropism and remains one of the most intriguing unanswered questions in cancer research [13].

Despite Stephen Paget’s 131-year-old “seed-and-soil” hypothesis [9], insufficient progress has been made towards decoding the mechanisms governing organ-specific metastasis. Subsequent studies investigating organ-specific metastasis focused largely on the role of intrinsic cancer cell properties, such as genes and pathways regulating colonization, in directing organotropism. Breast cancer cells express chemokine receptors, such as C-X-C motif receptor 4 (CXCR4) and C-C motif receptor 7 (CCR7), which partner with chemokine ligands expressed in lymph nodes (CXCL12) and lung (CCL21), thus guiding metastasis [14]. Tumor-secreted factors can also increase metastasis by inducing vascular leakiness, promoting the recruitment of pro-angiogenic immune cells , and influencing organotropism [15]. Furthermore, the ability of breast

cancer to form osteolytic lesions depends on osteoclast stimulating growth factors (for example, PTHRP and GM-CSF) released into the bone microenvironment [16]. Therefore, previous observations by the Lyden laboratory that metastatic melanoma-derived factors dictate organotropism are not surprising [17]. We found that medium conditioned by highly metastatic melanoma cells was sufficient to expand the metastatic repertoire of lung carcinoma cells that would typically only metastasize to the lung itself. This particular observation suggested that the formation of niches permissive for tumor outgrowth at future sites of metastasis could overcome the tumor cell's intrinsic metastatic properties and more importantly, that particular tumor-secreted factors could account for niche formation in distinct organs and this may determine metastatic organotropism.

1.4 – Pre-metastatic niches and organotropic metastasis

Fundamental discoveries revealed that tumors induce the formation of microenvironments in distant organs that are conducive to the survival and outgrowth of tumor cells before their arrival at these sites. These predetermined microenvironments are termed 'pre-metastatic niches' (PMNs) [18]. Although congruent with both Paget's and Ewing's theories, the concept of the PMN is unique as it proposes that the primary tumor preconditions specific organ sites for future metastatic disease (that is, before CTC arrival) via tumor-derived factors. Therefore, in contrast to the metastatic niche, which is initiated and shaped upon CTC arrival, the PMN represents an abnormal, tumor growth-favoring microenvironment devoid of cancer cells.

Since the existence of the PMN was first demonstrated, numerous studies have identified various molecules that regulate its stepwise evolution, highlighting the complex molecular and cellular changes that occur in the PMN to support future metastatic tumor growth [19]. PMNs are the result of the combined systemic effects of tumor-secreted factors and tumor-shed extracellular vesicles (EVs) that promote a temporal sequence of events during the evolution of PMNs. Vascular leakiness is the earliest event in this sequence, followed by the alteration of local resident cells, such as fibroblasts, and the recruitment of non-resident cells, such as bone marrow-derived cells (BMDCs), to these PMNs, subsequently attracting circulating tumor cells (CTCs) [19, 20]. Pre-metastatic niche formation requires S100 proteins and ECM deposition, such as fibronectin upregulation

by lung resident cells, as well as the recruitment of bone-marrow-derived myeloid cells in response to tumor-secreted factors [17]. It has become clear that vascular niche reshaping and extracellular matrix (ECM) remodeling is crucial for establishing the PMN. Moreover, PMNs are probable sites of immune deregulation, owing to the presence of a pro-tumorigenic, inflammatory milieu induced by tumor-secreted factors, which creates immunosuppression and coagulation disorders [5, 21] These events synergize to establish a favorable microenvironment that promotes the growth of disseminated tumor cells upon their arrival.

Although the mechanisms of lung PMN generation have started to be described, the cellular and ECM constitution and underlying molecular mechanisms of PMN formation in other metastatic organs remains to be characterized. Since distinct challenges are faced by cancer cells during metastatic colonization depending on the organ of metastasis, specific needs regarding the constitution of pro-tumoral microenvironments are likely to differ as well. This implies that the organ-specific mechanisms of metastatic colonization can offer potential targets for organ-specific metastatic therapy. The specific contribution of tumor-secreted factors and tumor-shed extracellular vesicles and exosomes is also not fully explored and requires deeper analysis. Action of these tumor agents is of particular interest in the context of brain metastasis, an organ in which metastases develop late but associate with poor outcome. This implies that brain metastasis usually happens late after primary tumor formation, with a long pre-metastatic phase during which tumor-secreted factors could affect the brain microenvironment and generate a PMN in the brain. The brain also poses particular challenges to metastasis that are unique to this organ, such as the presence of a restrictive vascular barrier structure, the blood-brain-barrier (BBB), that is much less permissive than other vascular beds as a result of their multi-cellular and complex composition and tight endothelial cell junctions. In addition, the brain microenvironment is suppressive and requires tumor cells to acquire additional survival mechanisms and specific signaling to colonize it. Due to the complexity of the brain metastatic process and limitations of the available pre-clinical models of brain metastasis, the development of therapeutic approaches for this dreadful type of metastasis is still lacking in comparison to other organs. Therefore, further understanding of the specific mechanisms involved in the formation of hospitable and

conducive environments to enhance tumor colonization in organs such as the brain, and improvements on the current research models, are required for development of effective anti-metastatic therapies.

Section 2

Brain Metastasis Biology

Section 2 – Brain Metastasis Biology

Metastatic spread to the brain remains one of the least understood and most detrimental outcomes of cancer. Brain metastases are estimated to occur in approximately 20% of all cancer patients and overshadow the incidence of primary brain tumors by more than ten-fold [22, 23]. Brain metastases present a unique set of clinical challenges and their presence is associated with poor survival, development of severe neurological issues, and ultimately death [24]. The brain microenvironment is vastly different from other organ environments, presenting complex anatomical structures, unique cell types, and particular immune and metabolic properties. Thus, the brain microenvironment imposes a very distinct and strong selective pressure on tumor cells that shapes the metastatic process and therapy responses. Importantly, the brain vasculature has emerged as a key determinant factor in brain metastasis, not only by due to its role in the initial seeding of circulating tumor cells and promoting vascular-associated tumor growth, but also due to its capacity to limit the access of systemic therapies to the brain [5]. The major limiting factor for the study of brain metastasis has been the scarcity of robust preclinical models that recapitulate the full process of metastatic spread to the brain and/or that allow to dissect out the key relationships between tumor cells and the brain microenvironment which allow for successful colonization of this organ [25]. Therefore, the study of brain metastasis and further characterization of their interaction with the brain microenvironment, and in particular the brain vascular niche, could unveil new therapeutic targets to address this unmet clinical need.

2.1 – Epidemiology of brain metastasis

Although the true prevalence of brain metastasis is not certain, epidemiological population-based studies estimate that their incidence ranges from 8.3 to 14.4 per 100,000 [26]. However, this value is likely an underestimate given that the majority of the epidemiological studies pre-date modern imaging technologies and no further information on disease course or subsequent involvement of metastatic sites was available for patients not presenting with neurological symptoms or brain metastasis at time of initial diagnosis. In support of this claim, autopsy studies suggest a higher incidence of

intracranial metastasis, detected in up to 40% of cancer patients [27]. Furthermore, it is also believed that while the improvement in cancer detection, patient care, and systemic therapies for extra-cranial metastasis implemented over the past decades, while having extended the life span of cancer patients, may account for and inversely correlate with the rising incidence of brain metastasis.

The incidence of brain metastasis largely depends on factors such as primary tumor site, stage of disease, subtype of cancer, and other key prognostic factors [22, 28]. Although any type of cancer has the ability to metastasize to the brain, the most common primary tumors associated with brain metastasis are lung (20 – 56% of patients), breast (5 – 20%), and melanoma (7 – 16%)[22, 26], followed by colorectal and renal cancers [22]. Within these, the type of primary tumor and its molecular subtype further impact the risk of developing brain metastasis. This is particularly well established in breast cancer, where tumors presenting triple-negative hormone-receptor status molecular subtype [i.e. estrogen receptor (ER)-negative, progesterone receptor (PR)-negative and normal human epidermal growth factor receptor 2 (ERBB2; also known as HER2) levels] or with HER2 amplification, have higher risk of developing brain metastases [29]. In lung cancer, patients with non-small cell lung cancer (NSCLC) or small-cell lung cancer (SCLC) primary tumor types are the most afflicted with brain metastases (15 – 26%, and 24% respectively) [30], with NSCLC molecular subtype with ALK rearrangements shown to be at increased risk [31].

In addition to these specific cancers and molecular subtypes, the risk of developing brain metastases also increases with more advanced primary disease [30], and can also be influenced by additional factors such as sex, age and ethnicity. Regardless, despite the factors described above and efforts to develop data-driven tools to specifically prognosticate brain metastasis patients earlier and more accurately (such as the graded prognostic assessment index – GPA, which takes into account performance of daily tasks by patients, treatment status, number of metastases, among others), their clinical value remains limited, as illustrated by the very short and poor survival estimates for brain metastasis patients [32].

Diagnosis of brain metastasis has improved during the last decades due to advancements in imaging technologies that allow earlier detection. However, current treatments for brain metastasis, such as whole-brain radiation therapy or local radiation therapy carry many toxic outcomes given that this is not a targeted therapy and therefore affects healthy normal brain cells as well. Due to the shortcomings of radiation, systemic treatments with efficacy in the CNS that target only tumor cells are needed. Thus, a better understanding of the molecular mechanisms driving brain metastasis are necessary for the development of novel and improved therapeutic approaches.

2.2 – Molecular mechanisms of brain metastatic colonization

A better understanding of the metastatic spread to the brain and the underlying molecular mechanisms governing it is necessary to address the dismal prognosis that brain metastasis patients currently face. From the analysis of preclinical models of brain metastasis, it has become apparent that cancer cells require two critical competences in order to successfully metastasize to the brain. First, they need to be able to reach and surpass the blood-brain-barrier (BBB) in order to enter the brain, and later they need to adapt to and remodel the brain milieu so they can survive and thrive within this new environment. The BBB is a multi-cellular and complex barrier structure that protects and insulates the brain and its neuronal signaling from systemic insults [24]. Alongside the blood-cerebrospinal fluid (CSF) barrier, the BBB comprises the most important functional barrier in the brain that tumor cells need to overcome to enter the brain. This structure consists of endothelial cells that are connected by strong tight junctions and present low transcytosis rates and expression of several efflux pumps. Furthermore, in addition to endothelial cells and their basement membrane, the BBB is composed by bordering pericytes and terminal processes of astrocytes, which further contribute for this barrier's functions and selective permeability. Due to the properties of the BBB, only small uncharged compounds are able to freely diffuse through it under normal conditions. However, inflammation occurring in the context of infections and autoimmunity, will open the BBB to immune cells. Through mechanisms which are still not completely elucidated, cancer cells can also overcome the BBB and gain access to the CNS [33].

Cancer cells are thought to arrive to the brain and arrest within the vasculature either as single cells or emboli. Their arrest is thought to be promoted by a combination of factors, ranging from aberrant sizes of cancer cells, slower blood flow movement at capillary branch points and activation of coagulation by cancer cells and the factors they secrete [34, 35]. Interestingly, several studies have shown that only a very small proportion of cells that arrest within the brain microvasculature form metastases, highlighting the importance of subsequent steps for successful brain metastatic colonization [35]. After arrest, the tumor cells' potential to extravasate into the brain and colonize the brain is mostly mediated by their ability to interact with brain endothelial cells. Successful interaction between tumor cells and brain endothelial cells is mainly determined by expression of adhesion factors, such as the membrane glycosyltransferase ST6GALNAC5, shown to specifically mediate circulating cancer cell adhesion to the endothelium of the brain [36]. During extravasation, tumor cells express factors that induce vascular permeability, promoting migration across the BBB, such as VEGF, COX2, and HBEGF. Additionally, recruitment of immune cells and activation of glial cells of the BBB by extravasating tumor cells results in VEGF signaling activation and release of proteinases such as cathepsin S and matrix metalloproteinases (MMPs), such as MMP9 [25]. The later are able to further contribute to this process by cleaving junctional adhesion molecules of the endothelial cell barrier and leading to focal extracellular matrix degradation, respectively. Once extravasation is completed, different cell fates might await tumor cells. They might undergo cell death due to the conditions of the brain microenvironment [24], remain in a dormant state with slow cell-cycling [36, 37] or survive and give rise to metastases.

Once within the brain, thriving tumor cells experience complex interactions with the brain microenvironment that govern their outgrowth. Although this process is not completely understood, the insights gathered so from pre-clinical models and analysis of patient samples indicates that the colonization process is characterized by induction of neuroinflammatory cascades and mechanisms of vascular niche reshaping. A particularly interesting observation is that surviving cancer cells appear to remain in proximity to the perivascular niche [35, 38]. This particular localization of tumor cells allows easy access to oxygen and nutrients from blood circulation, a settling contact point for attachment

within the basal lamina of vessels and exquisite access to angiocrine factors produced by endothelial cells that support tumor growth. Furthermore, brain metastatic tumor cells are known to exploit the vasculature of the brain rather than generate their own vascular supply system, through the process of angiogenesis, as commonly observed for extracranial metastases [24]. In the brain, tumor cells typically interact with the pre-existing vasculature and grow along the abluminal side, through a process known as vascular co-option [39]. Later, they reshape the architecture of the vasculature with which they associate in order to integrate it into the growing metastatic mass, a phenomenon typically observed in brain metastases and referred to as angiocentric growth. This mainly occurs through a process termed intussusceptive angiogenesis, where new vessels are formed by the remodeling and splitting of previously existing ones [40-43]. Adhesion molecules involved in vascular co-option include L1CAM and β1 integrin [38, 44]. Interestingly, another integrin family member, the αvβ3 integrin heterodimer, has been shown to promote cell adhesion to the endothelium and key signaling for initial colonization. In addition to their pivotal interaction with brain endothelial cells, tumor cells are exposed to and interact with other stromal cells of the brain microenvironment that can determine the success of their colonization. Of particular importance, tumor cells induce a prominent neuroinflammatory response, activating astrocytes and microglia. Astrocytes can influence tumor cell growth through pro-metastatic transfer of metabolites such as cGAMP thorough gap-junctions and secretion of inflammatory chemokines such as interferon-α and TNF, as well as anti-metastatic secretion of cell-death inducing plasmin [25]. In contrast, the complex role of microglia is equally acknowledged, but less explored. While microglia can hinder brain metastasis through cytotoxic effects which can be mitigated by tumor cell expression of neurotrophin-3 [45], they can also promote brain metastasis by producing pro-tumorigenic cytokines, such as CCL2 and other members of the CCL/CXCL family [46]. Finally, additional properties and adaptations by tumor cells that have been shown to assist in brain colonization include metabolic adaptations, impacting processes such as glucose metabolism or reactive oxygen species production [47]. As described in this section, the incomplete understanding of the roles that different brain stromal cells play in metastatic colonization, and the dependence of some of the mechanisms described to particular tumor types or circumstances, underscores the need

for improved brain metastasis pre-clinical models that allow the study of the interactions of tumor cells with the brain microenvironment and respective outcome for metastasis. Use of alternative models such as 3D organotypic brain slice *ex vivo* cultures [38, 48], or 3D multi-cellular cultures composed of different brain stromal cells *in vitro*, might be the key to help to bridge this gap.

Section 3

Exosomes in Cancer progression and Metastasis

Section 3 – Exosomes in cancer progression and metastasis

Among tumor-secreted factors, which are recognized as major contributors to the formation of pre-metastatic and metastatic niches, tumor-derived exosomes have recently arisen as crucial players in cell-to-cell communication and in the remodeling of distant microenvironments that favor organ-specific metastasis.

3.1 – Extracellular vesicle biology and exosome biogenesis

Exosomes are a class of extracellular vesicles (EVs) ranging in size between 30 –150 nm that derive from the multivesicular endosomal pathway [49]. This class of vesicles are secreted into circulation (blood, lymphatics fluid, saliva, urine, etc.) by both normal and tumor cells. In particular, tumor-secreted exosomes are critical mediators of intercellular communication between tumor cells and stromal cells in local and distant microenvironments, and therefore, are key modulators of tumor progression and metastasis.

EVs were first described in 1967 by work from Peter Wolf, who first demonstrated a role for platelet-secreted vesicles during blood coagulation [50]. In 1980, Trams et al. [51] uncovered the essential role that EVs play in intercellular transport of trophic substances or nutrients. In the 1980s, several groups described the role of secretory vesicles in reticulocyte maturation through recycling of transferrin and its receptor [52-54]. In addition, pioneer studies by Raposo et al. [55] further demonstrated the importance of EVs in immune modulation. Since then, many studies, including those from our group [17, 56, 57], have further demonstrated the crucial role of EVs in immune modulation, cell signaling, and onset and progression of disease.

EVs are classified on the basis of their size and origin. Microvesicles (>150 nm) are formed at the cell surface through a budding mechanism while exosomes (30–150 nm) are produced in a regulated manner by the endolysosomal and multivesicular body compartments for release outside the cell [1]. The biogenesis of exosomes starts with the invagination of endosomal limiting membranes which leads to the formation of intraluminal vesicles (ILVs) contained within the endosome. This compartment, termed a multivesicular body (MVB), fuses with the plasma membrane, culminating in the extracellular release of ILVs as exosomes. The machineries involved in the release of

exosomes, their docking and fusion during both physiological and pathological processes are still being deciphered. However, there is no doubt that exosome biogenesis is a multistep process which requires the coordinated efforts of several protein networks in the cell. Among these known actors are: 1) Rab GTPases, proteins which control endosomal trafficking; 2) endosomal sorting complexes required for transport (ESCRT), multiple protein complexes that regulate ILV formation; 3) tetraspanins, transmembrane proteins that induce membrane curvatures enabling vesicle formation; and 4) lipid-modifying enzymes (i.e. sphingomyelinase), that generate ceramides involved in promoting vesicle formation [58].

It has been shown that tumor cells are able to package and secrete, through exosomes, proteins (receptors, transcription factors, enzymes, extracellular matrix proteins) as well as nucleic acids (DNA, mRNA, microRNA [miRNA], and other non-coding RNAs), metabolites and lipids [59]. This exosome cargo becomes even more relevant once these vesicles are in circulation and taken up by other cells. This cargo can be transferred to recipient cells (tumor cells, stromal cells, immune cells, etc.) and influences their phenotype and/or function [1]. Therefore, exosomes are essential mediators of cell-cell communication. Remarkably, in addition to local signaling within the primary tumor microenvironment, tumors also signal over long distances to sites of future metastases to promote formation of a hospitable, pre-metastatic niche (PMN) that will foster growth of disseminated tumor cells upon their arrival [17, 56, 57].

Tumor-secreted exosomes can promote angiogenesis and coagulation, modulate the immune system, and remodel surrounding parenchymal tissue, which together support tumor progression [1]. Clinically, circulating exosomes and microvesicles isolated from cancer patients have been associated with metastasis or relapse, and therefore could serve as important diagnostic and prognostic markers as well as therapeutic targets [59].

3.2 – Exosome-mediated biological functions

Through their cargo, exosomes mediate several biological functions that cooperate to promote tumor progression and metastasis. Tumor-derived exosomes can transfer

oncogenic molecules as cargo between tumor cells within the primary tumor or distant metastatic sites [60]. A large number of studies have now demonstrated that exosomal proteins varies between different cancer types and even between cancers with different metastatic potential but with a similar origin. These unique patterns of exosomal protein cargo seem to also influence the metastatic capabilities of their cells of origin since exosomes from more aggressive tumor cells are more efficient at promoting metastasis than exosomes derived from less metastatic cells [17]. Furthermore, this differential and selective packaging also occurs in cancer with specific metastatic tropism (organotropism). For instance, packaging of distinct integrins in exosomes from different cancer types has a role in determining the organs that take up tumor exosomes [56]

As tumors form and progress, they modify the stroma through soluble factors, exosomes, and direct cell-cell interaction. Therefore, tumor-derived exosomes exert also complex effects on neighboring stromal cells, such as endothelial cells and fibroblasts. Conversely, exosomes secreted by tumor stroma can also influence tumor progression [61]. Therefore, exosomes mediate bidirectional communication between tumor cells and their environment and are central effectors of a feedforward signaling loop that shapes the ever-evolving tumor microenvironment.

The properties of cancer exosomes in metastatic tumor progression as well as their presence in numerous fluids and tissues have made them a promising new source of biomarkers for cancer progression and as novel targets for future anticancer therapies.

3.3. – Regulation of metastasis by tumor exosomes

Tumor cell-derived EVs fuse with resident cells in both PMNs and tumors, transferring their cargo, including genetic material (DNA, mRNA and miRNA), metabolites (lipids and small metabolites) and protein. Pioneering studies demonstrated that platelet-derived EVs (particularly microparticles) induced angiogenesis and metastasis in lung and breast cancers [62, 63]; however, the relevance of EVs in PMN formation was not evaluated in these studies. Since then, EVs have been shown to contribute to the recruitment and transfer of material to other stromal cell types, including those populating PMNs [64, 65].

Tumor-derived exosomal miRNA and proteins reprogramme or educate target cells that take up exosomes towards a pro-metastatic and pro-inflammatory phenotype, creating

the PMN [17, 57]. Education of stromal cells depends on the cancer type and pre-metastatic organ analysed. In melanoma, the hepatocyte growth factor receptor, MET, which is secreted in B16-F10 melanoma-derived exosomes, reinforces the expression of tyrosine kinase with immunoglobulin (Ig) and epidermal growth factor (EGF) homology domains 2 (TIE2) and MET in blood-circulating BMDCs, and promotes pro-vasculogenic and pro-migratory properties in these cells. These re-educated BMDCs then exit the bone marrow and contribute to the formation of PMNs in lungs [17]. Importantly, exosomes secreted by B16-F10 melanoma cells promote vascular leakiness in lung PMNs, inducing a pro-inflammatory response by increasing the expression of cytokines and chemokines such as TNF, S100A8 and S100A9, which, in turn, recruit BMDCs to these PMNs [17]. However, the source of S100 proteins was not defined in this study. Breast and pancreatic cancer cell-secreted exosomes express integrins on their surface, which promotes their homing to PMNs [56]. Expression of the integrin α6β4 heterodimer on the surface of tumor-derived exosomes promotes their homing to lung PMNs, whereas αvβ5 targets them to liver PMNs. The homing of exosomes to these organs caused an increase in pro-inflammatory S100 family proteins in the PMN, generating a supportive microenvironment for subsequent metastasis [56].

Regarding liver PMNs, pancreatic tumor-derived exosomes expressing MIF promote TGFβ secretion in Kupffer cells, stimulating hepatic stellate cells to secrete fibronectin and promoting the recruitment of BMDCs [57].

Interestingly, genomic content (that is, miRNAs) is also packaged selectively within EVs and is involved in PMN formation [66, 67]

Recently, RNAs packaged within primary tumor-derived exosomes were found to be involved in the activation of TLR3-dependent signalling in lung epithelial cells, inducing chemokine secretion in the lung and promoting PMN formation by recruiting neutrophils [68]. These findings only encompass the beginning of our understanding on how tumor-derived EVs are involved in metastasis and opens the door for the pursuit of their roles in PMN BrM formation, which were remained completely unexplored at the starting time of this thesis.

Section 4

Background and Research Aims

Section 4 – Background and Research Aims

Despite increased research interest in the molecular mechanisms driving BrM, there have been few advances in the early diagnosis and therapeutic targeting of this disease. The role of tumor-derived exosomes, emerging players in the interaction between tumor cells and the host microenvironment, remains widely unexplored in the brain metastatic process. Hence, gaining insight into the mechanisms of BrM and the specific contribution of tumor-derived exosomes to this process may open new avenues of investigation with potential clinical applications. Due to the aforementioned functions of tumor exosomes in regulating cancer metastasis, we aimed to determine the role of tumor-derived exosomes in the remodeling of the brain microenvironment and their specific contribution to supporting metastatic colonization of the brain.

The main objectives of the work presented in this manuscript are the ensuing:

- Characterize the brain biodistribution of tumor exosomes and their interaction with brain cells **(Chapter III)**
- Evaluate if tumor exosome uptake by the brain microenvironment generates a pro-metastatic niche supportive of metastatic colonization **(Chapter IV)**
- Identify candidate exosomal molecule(s) with functions in brain metastasis and characterize their biological mechanisms of action **(Chapter V and VI)**
- Address the potential significance of candidate exosomal molecule(s) for brain metastasis in cancer patients **(Chapter VII)**

The findings documented for each of these objectives will be discussed further on **Chapter VIII**. We expect that our understanding of the role of tumor-derived exosomes in the reshaping of the brain microenvironment for successful metastatic colonization can provide significant advances to the brain metastasis research field. Furthermore, we contemplate that new brain metastasis targets may be identified from this study and potentially applied to the diagnostic and therapeutic management of brain metastasis in cancer patients.

CHAPTER II

Materials and methods

Cancer cell lines and cell culture. All cancer cell lines used in this study are of human breast or lung cancer origin. The breast cancer cell lines were provided as follows: brain-tropic 231BR cells by P. Steeg (NCI); brain-tropic MDA-MB-231-HM cells [69] by S. Wang (UC San Diego); MDA-MD-231 organotropic 831 (brain-tropic), 4175 (lung-tropic) and 1833 (bone-tropic) cells by J. Massagué (MSKCC); and lung-tropic 4173 cells by A. Minn (University of Pennsylvania). The brain metastatic derivative N2LA-BR of the lung cancer cell line N2LA (N2LA-JHH-VKR) was generated from a patient with metastatic lung cancer by V. Rajasekhar (MSKCC). The breast cancer cell line MDA-MB-231 (parental) was purchased from American Type Culture Collection (ATCC). Breast cancer cells were cultured in Dulbecco's Modified Eagle Medium (DMEM) and lung cancer cells in RPMI, both supplemented with 10% fetal bovine serum (FBS) (Gibco, Thermo Scientific), L-glutamine (1mM), and Penicillin/Streptomycin (100 IU/mL and 100 µg/mL). For exosome isolation from tissue culture supernatants, cells were cultured in exosome-depleted FBS. Depletion of endogenous serum exosomes was achieved by FBS ultracentrifugation at 100,000xg for 70 min. All cancer cells were maintained in a humidified incubator with 5% CO_2 at 37 ºC. All cell lines used were routinely tested for mycoplasma (Universal Mycoplasma Detection Kit, ATCC) and found to be negative.

Exosome purification, labelling, characterization and analysis. Exosomes from cell lines were purified by sequential ultracentrifugation as previously described [56]. Briefly, the fresh cell culture supernatant of a 3-day confluent culture was centrifuged at 500*x*g for 10 min, to remove any cells, and then at 12,000*x*g for 20 min, in order to clear away any cell debris or apoptotic bodies that might be present in the culture media. Exosomes were then collected from the latter supernatant by an ultracentrifugation step of 100,000*x*g for 70 min. Exosome collection was followed by a washing step through resuspension of the pellet in 1xPBS followed by centrifugation at 100,000*x*g for 70 min. For exosome imaging purposes, purified exosomes were fluorescently-labelled using the PKH67 (green) or PKH26 (red) lipophilic membrane dyes (Sigma), or the CellVue Maroon kit (far red) (Polysciences). Labelled exosomes were washed in 20 mL of 1xPBS and subjected to an additional round of ultracentrifugation at 100,000*x*g for 70 min. The final exosome

pellet was then resuspended in a low volume of 1xPBS (50-200 µL) and maintained at 4 ºC until subsequent use in any biological assays. All exosomes used in biological assays were purified from freshly cultured media, collected and maintained in sterile conditions, and kept on ice at all times when not in use. Exosome preparations for non-biological assays or *in vivo* education experiments, that required large amounts of exosomes, were aliquoted and frozen until use at -80 ºC. All centrifugation steps were performed at 10 ºC using the Beckman 45Ti or 70Ti rotor, depending on the starting cell culture supernatant volume. The protein concentration of each final exosome preparation was determined by BCA assay (Pierce, Thermo Scientific). Exosome size distribution and particle number were analyzed using the DS500 nanoparticle characterization system (NanoSight, Malvern Instruments), equipped with a blue laser (405 nm), as previously described [56]. Exosome preparations were verified by negative stain transmission electron microscopy (TEM) analysis, as previously described [70].

Brain slice assay. To study the biological effects of tumor-derived exosomes on the brain microenvironment in the context of metastasis, organotypic brain slice cultures were prepared by adapting a previously described protocol for the generation of mouse brain cortical slices to study neuron development [71]. In brief, brains from 6 to 8 week-old athymic NCr nude female mice (Taconic) or outbred *Foxn1*$^{-/-}$ mice (Jackson Laboratories, cat # 007850), were dissected in complete HBSS, supplemented with HEPES (pH 7.4, 2.5mM), D-glucose (30mM), $CaCl_2$ (1mM), $MgSO_4$ (1mM), and $NaHCO_3$ (4mM), after cardiac perfusion of the whole mouse with 10 mL of cold sterile PBS. Freshly dissected brains were blotted for excess of dissection media and embedded in microwave-preheated 4% low-melting agarose (Lonza) in complete HBSS. The temperature of the preheated agarose solution was monitored with a thermometer and embedding is carried out when the temperature cools down to 37 ºC and the solution presents itself transparent and homogeneous in viscosity. Once the agarose had solidified, the embedded brains were cut into 250 µm coronal slices (consistently from within the region defined by bregma -2mm to +2mm) using a VT 12000s vibratome (Leica). On average, approximately 12-14 complete coronal slices were obtained per mouse brain. Whole brain coronal slices were

dissected across the midline that separates both brain hemispheres, generating two symmetric halves. Brain slices displaying loss of tissue integrity or signs of tissue damage due to issues in tissue sectioning and/or handling were not placed in culture. Brain slices generated from different positions across the brain anterior-posterior axis were distributed equally across conditions so that each experimental group was comprised by an identical group of slices representative of the brain region sectioned, ensuring a similar composition of different brain regions. With the aid of a wide-opening plastic transfer pipette, groups of three individual half-brain slices were placed flat on top of 0.4 µm pore polycarbonate (PC) membrane cell culture inserts (#Z353086 Sigma or #140660 Thermo Scientific) in 6-well plate format, with brain slice media (DMEM supplemented with 25% complete HBSS, 5% FBS, L-glutamine (1mM), Penicillin/Streptomycin (100 IU/mL and 100 µg/mL), and Normocin (Invivogen, 50 µg/mL)) in the bottom well. In order to establish a defined, constant and restrained region for exosome treatment and cancer cell administration to brain slices, a sterilized transparent PC ring (Small Parts), with a 3 mm inner diameter, was placed on top of each slice using forceps. Rings were positioned onto slices in a central position so that the inner-limit of the ring was always within the boundaries of the brain slice, ensuring the containment of exosomes and cancer cells administered to a well-defined region of interest. Even though any brain slice presenting loss of tissue integrity or damage during the course of the *ex vivo* culture portion of the experiment was readily discarded, the long processing and immunostaining procedure that starts after tissue fixation of the brain slices, involving numerous rounds of “free-floating” washes in buffer containing detergent, can also affect tissue integrity and quality. Although we took precaution to minimize tissue damage during processing after fixation, invariably some tissue disruption happened and unless presenting severely compromised structure that prohibits analysis, we strived to evaluate all available brain slices as long as they presented inner-ring brain slice regions with intact architecture and sufficient area for analysis.

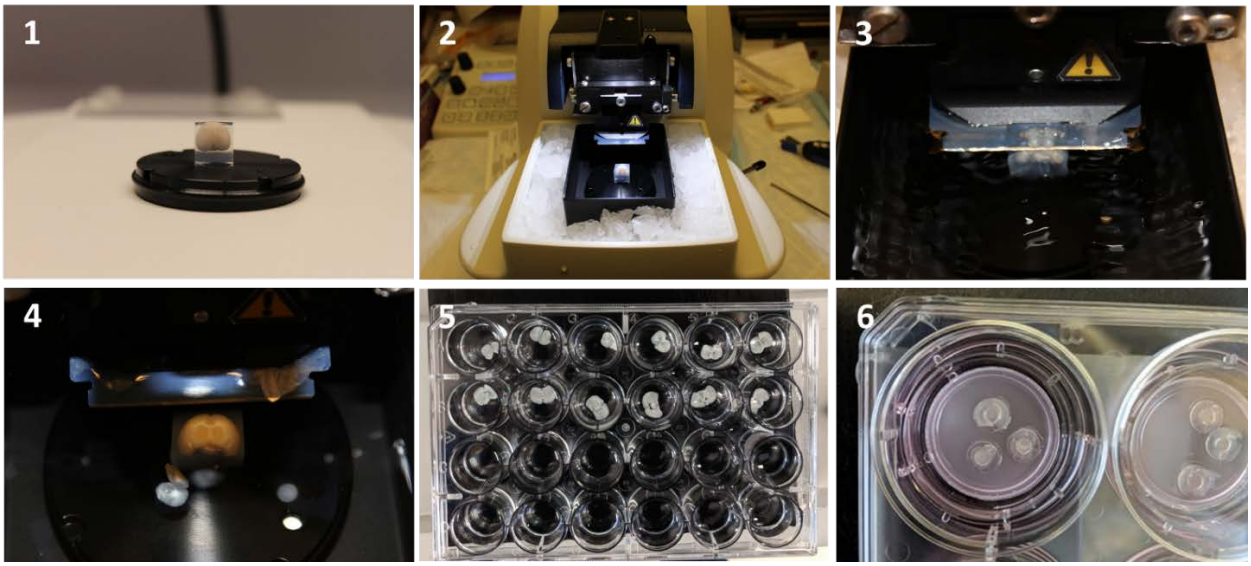

Scheme of Brain slice generation and culture. 1) Mounting of agarose-embedded brain for vibratome sectioning; 2) Brain specimen and vibratome setup; 3) Generation of the first brain slice from the defined region of interest (bregma -2mm to +2mm); 4) Top view of vibratome sectioning; 5) Representative series of brain slices generated from one mouse brain (top left to bottom right, most anterior to most posterior brain sections); 6) Culture of brain slices. Note the distribution of brain slice halves from different brain regions in individual culture inserts (6) and how all brain slices selected for culture show no signs of loss of integrity (5 and 6).

For exosome treatment and cancer cell administration, a volume of 3 µL containing 1xPBS-resuspended exosomes (5 µg); 7,500 231 BrT1 cancer cells; or 20,000 231 parental cancer cells, were added to the inner region of the rings. For brain colonization studies, brain slices were pre-treated with PBS or exosomes for two consecutive days prior to the addition of the cancer cells. Exosome treatment is administered before adding cancer cells in order to ensure that potentially pro-tumoral changes triggered by exosome treatment were limited to and derived from changes in brain resident cells and its microenvironment. Cancer cells were added 24 hours after the last treatment and incubated for a period of 72 hours. Brain slices were maintained in a humidified incubator with 5% CO_2 at 37 ºC for a maximum of 5 days, changing the media every two days. Dead cells and debris were washed off the top of the brain slices with three 1xPBS washes on

a platform rocker before brain slice fixation in 2% paraformaldehyde (PFA) for 2 hours at 4 ºC. Tissue processing and immunofluorescence followed in order to allow analysis of tumor cell colonization, tissue invasion, and interaction with vessels in the brain microenvironment. Tumor cell colonization was measured by quantifying the average number of cancer cells growing on top of brain slices. Tumor cell invasion was measured by quantifying the average number of invading cancer cells (cancer cells observed below the first layer of brain cells on the top of the brain slice) on transversal sections of brain slices. Tumor cell interaction with vessels in the brain microenvironment was measured by quantifying the average number of cancer cells growing on top of brain slices in association with brain vessels displaying spindle-like morphology. Images of brain slice representative fields of view were taken at 10X objective amplification and cancer cells were counted manually with multi-point tool in ImageJ software (version 1.52a). For characterization of exosome adhesion and uptake studies, co-localization of exosome fluorescent signal in brain endothelial cells and other brain cell types was evaluated after one treatment with fluorescently-labelled exosomes (5 µg). Exosomes were administered to the top of the slice and incubated for 12h for adhesion studies, or 24 hours for uptake studies, before undergoing the washing and fixation steps, proceeding to tissue processing and analysis of exosome-positive cells by immunofluorescence analysis.

Proteomics methods and data analysis. Mass spectrometry of exosomes was performed at the Rockefeller University Proteomics Resource Center as previously described [56]. Briefly, exosome-enriched samples were denatured, reduced, and alkylated followed by proteolytic digestion with LysC (Wako Chemicals) and trypsin (Promega). Approximately 1µg of each desalted [72] sample was analyzed by nano-LC-MS/MS system (Ultimate 3000 coupled to a QExactive Plus, Thermo Scientific). Peptides were separated using a 12 cm x 75µm C18 column (3 µm particles, Nikkyo Technos Co., Ltd. Japan) at a flow rate of 200 nL/min, with a 6-56% gradient over 130 minutes (buffer A 0.1% formic acid, buffer B 0.1% formic acid in 80% acetonitrile). Data were quantified and searched against Human Uniprot database (July 2014) using MaxQuant (version 1.5.0.9) [73]. Oxidation of methionine and protein N-terminal acetylation were allowed as

variable modifications, cysteine carbamidomethyl was set as a fixed modification and two missed cleavages were allowed, and the “match between runs” option was enabled. Perseus software (version 1.5.0.9) was used for bioinformatics and statistical analysis. Protein abundances were expressed as LFQ (label free quantitation) values. Only proteins quantified in at least two out of three replicates in at least one group were retained, and missing values were imputed. A multiple sample ANOVA test was performed and corrected for multiple hypotheses testing using a permutation-based FDR threshold of 0.05. GENE-E software was used for heatmap generation and data display.

Western blot analysis. Exosomes and cells were lysed on ice with RIPA buffer supplemented with a protease inhibitor cocktail (Roche). Lysates were cleared by centrifugation at 12,000*x*g for 20 min at 4 ºC using a bench top centrifuge and the supernatant fraction was used for western blot. Protein concentration was determined by BCA assay and a standardized amount of protein for all samples (5-15 µg) was loaded on a Novex 4-12% Bis-Tris Plus Gel (Life Technologies) and ran alongside a pre-stained broad range molecular weight protein ladder (Abcam; ab116028). After gel electrophoresis, protein samples were transferred onto a PVDF membrane (BioRad) for 2 hours at 4 ºC. Ponceau red staining was performed for each membrane to ensure proper transfer, followed by 1 hour blocking incubation in PBS solution with 0.1% Tween-20 (Santa Cruz Biotechnology) (PBS-Tw) with 3% BSA at room temperature and incubation with primary antibody in blocking solution shaking overnight at 4 ºC. Antibodies against the following proteins were used for western blot analysis: CEMIP (1:5,000, Novus biologicals; 4575.00.02), HSP70 (1:1,000, System Biosciences; EXOAB-Hsp70A-1), Syntenin-1 (1:200, Santa Cruz biotechnology; sc-100336), CD81 (1:1000, Santa Cruz biotechnology; sc-166029), and ACTB (1:1,000, Cell Signaling; 4967L [unconjugated], or 1:20,000, Sigma; A3854 [peroxidase-conjugated]). Anti-Mouse/Rabbit Whole IgG Affinity-Purified antibodies conjugated with horseradish peroxidase (HRP) (1:5,000, Jackson ImmunoResearch Laboratories) were used as secondary antibodies. To remove excess antibody, membranes were subjected to three PBS-Tw washes after each antibody incubation. Pierce ECL Western Blotting Substrate (Thermo Scientific) was used as a

substrate for HRP. For CEMIP relative quantification, the ratio between the CEMIP band intensity and respective ACTB band for each sample was measured, using ImageJ software. For subcellular analysis of CEMIP in brain metastatic cancer cells, protein from different subcellular compartments was extracted from cells using the Compartment Protein Extraction kit (Millipore), following the manufacturer's protocol.

OptiPrep™ density gradient (ODG) exosome isolation. To prepare the discontinuous iodixanol gradient, 40% (w/v), 20% (w/v), 10% (w/v) and 5% (w/v) solutions of iodixanol were made by diluting a stock solution of OptiPrep™ (60% (w/v) aqueous iodixanol from Sigma) with 0.25 M sucrose/10 mM Tris, pH 7.5. The gradient was formed by adding 3 mL of 40% iodixanol solution to a 14 x 95 mm ultra-clear tube (Beckman Coulter), followed by gently layering 3 mL each of 20% and 3mL of 10% solutions, and 2.5 mL of 5% solution. A pellet of exosomes, isolated as described above, was resuspended in 500uL of 1xPBS and overlaid onto the top of the gradient [74]. A portion of the exosome pellet sample was saved as input. The gradient was centrifuged at 100,000*x*g for 16 h at 10 °C using a SW-40 Ti Rotor. Twelve individual 1 mL gradient fractions were collected manually from top to bottom. Fractions were diluted with 2 mL PBS and centrifuged at 100,000g for 3 h at 10 ºC followed by washing with 1 mL 1xPBS, and resuspended in 30uL of RIPA buffer. Fractions (5µg of protein) were monitored for the expression of exosomal markers CD81, Syntenin-1, and HSP70 and for the CEMIP protein by western blot analysis. The density of each fraction was determined by measuring the weight of each fraction (µg/mL).

Mouse studies. All mouse work was performed in accordance with institutional, IACUC and AAALAS guidelines, as described in our Weill Cornell Medicine animal protocol 0709-666A. All animals were monitored for signs of stress, illness or abnormal tissue growth, and euthanized if deterioration of the animal's health was observed. Mice that died before the predetermined end of the experiment were excluded from the analysis. All exosome, brain slice and brain metastasis *in vivo* experiments used 6 to 8 week-old athymic NCr nude female mice (Taconic) or outbred *Foxn1*$^{-/-}$ mice (Jackson Laboratories, cat #

007850). For characterization of *in vivo* distribution of exosomes in lung, liver and bone, 10 µg of fluorescently-labelled exosomes in a 100 µL volume of 1xPBS were injected via the retro-orbital venous sinus, the tail vein or intracardially. Exosome distribution patterns were consistent regardless of the route of injection. For brain distribution, exosomes were injected through intracardiac injection. For characterization of *in vivo* brain biodistribution of exosomes, 10 µg of fluorescently-labelled exosomes in a 100 µL volume of 1xPBS were administered *via* intracardiac injection. *In vivo* organ distribution of exosomes was evaluated in tissue sections of brains and other organs collected 24 hours post-injection. For exosome-tracking purposes, purified exosomes were fluorescently labelled using PKH67 (green) or PKH26 (red) membrane dye (Sigma-Aldrich). Labelled exosomes were washed in 20 ml of PBS, collected by ultracentrifugation and resuspended in PBS. To measure exosome uptake by specific cell types, labelled exosomes were injected 24 h before tissue collection and tissues were analysed for exosome positive cells by immunofluorescence. Mice were euthanized, perfused with 1xPBS and processed for sectioning and subsequent immunofluorescence staining. Pictures of exosome-positive cells in representative organs sections and whole-brain sagittal sections were taken with an E800 Eclipse microscope (Nikon) at 400x magnification. To evaluate exosome-induced vascular leakiness, 2 mg of Rhodamine or Texas-Red-lysine fixable dextran 70,000 MW (Invitrogen) was administered *via* retro-orbital injection 23 hours after exosome treatment with 10 µg of PKH67 labelled exosomes in a 100 µL volume of 1xPBS that was administered *via* intracardiac injection. One hour post-dextran injection mice were perfused with 1xPBS and euthanized. Tissues were collected and processed for sectioning. Pictures were taken with an E800 Eclipse microscope (Nikon) at 400x magnification. For experimental brain metastasis studies using the 231 BrT1 breast cancer model, $1x10^4$ fluorescently-labelled and/or luciferase positive cancer cells resuspended in 100 µL of 1xPBS were injected by intracardiac injection in the left ventricle of the heart. For experimental brain metastatic tumor *in situ* growth studies using the 231 BrT1 breast cancer model, $1x10^5$ fluorescently-labelled and luciferase positive cancer cells resuspended in 2 µL of 1xPBS were injected by intra-cranial injection in the right brain hemisphere with a low-volume Hamilton syringe and the aid of a stereotactic apparatus. Cancer cell suspension was injected at a rate of 0.2 µL/min, at 2.5 mm depth

from the surface of the brain and coordinates 0.1 mm posterior and 2.0 mm lateral to the bregma. For primary tumor *in situ* growth studies using the 231 BrT1 breast cancer model, $1x10^6$ cells in 50 µL of growth factor reduced Matrigel (Corning), were injected in the 4th mammary fat pad of mice. For experimental brain metastasis education studies using the 231 BrT1 breast cancer model, 10 µg of exosomes were administered to mice every other day intravenously by retro-orbital injection for three weeks, mimicking the continuous and systemic release of exosomes by growing primary tumors. One day after the last treatment of the exosome education, mice were injected with $1x10^4$ 231 BrT1 fluorescently-labelled and luciferase positive cancer cells resuspended in 100 µL of 1xPBS, by intracardiac injection in the left ventricle of the heart. For *in vivo* metastasis imaging of experimental brain metastasis ability and metastatic tumor *in situ* growth capacity, as well as for brain metastasis exosome education studies, mice were imaged by IVIS SpectrumCT bioluminescence imaging system (PerkinElmer) once a week for the duration of the experiment. Mice were imaged in supine position except for evaluation of brain metastatic tumor *in situ* growth experiments, in which mice were imaged in prone position given the dorsal location of tumor cells injected intracranially. *In vivo* cranial bioluminescence intensity was analyzed by quantification of total cranial photon flux (p/s) and was performed using Living Image software (Caliper Life Sciences). Negative photon flux values were considered to be equal to zero. At the described experimental endpoint, mice were euthanized, perfused with PBS and brains were processed for sectioning and subsequent staining (see Methods – “Tissue processing and immunostaining”). The presence of brain metastases was confirmed by immunofluorescence analysis of representative sagittal brain sections with antibodies against cancer cell-expressed green fluorescent protein (GFP) (1:200, Aves Labs; GFP-1020) and/or haematoxylin/eosin (H&E) staining. Brain metastatic burden was further characterized by histological evaluation and quantification of the number of lesions and total brain metastatic lesion area at 260x magnification, scoring two whole brain sagittal sections representative of different brain areas per mouse, stained with anti-GFP and DAPI or H&E. Tumor cell clusters in the brain composed of 10 or more cancer cells were considered as metastatic foci or lesions. Pictures were taken with an EVOS FL Cell Imaging System microscope (Thermo Scientific) and images were analyzed with ImageJ software. For analysis of

tumor vasculature caliber in experimental brain metastasis studies, the diameter of vessels within metastatic foci and in nearby normal brain regions was analyzed in two whole brain sagittal sections representative of different brain areas per individual and measured with ImageJ software. Briefly, the diameter of each vessel was calculated as the average of three individual measurements along the length of the vessel at 260x magnification, scoring up to five different tumor/normal vessels per individual. Vessel diameter was evaluated in metastatic foci within the same size range across different experimental conditions. For primary tumor *in situ* growth studies tumor size was measured manually with a vernier caliper (Scienceware) once a week throughout the duration of the experiment. Tumor volume was calculated using the formula for an ellipsoid, $V = \pi/6 \ (L \times W \times H)$, as previously described [75]. No statistical method was used to pre-determine sample size and no method of randomization was used to allocate animals to experimental groups. Living Image (version 4.5, Caliper Life Sciences, Perkin Elmer) was used for acquisition and analysis of IVIS data.

Tissue processing and immunostaining. For histological analysis of exosome and brain metastasis *in vivo* experiments, tissues were freshly harvested from mice and dissected in cold PBS. Dissected brains were directly embedded in Tissue-tek O.C.T. compound (Electron Microscopy Sciences) and frozen in a dry ice/ ethanol bath. Dissected lungs and other organs were fixed in 4% PFA overnight at 4 ºC, incubated in a 30% sucrose solution for 12 hours at 4 ºC, and then embedded and frozen. For immunofluorescence, tissue blocks were cryosectioned in 10 µm-thick sections onto pre-cooled Superfrost plus slides (VWR) using a CM3050 S cryostat (Leica). Tissue sections were fixed in 4% PFA for 5 min at room temperature (RT), air-dried for 10 min, permeabilized in 1xPBS solution with 0.25% Triton X-100 (Sigma) (PBS-T) for 15 min, blocked in PBS-T with 3% bovine serum albumin (BSA) and 5% normal goat serum (NGS) for 1 hour at RT and incubated overnight in a wet chamber at 4 ºC in the latter solution with antibodies against the following proteins: GFP, mCherry, Collagen IV (1:500, abcam; ab6586), PECAM-1/CD31 (1:50, Santa Cruz Biotechnology; sc-18916), Glut-1 (1:100, abcam; ab40084), Iba-1 (1:200, Wako; 019-19741), GFAP (1:500, abcam; ab7260),

PDGFRb (1:100, R&D systems; AF1042), NeuN (1:500, Millipore; ABN90), Ki-67 (1:500, abcam; ab66155), and KIAA1199/CEMIP (1:100, abcam; ab76849). Unbound antibody was washed off with three PBS-T washes before incubating in blocking solution with secondary antibodies conjugated to AMCA, Alexa Fluor 488, 568 and 647 (1:500, Thermo Scientific, Life technologies - A11001, A11008, A11036, A11039, A11077, A21244, A21247, A27040; and Vector laboratories - CI-2000) for 2 hours at RT. Unbound secondary antibody was washed off with five PBS-T washes before incubating with DAPI (1:10000, Sigma; D9542), for 15 minutes. Slides were then washed twice in 1xPBS and mounted with Prolong Diamond antifade reagent (Invitrogen). For histological analysis of brain metastasis with H&E stain, dissected brains were fixed in 4% PFA overnight at 4 ºC, dehydrated in a sequence of ethanol series (50%, 70%, 85%, 95%, 100%) and embedded in paraffin. Tissue blocks were sectioned in 10 µm-thick sections, which were rehydrated, stained and then dehydrated again before mounting with VectaMount medium (Vector). For brain slice experiments, the PC ring was removed from the freshly fixed slices, which were then washed in 1xPBS, permeabilized with PBS-T, and prepared using the same protocol described for tissue sections, with the distinction that immunofluorescence was carried out in free-floating conditions. In the particular case of analysis of brain slice tissue invasion, fixed slices were washed in PBS, had the outer-ring regions dissected out and then were directly embedded in Tissue-tek O.C.T. compound and frozen. These tissue blocks were cryosectioned in 10 µm-thick sections perpendicular to the plane of the embedded inner-ring tissue slice and followed the same immunofluorescence protocol described for tissue sections.

Generation of CEMIP knockout and overexpression cell lines. Knockout of CEMIP in 231 BrT1 cells was achieved by transfection of cells with the Cas9-expressing PX458-DsRed mammalian backbone vector with cloned gRNAs targeting human CEMIP (gRNA KO1, CGTACCAACGGGCCCCTCCG; and gRNA KO2, GCGGCTTGGACCATAGCGGA). Vectors for CEMIP knockout were prepared by MSKCC Gene Editing and Screening Core Facility and sgRNAs were chosen based on highest cutting specificity and fewest off-target effects using Guidescan (MSKCC). Oligos

(Thermo Scientific) were annealed and ligated into BbsI-cut PX458 vector. Ligated product was transformed into Stbl3 Competent cells (Thermo Scientific) and colonies were Sanger sequenced to identify positive clones before proceeding with mammalian cell transfection. Cancer cells were then transfected with the prepared vectors for CEMIP knockout using Lipofectamine LTX/PLUS (Invitrogen, 15338100) according to the manufacturer's instructions. Approximately 48h after cancer cell transfection, transiently $DsRed^+$ expressing cells were single cell-sorted into 96-well plate format and grown as clones. CEMIP targeting and depletion in selected clones displaying unaltered proliferative ability *in vitro* were evaluated by analysis of exosomal protein expression through western blot analysis and validation of CEMIP CRISPR editing was further supported by identification of complex indels in DNA isolated from selected clones through Sanger sequencing analysis. Overexpression of CEMIP in 231 parental cells was achieved by lentivirus-mediated stable expression of CEMIP. For lentiviral expression, pLentiCMV-CEMIP-blast was generated by PCR amplification of full length human CEMIP from pcDNA3.2V5DEST_wtKIAA1199 (a gift from Dr. G. Marra, Institute of Molecular Cancer Research, University of Zurich) using the following primers: forward (with 5' PspXI restriction site) 5'-ACGTACTCGAGCACCATGGGAGCTGCTGGGAGGCA-3' and reverse (with 3' NheI restriction site) 5'-ACGTGCTAGCCTACAACTTCTTCTTCTTCAC-3'. The CEMIP amplicon was then subcloned into the SalI/XbaI restriction sites of pLentiCMV-blast (provided by E. Campeau, University of Massachusetts Medical School, Worcester, MA; Addgene #17486) [76]. As a control, 231 parental cells were infected with pLentiCMV-blast empty-vector lentivirus. Lentivirus was produced using a third-generation system with four plasmids [77] by co-transfecting a 10 cm dish of HEK-293T cells using Lipofectamine LTX/PLUS (Life Technologies) with 12 µg of expression cDNA and packaging and envelope vectors (2 µg of pRSV-REV, 2 µg of pMD2Lg/pRRE, and 4 µg of pMD2.g). Lentiviral packaging and envelope plasmids pRSV-REV, pMD2Lg/pRRE, and pMD2.g were gifts from D. Trono (École Polytechnique Fédérale de Lausanne, Lausanne, Switzerland; Addgene #12253, #12251, and #12259). Lentiviral supernatants were collected 48 hours after transfection, filtered through a 0.45 µm filter, and stored at –80°C. For infection, $1x10^5$ cells were seeded into 6-well plate format one day before

infection and incubated overnight with virus-containing supernatants supplemented with 8 µg/ml polybrene (Sigma-Aldrich). Stable cell lines were obtained by selecting with 10 µg/ml blasticidin (Invitrogen), and overexpression was confirmed by analysis of exosomal protein expression through western blot analysis. After stably transduced cells were obtained, cells were cultured for exosome collection in the absence of selection agents. For *in vivo* bioluminescent tracking of cancer cells, we generated 231 BrT1 luciferase-expressing cells by infecting them with lentiviral particles expressing the firefly luciferase gene under CMV promoter and GFP-Puromycin selection markers (Gentarget), according to the manufacturer's instructions and confirmed *in vivo* bioluminescent signal after puromycin (Invivogen) selection *in vitro* for two weeks at the concentration of 2 µg/ml.

Proliferation and invasion *in vitro* assays. For proliferation assays, $2x10^6$ 231 BrT1 cells from each experimental condition (WT, CEMIP KO1 and CEMIP KO2) were plated in T175 flasks and cell number was quantified 72h-post seeding. For invasion assays, cells were serum-starved for 24 hours previous to plating $2.5x10^4$ cells in 24-well plate format with transwell inserts (8-µm pore size, Corning) previously coated with 50 µL of growth factor reduced Matrigel (Corning). Cell suspensions were added into inserts containing media with 1% FBS on the top and complete media with 10% FBS in the bottom chamber and were incubated at 37 ºC for 48 hours. Cells that remained in the upper part of the transwell insert were removed with cotton swabs and inserts were fixed with 1% PFA overnight at 4 ºC, followed by two 1xPBS washes and mounting with Prolong Gold antifade reagent with DAPI (Invitrogen) for cell nuclei visualization and counting. Pictures were taken with an EVOS FL Cell Imaging System microscope (Thermo Scientific).

Brain endothelial cell isolation, culture and assays. Brain endothelial cells were isolated from C57BL/6J mouse brains harvested from young adults and processed to a single cell suspension with a collagenase/dispase digestion cocktail as described previously [78]. Single cell suspensions were plated on fibronectin-coated plates (Sigma, 1 mg/mL in 1xPBS) in mEC media as described previously [78]. In order to select for brain

endothelial cells, puromycin (Invivogen) was added to the media up to the first cell culture passage at a concentration of 4 µg/ml. Cells were infected with E4ORF1-carrying lentiviral particles 96 hours after isolation [79, 80]. E4ORF1 expression enables robust expansion of endothelial cells, improving their survival in low serum and serum-free conditions while maintaining their angiocrine repertoire. Accutase was used as a cell detachment solution and cells were expanded for experiments in 6-well plate format (1.5 mL of media volume per well) after endothelial purity was confirmed by confocal microscopy and flow cytometry analysis of VE-Cadherin and CD31 marker expression and absence of CD45 expression. Cells were sub-cultured in Advanced DMEM/F12 supplemented with 20% exosome-depleted heat-inactivated FBS, 1% Antibiotic-Antimycotic 100X-solution (Invitrogen), 1% Glutamax 100x-solution (Life Technologies), 1% Non-essential Amino Acids (Life Technologies), 1% CD Lipid Concentrate (Life Technologies), HEPES (20mM), Heparin (100 µg/mL), Endothelial cell mitogen (Alfa Aesar, 50 µg/mL), SB431542 (R&D systems, 5 µM). For *in vitro* treatment with exosomes brain endothelial cells were grown up to 80% confluence and switched to starvation media (5% FBS) 6 hours before exosomal treatment start. Brain endothelial cells were maintained in a humidified incubator under hypoxic conditions (5% O_2) and 5% CO_2 at 37 ºC. The Cultrex In Vitro Angiogenesis Assay tube formation kit (Trevigen) was used for endothelial tube formation assay according to the manufacturer's instructions. Briefly, $1x10^4$ calcein AM-labelled brain endothelial cells, pre-treated for 24 hours with PBS or 10 µg of exosomal protein per mL of cell culture media (total volume of 1.5mL per 6-well plate well), were seeded in µ-Slide Angiogenesis chambers (Ibidi) and allowed to form vascular networks for 4 to 6 hours. Pictures were taken with an EVOS FL Cell Imaging System microscope (Thermo Scientific) at 260x magnification and images were analyzed with ImageJ's tool "Angiogenesis Analyzer" (by Gilles Carpentier) according to the instructions provided by the developer. The "Angiogenesis Analyzer" allows an automated and quantitative evaluation of vessel-like cellular network organization and therefore extraction of characteristic information from the pseudo capillary network formed and improved interpretation of the assay's results. Quantitative analysis of the number of junction elements (correspond to nodes or groups of fusing nodes – pixels with 3 neighbors), number and length of branches (elements of a ramification delimited by a junction and

one extremity) or isolated segments (binary lines that are not branched or connected to other vascular structures) allowed overall assessment of topology and complexity of the vascular meshed network formed. Basic topology of the vascular tree is emphasized by the highlight of master segments in yellow (tree segments delimited by two junctions in which none is exclusively implicated with one branch) and the tree's master junctions in red (tree junctions linking at least three master segments).

FACS analysis. Brain slices were pre-treated with PBS or green fluorescently-labelled exosomes (5 µg/slice) for two consecutive days, then had their outer-ring areas dissected out and the PC ring removed. Inner-ring brain slice tissue was transferred to a 6-well plate with cold PBS and washed three times before digestion with Dispase/Collagenase digestion mix (Roche; Dispase II at 1 U/mL and Collagenase A at 2.5mg/mL final concentration) for 15 minutes at 37 ºC on agitation (70 RPM). Full dissociation of the tissue and single-cell suspension was obtained by pipetting up and down gently. The cell suspension was filtered through a 100µm cell strainer. Cells were washed with MACS buffer (PBS Ca^{2+}/Mg^{2+}-free, 1% BSA, 2mM EDTA) and collected by centrifugation at 300*x*g for 5 min at 4 ºC. Single-cell suspensions were incubated with Myelin Removal Beads (Miltenyi) according to the manufacturer's instructions. Myelin-free cell suspensions were resuspended in MACS buffer and incubated with conjugated antibodies against the following cell markers: CD45 (EBioscience, 56-0451-82; 1:100); CD31 (BD Biosciences, 561073; 1:40); CD11b (BD Bioscience, 550993; 1:200); and CD49d (Biolegend, 103618; 1:100). Brain endothelial cells were defined by $CD45^-$ $CD31^+$ marker expression and microglial cells by $CD45^+$ $CD11b^{low}$ $CD49d^{low}$ [81] marker expression. After incubation in the dark for 30 min at 4 ºC cell suspensions were washed with MACS buffer, filtered through a 40-µm cell strainer and resuspended in a DAPI solution. Unstained and single-stained cell suspensions were prepared in parallel and used for cell sorter set-up. $DAPI^+$ dead cells were excluded. Sorting was performed on a FACS Aria (Becton Dickinson) and endothelial cells ($DAPI^-$ $CD45^-$ $CD31^+$) and microglia cells ($DAPI^-$ $CD45^+$ $CD11b^{low}$ $CD49d^{low}$) that had uptaken PKH67 green fluorescently-labelled exosomes were sorted directly into RLT buffer (Qiagen) supplemented with 2-

Mercaptoethanol, vortexed, and subsequently frozen on dry ice. Becton Dickinson Diva Software was used for flow cytometry cell sorting and data acquisition and TreeStar FlowJo 10.5.3 was used for flow cytometry data analysis.

RNA preparation, sequencing and data analysis. RNA was extracted from brain slice FACS-sorted exosome positive endothelial or microglia cells using the RNeasy Micro kit following the manufacturer's protocol (QIAGEN). RNA was quantified using Qubit 2.0 Fluorometer (Life Technologies, Carlsbad, CA, USA) and RNA integrity was checked with TapeStation (Agilent Technologies, Palo Alto, CA, USA). RNA library preparations, sequencing reactions, and initial bioinformatics analysis were conducted at GENEWIZ, LLC. (South Plainfield, NJ, USA). SMART-Seq v4 Ultra Low Input Kit for Sequencing was used for full-length cDNA synthesis and amplification (Clontech, Mountain View, CA), and the Illumina Nextera XT library was used for sequencing library preparation. Briefly, cDNA was fragmented and an adaptor was added using Transposase, followed by limited-cycle PCR to enrich and add index to the cDNA fragments. The final library was assessed with Qubit 2.0 Fluorometer and Agilent TapeStation. The sequencing libraries were multiplexed and clustered on one lane of a flow cell. After clustering, the flow cells were loaded on the Illumina HiSeq instrument according to manufacturer's instructions. The samples were sequenced using a 2x150 Paired End (PE) configuration. Image analysis and base calling were conducted using the HiSeq Control Software (HCS) on the HiSeq instrument. Raw sequence data (.bcl files) generated from Illumina HiSeq were converted into fastq files and de-multiplexed using the Illumina bcl2fastq v. 2.17 program. One mismatch was allowed for index sequence identification. After demultiplexing, sequence data was checked for overall quality and yield. RNASeq fastq files were analyzed with FastQC v0.11.7 to assess sequence base quality, per-base sequence content, GC content, N content, and the sequence length distribution. Reads were subsequently trimmed using Trimmomatic [82] v0.38, to remove Illumina adapter content, low quality leading and trailing bases with score ≤ 3, all bases after the sliding window average ≤ 15, and all edited reads ≤ 36 bp. Reads were aligned to *Mus musculus* annotation GRCm38.p6 using Salmon [83] v0.10.0. Default parameters were used for building the

mouse index and for alignment of transcripts. DESeq2 [84] v1.18.1 was used to assess differential gene expression using the likelihood ratio test, with the model [~ replicate + condition] analyzed against the reduced model [~ replicate]. Variance Stabilized Transformed gene counts were used to identify and remove outliers, using both Principal Component Analysis and sample clustering (using the euclidean distance metric and the complete clustering method). Two samples - WT replicate C and KO2 replicate A – were identified as outliers and removed from further analysis. To identify significant differences between treatments, a post-hoc analysis of genes differentially expressed according to LRT analysis was performed. DESeq2 was used to perform the binomial Wald test for contrasts between PBS, WT, KO1 and KO2. The focal gene set of interest was identified as those genes for which: a) the likelihood ratio test was significant ($p \leq 0.05$); b) there were significant expression differences between WT and PBS ($p \leq 0.05$); c) WT expression was significantly different from both KO1 and KO2 ($p \leq 0.05$ in each contrast); and d) expression was concordantly up- or down- regulated in KO1 and KO2 relative to WT. Log2(Fold change) values and p values are reported according to the Wald tests. Gene names were mapped to Entrez gene identifiers using Ensembl Biomart [85], mouse version GRCm38.p6. All scripts and output of the differential analysis are available at doi: 10.5281/zenodo.2574121. The R Script used for differential expression analysis can be found in the Supplementary file differential-expression-analysis.R. The Python script used for subsequent post-hoc analysis can be found in the Jupyter notebooks endothelial_expression_analysis.ipynb and microglial_expression_analysis.ipynb. Ingenuity Pathway Analysis (IPA, Qiagen, version 01-13) was used for molecular pathway analysis of gene expression data.

Human studies. Tissue microarrays of tumor samples (TMAs) from both primary and metastatic lesions were generated from formalin-fixed, paraffin-embedded archival samples approved for research use through the Institutional Review Board at Weill Cornell Medicine. Tissue microarray-based studies and fresh tissue studies were conducted in accordance with Weill Cornell Medicine IRB approved protocols (IRB Protocol#1312014589 and 0604008488) and individuals provided informed consent for

blood and tissue donation on these approved institutional protocols. For the tissue microarray studies, samples from 317 distinct tumor resections (213 primary tumors and 104 metastatic tumors) over 278 unique patients were used. At the time of their surgery, patients ranged in age from 28 - 95 years. 100% of breast carcinoma samples and 45% of lung carcinoma samples were derived from female patients. All patients used for this study had been diagnosed with invasive breast carcinoma (35% of samples) or non-small cell carcinoma of the lung (65% of samples). Within the lung carcinoma cohort, 72% of patients were diagnosed with adenocarcinoma, 15% with squamous cell carcinoma, and the remainder with non-small cell carcinoma. Paraffin blocks were cored in representative areas of tumor and H&E stained. Microarrays were reviewed for the presence of tumor. Immunohistochemistry staining was performed on a Leica Bond system using the standard protocol F. The array was pre-treated using heat-mediated antigen retrieval with Sodium Citrate buffer, pH 6 (epitope retrieval solution 1) for 30 min. The section was then incubated with anti-human CEMIP/KIAA1199 (ab76849) (1:100 dilution) for 25 min at room temperature and detected using an HRP conjugated compact polymer system. DAB was used as the chromogen. Anti-human CD3 and “no primary antibody” controls were used to confirm the specificity of CEMIP staining. The TMA sections were then counterstained with hematoxylin and mounted with Leica Micromount. Tumor cores (between 1 – 3 per sample) were scored for intensity of CEMIP staining in tumor cells by two independent pathologists on a scale from zero (no expression) to four (very high expression). For those tumor samples where more than one core was available for analysis, the average intensity over all cores was calculated. Based on the CEMIP expression levels observed across the different tumor samples analyzed, pathologists defined a threshold cutoff value of expression (CEMIPexp>2) and assigned the according binary score (CEMIP $^{low/high}$) to each tumor sample. Particular brain metastasis cases for which brain metastasis coincided or preceded primary diagnosis, and cases for which there was no information regarding time of primary diagnosis, were excluded from subsequent survival analyses. Progression Free Survival (PFS) was based on CEMIP $^{low/high}$ expression in primary tumor and defined as the time interval between primary tumor diagnosis and the earliest brain metastasis detected. Outlier cases presenting abnormally long time period from primary tumor diagnosis to brain metastasis (>10 years) were

omitted from analysis. Overall Survival (OS) was based on CEMIP $^{low/high}$ expression in brain metastatic tumor and defined as the time interval between primary tumor diagnosis and patient date of death or last follow up. Kaplan-Meier survival curves were compared using Log-rank (Mantel-Cox) test. Correlation of CEMIP expression in primary tumor samples with metastatic status (overall metastasis, non-brain metastasis, and brain metastasis) was determined by calculation of the Spearman correlation coefficient. For isolation and characterization of exosomes from surgically-resected fresh patient primary and metastatic tumor samples, tissue was collected and received within two-hours post-surgery, dissected into 2mm x 2mm pieces and placed in serum-free DMEM culture media supplemented with L-glutamine (1mM) and Penicillin/Streptomycin (100 IU/mL and 100 µg/mL). Patient tissue explant cultures were maintained in a humidified incubator with 5% CO_2 at 37 ºC and tissue-derived exosomes were obtained from the culture supernatant after 24 hours. For evaluation of CEMIP expression in patient-derived tumor exosomes we analyzed 5 µg of exosomal protein per sample by western blot.

Data presentation and statistical analysis. Error bars in graphical data represent mean ± SEM. Reference to the number of independent biological replicates performed for each experiment, as well as the sample size of each experimental group/condition, is provided in the respective figure legend of each experiment. Statistical significance was determined with two-tailed Student's t-test or one-way ANOVA, in which P values smaller than 0.05 were considered statistically significant. Variance was similar between the groups that were statistically compared. Prism 8 (version 8.0.2) was used for statistical analysis and graphical data presentation (Graphpad software). ImageJ (version 1.52a) was used for image processing and analysis. Photoshop CC (version 20.0.3, Adobe) and Illustrator CC (version 23.0.2, Adobe) were used for image editing and presentation and for figure panel generation.

CHAPTER III

Biodistribution and vascular interaction of metastatic tumor exosomes in the brain

Specific aims

Under the hypothesis that tumor-derived exosomes contributed to remodeling of the brain microenvironment and promoted a pro-metastatic niche advantageous for metastatic colonization of the brain we decided to first explore which could be the main stromal cell players involved in interacting with these extracellular vesicles and that could therefore be mediating this process. To test this hypothesis we started by characterizing how brain metastatic exosomes distributed among different organs *in vivo*, analyzing their biodistribution within the brain and describing their interaction with brain cells.

For that, we pursued the following aims:

a. evaluate the *in vivo* biodistribution of tumor exosomes from brain metastatic cell models compared to other models with distinct metastatic organotropisms

b. characterize the major cell types in the brain interacting with tumor exosomes *in vivo*

c. describe consequences of tumor exosome uptake in the brain *in vivo*

Exosomes from brain metastatic cells preferentially localize to the brain

The Lyden laboratory was the first to describe the role of tumor-derived exosomes in pre-metastatic niche formation [17]. The work laid the foundation for further exploring the interaction of tumor exosomes with the stromal cells that make up pre-metastatic niches in different organs and dissecting their distinct pro-metastatic functions. A key question raised by this initial study was if exosomes from tumor cells displaying particular metastatic organotropism would recapitulate the tropism of their cells of origin. This question is of particular relevance given that if so, primary tumors could dictate and prepare their future metastatic sites, also known as pre-metastatic niches, through the exosomes they release. The growing angiogenic tumors, capable of shedding millions of exosomes into blood circulation, would create hospitable niches in the future organs of metastasis and influence the metastatic spread pattern accordingly. Therefore, to examine whether tumor exosomes colonize specific organ sites, we isolated exosomes from human metastatic breast cancer cell model MDA-MB-231 (231 parental), its derivative organotropic metastatic subline 831-BrT (231 BrT2) that displays specific brain metastatic organotropism *in vivo* [86], or from 4175-LuT lung (231 LuT1) and 1833-BoT bone (231 BoT1) metastatic MDA-MB-231 derivative sublines, which do not metastasize to the brain but to the lung and bone, respectively [36, 86-89] and evaluated if they would also exhibit organ tropism. These models present the advantage of being generated by the same laboratory and therefore being true organotropic “sibling” sublines generated from one parental cell population through several *in vivo* rounds of organ-specific metastatic selection [36, 86-89]. Although exosomes from the MDA-MB-231 variants were similar in size and morphology [56], we observed that their organ distribution 24h after systemic circulation injection varied. For studies on brain exosome biodistribution, mice were injected with tumor exosomes intracardiacally, allowing for unbiased exosome distribution through every organ following direct injection in the left ventricle of the heart. For lung and liver quantification, exosomes were injected intravenously by retro-orbital or tail vein injection. The later implies that exosomes pass through the lung before having the chance to spread to all organs, due to the venous nature of the administration. Therefore, although intravenous injection is a fast, repeatable, and reproducible method of exosome administration it is less efficient in delivering exosomes to the brain since a

proportion of these will be passively retained in the lung before entering the heart for whole-body distribution. When analyzing brains of mice injected with different organotropic-derived exosomes (Fig. 1b) we observed that 831-BrT exosomes efficiently localized to the brain with a more than fourfold increase compared to 1833-BoT and 4175-LuT exosomes (Fig. 1c). Similarly, lung-tropic 4175-LuT exosomes preferentially localized to the lung, thus suggesting that exosomes home to specific organs that correlate with the future metastatic sites of the cell of origin.

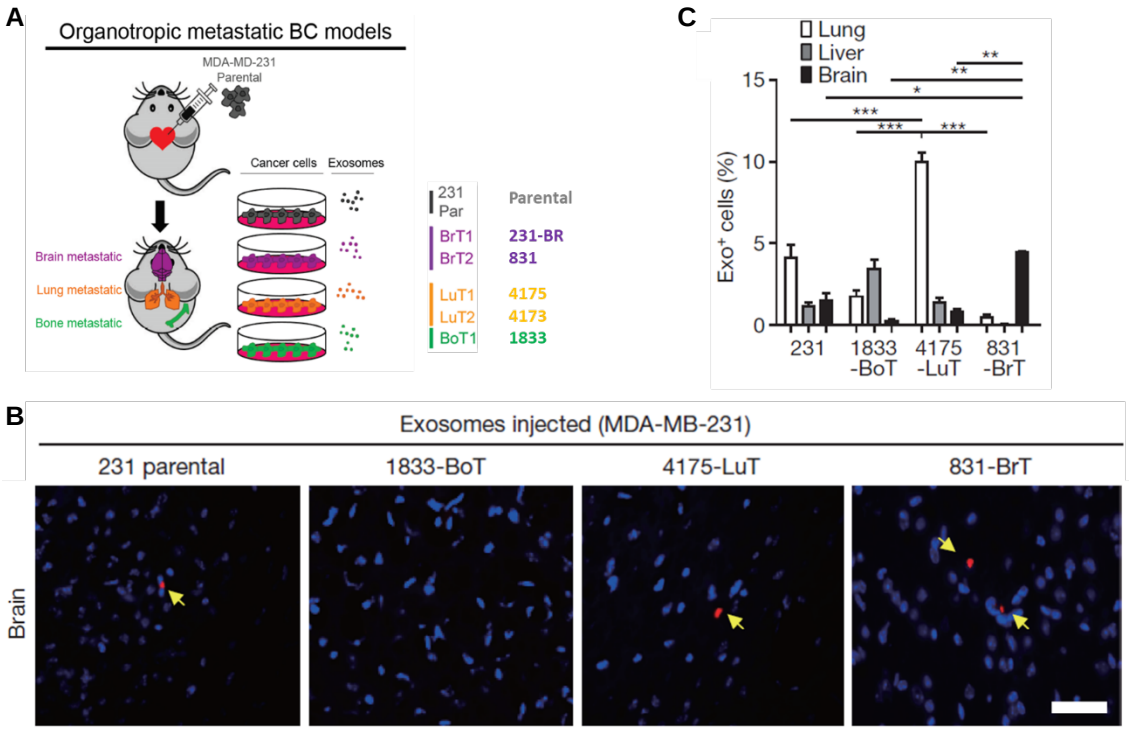

Figure 1. Tumor exosomes derived from brain metastatic models are preferentially uptaken in the brain relative to other organotropic models. A, Illustration of organotropic metastatic derivatives of MDA-MB-231 breast cancer cell model (parental (gray) and brain (purple), lung (orange), and bone (green) metastatic) and respective cell-derived exosomes analyzed. **B**, Fluorescence microscopy depicting representative images of brains from mice injected with different organotropic MDA-MB-231 subline-derived exosomes. Arrows indicate exosome foci. Immunofluorescence images are representative of five random fields. **C**, Immunofluorescence quantification of exosome-positive cells (n = 5 animals pooled from two independent experiments). Exosome signal quantification in the brain is represented by black bars. Scale bars, 50 µm (**B**) Error bars depict mean ± SEM. P values were calculated by ANOVA (**C**); * $P < 0.05$; ** $P < 0.01$; *** $P < 0.001$.

Next, we sought to determine if tumor exosomes from cancer cell models with different metastatic tropisms displayed different biodistribution patterns in the brain, in addition to the overall quantitative differences observed above. To analyze tumor exosome biodistribution we generated sagittal sections of the brains of exosome-injected mice and mapped the location of fluorescent cellular exosome uptake signals within arbitrarily defined quadrants covering the entire brain (Fig. 2a). The number of exosomes per quadrant was quantified in each individual and the data from all individuals in the same group was merged into a single map (Fig. 2b, left) and presented as a heatmap displaying the average number of exosomes per brain area (Fig. 2b, right). Interestingly, the biodistribution pattern of tumor exosomes was different depending on the organotropic metastatic cell of origin (Fig. 2b, right). In particular, when analyzing the brains of mice injected with brain metastatic cell-derived exosomes we detected hotspots of exosomal signal in the regions between the cerebellum and the pons, the cerebellum and the midbrain, and the hippocampus region, that were not found in mice injected with lung or bone metastatic cell-derived exosomes (Fig. 2b, right). Of interest, in the mice injected with exosomes derived from parental cells (heterogeneous tumor cell population with no particular metastatic organotropism), exosome biodistribution in the brain had an intermediate pattern, in between what was observed for the brain *versus* lung and bone groups. Given that exosomes were injected into the systemic circulation, we contemplated a potential link between the localization of exosome hotspots and the architecture of the brain vasculature. Indeed, the specific brain metastatic exosome signal hotspots appeared to overlap with the endings of main arterial vessels that supply blood to the brain, in particular the posterior cerebral artery (PCA; magenta 3D vessel tree), the superior cerebellar artery (SCA; blue 3D vessel tree), and the internal carotid artery (IC; dark green 3D vessel tree) (Fig. 2c).

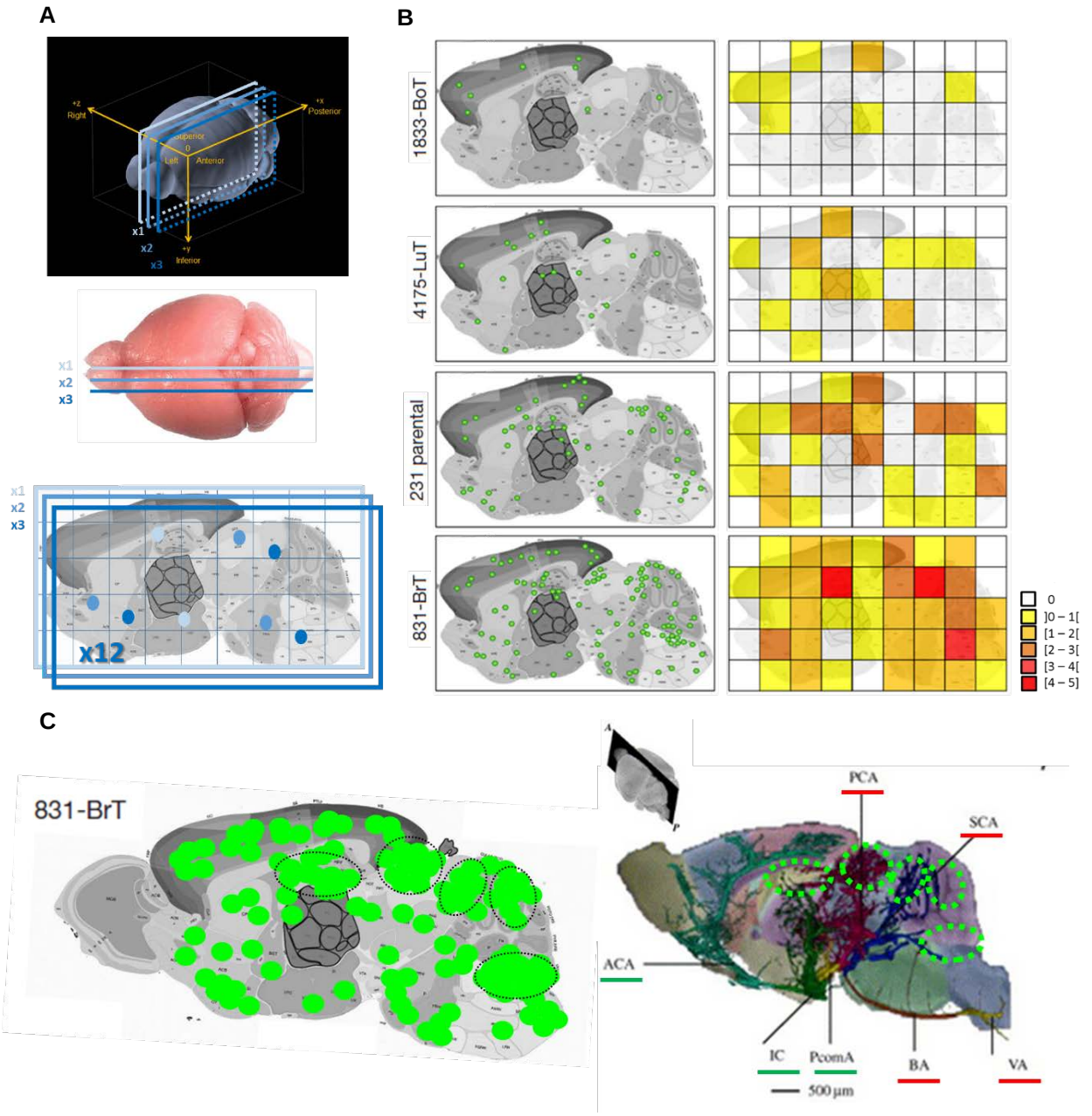

Figure 2. Exosome biodistribution analysis in the brain. Top, 3D view of the brain (adapted from *Allen Brain Atlas*) showing serial sagittal planes (in shades of blue). Middle, dorsal view of a fixed mouse brain (adapted from *Airey DC (2001), J Neuroscience*) and series of sections (in shades of blue) spanning the inner 1200 µm from the sagittal midline. The region selected for analysis comprises a representation of the majority of internal anatomical structures of the brain. Bottom, representative whole-brain sagittal section with overlaying grid (blue quadrants) and cumulative mapping of exosomal signals (dots in shades of blue) over 12 independent 10 µm cryosections per individual. **B**, Left, exosome biodistribution maps displaying the merged exosomal signal events (green dots) from individual mouse brains (*n* = 3 animals per

experimental group). Right, heatmap displaying the average exosome density observed in different brain areas. **C**, Left, representative whole-brain sagittal section displaying cumulative mapping of exosomal signals (green dots) from 831-BrT cell model (*n* = 5 animals). Black dotted line represents hotspots of exosome signal in the brain. Right, 3D vasculature of the mouse brain (adapted from *Dorr A (2007), Neuroimage*) depicting the main cerebral arteries. Colors distinguish vasculature origin - vasculature of vertebral artery origin (from subclavian arteries; red) and vasculature of internal carotid origin (from common carotid arteries; green). Green fluorescent dotted line represents hotspots of exosome signal in the brain.

Circulating tumor-derived exosomes predominantly interact with brain ECs

To identify the cells uptaking tumor exosomes in each organ, we intravenously injected red fluorescently-labelled exosomes isolated from 831-BrT, 4175-LuT or parental cells into mice. Interestingly, we found that the specific cell type responsible for exosome uptake varied depending on the metastatic organ. Brain-tropic 831-BrT exosomes interacted mainly with CD31-positive brain endothelial cells (98% of exosome-positive cells; Fig. 3a, left), whereas lung-tropic 4175 exosomes mainly co-localized with S100A4-positive fibroblasts and surfactant protein C (SPC)- positive epithelial cells (40% and 30% of exosome- positive cells, respectively) in the lung (Fig.3a, right). The remaining population of exosome-positive cells in the lung could not be defined but were likely largely comprised of lung endothelial cells. Moreover, in the brain, we observed that regardless of the cellular source of tumor exosomes administered (831-BrT, 4175-LuT or parental cells), exosomes were predominantly uptaken by endothelial cells (Fig. 3b). Immunofluorescence analysis also indicated that the second most common cell type uptaking brain metastatic tumor exosomes from systemic circulation were $PDGFRb^+$ cells, pericytes, which also express $CD31^+$. Collectively, these data demonstrate that although specific tissue-resident stromal cells differentially uptake tumor exosomes in metastatic target organs, and brain-metastatic derived exosomes preferentially home to the brain compared with other organotropic models, endothelial cells and perivascular cells are the main players in the brain interacting with tumor exosomes from circulation *in vivo*. Interestingly, the observation that tumor exosomes were not taken up by other stromal cells within the inner brain microenvironment directly from circulation may indicate that tumor exosomes might not be able to directly reach these cells from circulation,

considering the scenario of single exosome administration, and need to either first interact with brain endothelial cells or have this first endothelial barrier already open.

In addition to evaluating the 831-BrT (BrT2) brain metastatic cell model, we extended our analysis on tumor exosome brain endothelial cell tropism to a second MDA-MB-231 organotropic brain metastatic model, 231-BR (BrT1) [86], which displayed consistent and improved brain metastatic efficiency and accelerated progression kinetics compared to BrT2 in experimental brain metastasis in *in vivo* assays and therefore represented an improved brain metastasis model for these studies.

Consistent with our BrT2 cell-derived exosome data, BrT1 tumor cell-derived exosomes localized to the brain and were predominantly uptaken BrECs *in vivo* (Fig. 4a). Strikingly, *in vivo* uptake of brain metastatic tumor-derived exosome by BrECs after a single intracardiac injection of 10 µg of fluorescently-labelled 231 BrT1-derived exosomes was also accompanied by disruption of the blood-brain barrier (BBB) vascular integrity, as evidenced by the visualization of extravasated high molecular weight dextran in exosome-positive blood vessels (Fig. 4b), an effect also observed for 831-BrT (BrT2) exosomes [56].

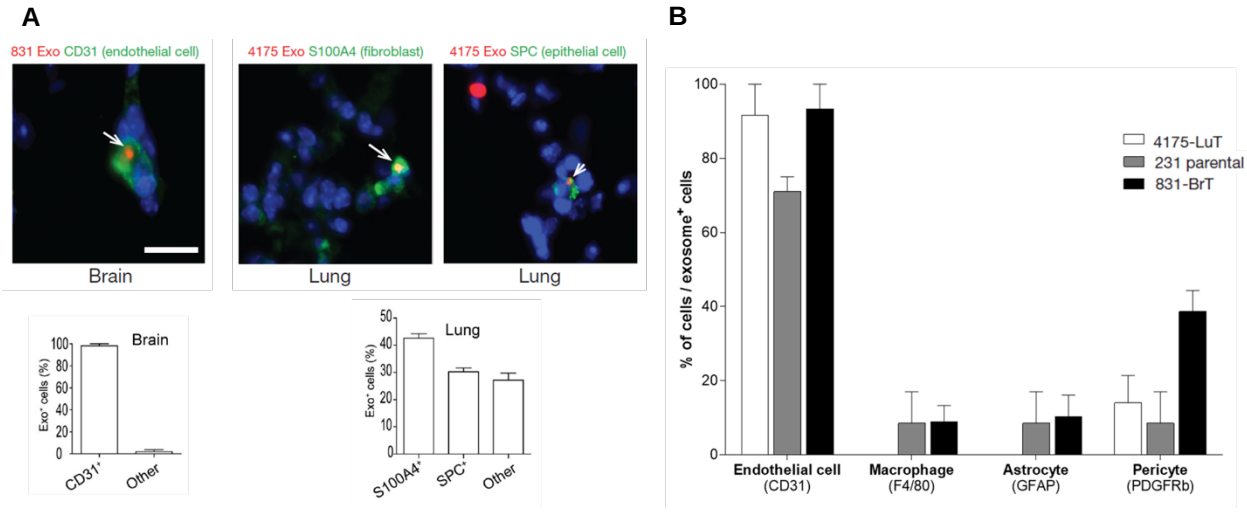

Figure 3. Organ-specific metastatic cell-derived exosomes interact with distinct resident cell types in different organs. A, Analysis by immunofluorescence of exosome distribution (red) and different resident cell types (green). Left, brain co-staining with CD31 (endothelial cells) and 831-BrT exosomes. Right, lung co-staining with 4175-LuT exosomes and S100A4 (fibroblasts) or SPC (epithelial cells). Scale bar, 30 µm. Immunofluorescence images are representative of five exosome-positive cells each, from *n* =

5 mice. Quantification of organotropic exosome uptake by target cells *in vivo*: Left bottom graph, quantification of the frequency of 831-BrT exosome-positive endothelial cells by immunofluorescence microscopy (*n* = 5 mice). Right bottom graph, quantification of the frequency of 4175-LuT exosome-positive fibroblasts and epithelial cells (*n* = 4 mice). **B**, Quantification of organotropic exosome uptake by brain stromal cells *in vivo* by immunofluorescence microscopy. Endothelial cells (CD31); Macrophage (F4/80); Astrocyte (GFAP); and Pericytes (PDGFRb), (*n* = 3 mice).

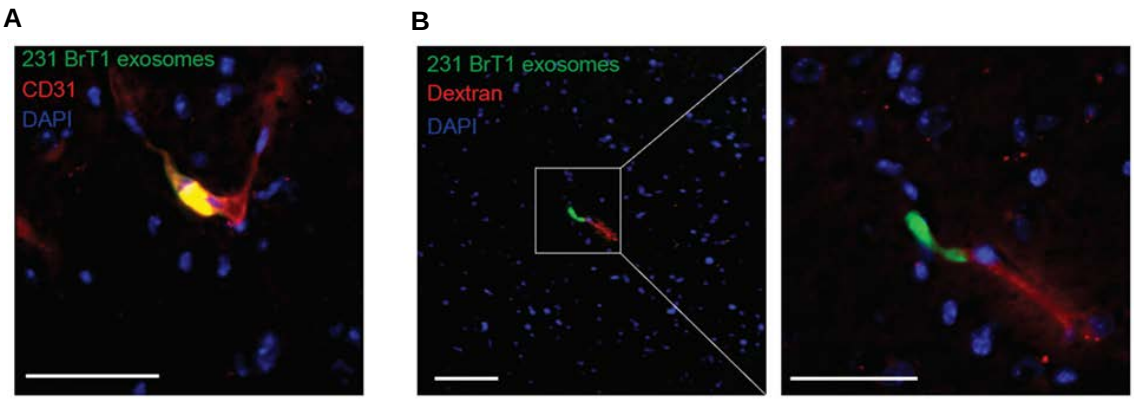

Figure 4. Brain metastatic tumor exosomes interact with BrECs and promote loss of vascular integrity *in vivo*. A, Representative fluorescence image of BrT1 exosomes (green) interacting with CD31+ BrECs (red) *in vivo* 24 hours post-intracardiac injection of labelled exosomes. **B**, Representative fluorescence image of BrT1 exosomes (green) and associated extravasated rhodamine-labelled Dextran (red) in the brain 24 hours post-intracardiac injection of labelled exosomes (right, enlarged inset). Immunofluorescence images of *in vivo* exosome uptake by BrECs and vascular leakiness are representative of three independent biological replicates (**A**, **B**). Scale bars, 50µm (**A**), 50µm and 100µm (**B**).

Taken together, these results indicate that brain metastatic cell-derived exosomes are predominantly taken up by brain endothelial cells, have the ability to affect brain vascular cell behavior and promote BBB opening and may thus contribute to pro-metastatic processes such extravasation, known to facilitate metastasis.

CHAPTER IV

Ex vivo modeling of brain metastatic colonization for tumor exosome studies

Specific aims

Although the *in vivo* models used in the previous chapter were useful for the characterization of the interaction of tumor exosomes with cells in the brain microenvironment, they presented limitations for their use in the study of tumor exosome-mediated effects on the brain microenvironment. To study the ability of tumor exosomes to generate a pre-metastatic niche in the brain, we required a model that allowed repeated, reproducible, and efficient administration of exosomes to the brain, which was not possible *in vivo* due to high mortality risk in animals following repeated intracardiac injections. Thus, knowing that tumor exosomes compromise the BBB and allow for the exposure of the inner brain microenvironment to subsequent tumor-secreted exosomes and other factors, and in order to overcome the hurdles posed by the pre-clinical models currently available for BrM research [90], we optimized an *ex vivo* organotypic brain slice culture system [71] to help us define the specific contribution of tumor-derived exosomes to brain microenvironment remodeling for metastatic colonization. Based on our previous findings that tumor-derived exosomes from brain metastatic cells present specific brain biodistribution, cellular uptake and biological effects, we decided to investigate if they can generate a niche in the brain supportive of metastatic colonization.

The specific aims for this chapter are as follows:

a. devise and test an *ex vivo* organotypic brain slice assay for the study of tumor exosomes in brain metastatic colonization

b. describe the effects of tumor exosomes from cell models with different metastatic organotropisms in *ex vivo* brain metastatic colonization

c. characterize the major cell types in the brain interacting with brain metastatic tumor exosomes *ex vivo*

Exosomes from brain metastatic cells promote cancer cell colonization of the brain *ex vivo*

Adaptation of an organotypic brain slice 3D model previously developed for the study of neurobiology [71] provided a system in which we could distinguish the effects of tumor exosomes from those of the cancer cells of origin. This brain metastasis model comprised of a live 3D brain microenvironment with an intact architecture but that allow us to study and visualize the different processes in brain metastatic colonization such as the growth and invasion of cancer cells into the brain parenchyma. In addition to providing better control of experimental conditions in comparison with *in vivo* models, adoption of an *ex vivo* approach also yielded production of several brain slices per individual brain, allowing to have a high number of individual data points for analysis in different experimental groups that could be generated from a single mouse (Fig. 1a). Furthermore, to allow for the addition of exosomes, I have improved this system by adding a small polycarbonate ring, a cell culture-suited material, to the top of the brain slice. This modification allowed us to limit and standardize the area of tumor exosome effect, as well as to better control the spread of exosomes and tumor cells over the brain slice (Fig. 1b).

Having adapted the *ex vivo* model for the study of tumor exosomes in brain metastasis (Fig. 1a, b) we set to determine if exosomes derived from brain metastatic cancer cells specifically alter the brain microenvironment and impact tumor cell colonization. For that, we pre-treated brain slices with a physiological dose of 5 µg of exosomes isolated from brain-tropic 231-BR (231 BrT1), lung-tropic 4175 (231 LuT1), bone-tropic 1833 (231 BoT1), or parental MDA-MB-231 (231 Parental) human breast cancer metastatic cells [36, 86] (Chapter III, Fig. 1a), for two consecutive days, then added GFP^+ 231 BrT1 cancer cells, measuring tumor cell colonization three days later (Fig. 1b, c – cancer cell number).

Pre-treatment of brain slices with 231 BrT1-derived exosomes increased colonizing 231 BrT1 cell number four-fold compared to PBS, and two-fold or more compared to pre-treatment with 231 parental and lung- or bone- metastatic exosomes (Fig. 2a, b), respectively. Pre-treatment with non-brain tropic exosomes did not induce significant cancer cell growth compared to PBS (Fig. 2a, b).

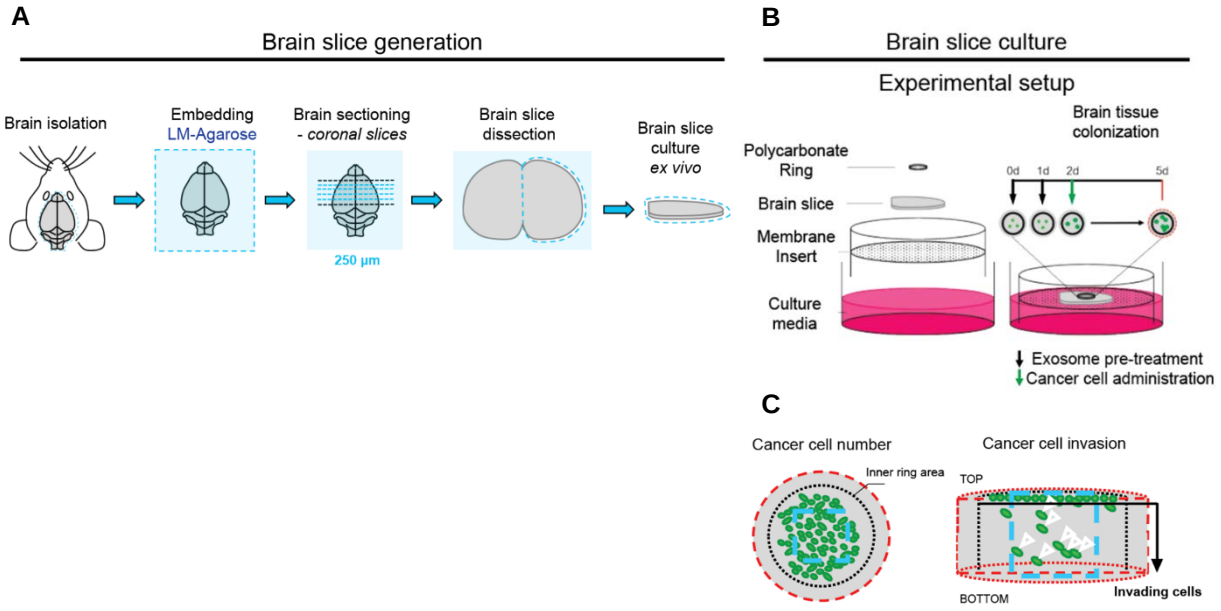

Figure 1. Development of a brain slice model to study the role of tumor exosomes in metastatic colonization. A, Schematic representation of the *ex vivo* brain slice model optimized for the study of exosome-mediated cancer cell brain colonization. **B**, Schematics of the brain slice culture and experimental setup used for the study of tumor exosome pre-treatment effects on the brain microenvironment during metastatic colonization. **C**, Cancer cell phenotypes analysed (left, cancer cell number – of brain slice whole mount; and right, cancer cell invasion – brain slice transversal section). Invading cells (white arrows) inside the region of interest, denoted by the blue square, are comprised of all cancer cells below the first layer of brain cells on the top of the brain slice.

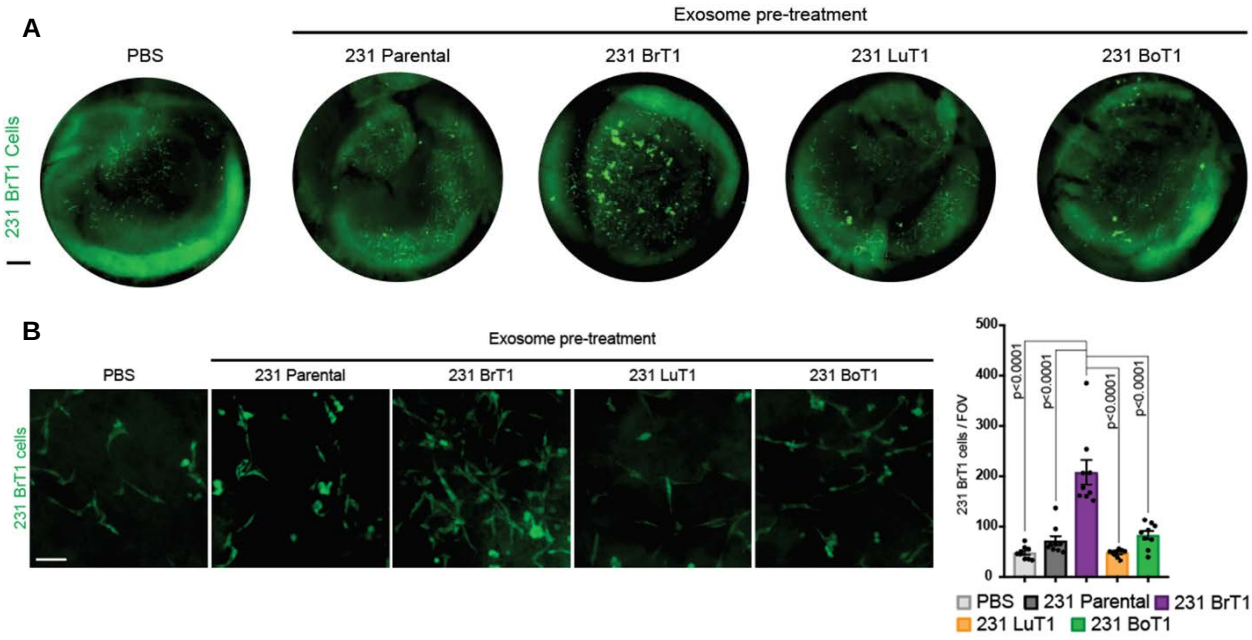

Figure 2. Exosomes from brain metastatic cells promote cancer cell growth in brain metastatic colonization. A, Representative whole slice fluorescence images of 231 BrT1 GFP^+ cells growing on top of brain slices pre-treated with exosomes or PBS. **B**, Left, representative images of 231 BrT1-GFP^+ cells growing on top of brain slices pre-treated with exosomes or PBS. Right, quantification of cancer cell number. The number of cells per field of view (FOV) are averages ± SEM, from *n* = 9 individual brain slices, scoring two fields per slice (**B**). A representative experiment of three independent biological replicates is shown. Scale bars, 500 µm (**A**) and 100µm (**B**). Error bars depict mean ± standard error of the mean (SEM). *P* values were calculated by ANOVA (**B**).

Next, we asked if pre-conditioning with brain metastatic tumor-derived exosomes impacted brain metastatic cell invasiveness. Three days after tumor cell addition, we quantified invading 231 BrT1 cells in transversal sections of brain slices pre-treated with 231 BrT1 or 231 parental-derived exosomes (Fig. 1c – cancer cell invasion) and determined that 231 BrT1 exosome pre-treatment augmented 231 BrT1 cell invasiveness three-fold compared to 231 parental-derived exosomes or PBS, respectively (Fig. 3a). Moreover, Ki-67 immunostaining showed that 231 BrT1 exosome pre-treatment bolstered invading 231 BrT1 cell proliferation over four-fold compared to 231 parental exosomes (Fig. 3b).

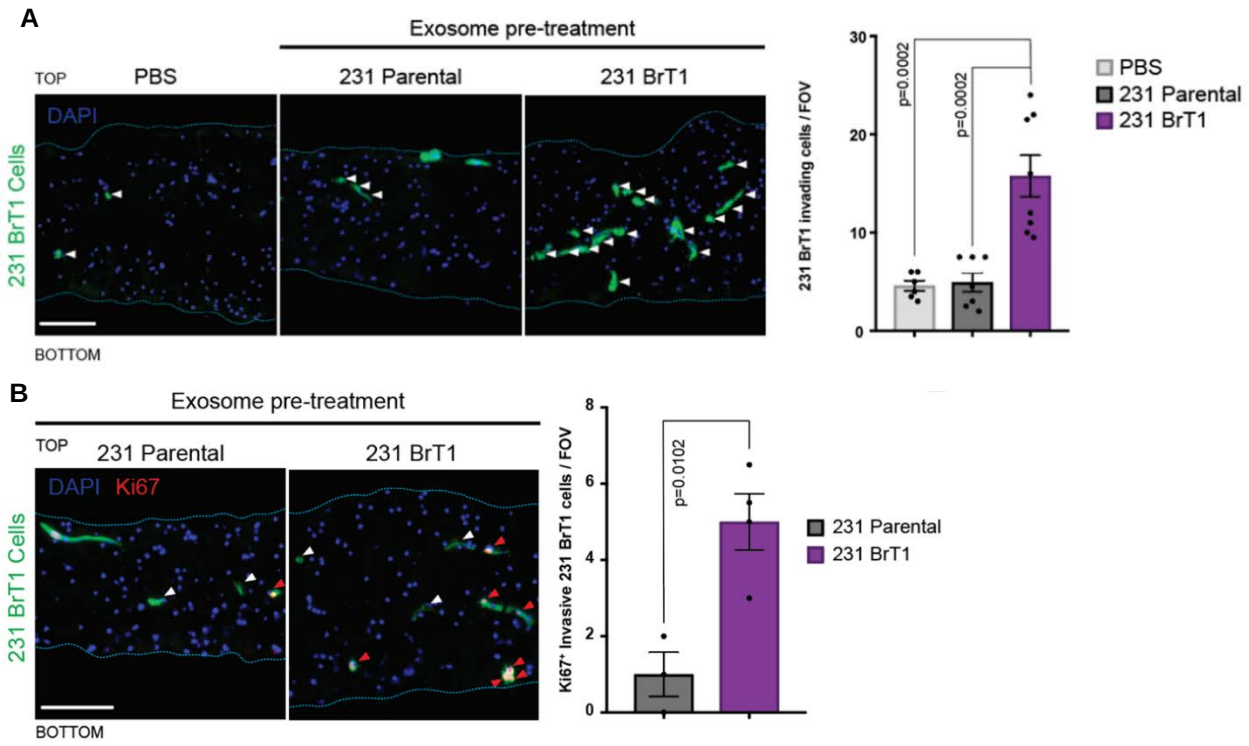

Figure 3. Exosomes from brain metastatic cells support brain colonization and proliferation of invading cancer cells. A, Left, representative images of 231 BrT1-GFP+ cells invading brain slices pre-treated with exosomes or PBS. Right, quantification of invading cancer cell number. **B**, Left, representative immunofluorescence microscopy images of proliferating Ki-67+ BrT1 GFP+ cells invading brain slices pre-treated with exosomes. White and red arrows indicate invading Ki-67- or Ki-67+ cells, respectively. Right, quantification of Ki-67+ invading cancer cell number. Brain slice sections were stained with DAPI (blue); dotted blue lines delineate the top and bottom limit of the brain slice (**A**, **B**). The number of cells per field of view (FOV) are averages ± SEM, from *n* = 6, 7, 8 (**A**), or from *n* = 3, 4 individual brain slices (**B**), scoring two fields per slice (**A**, **B**). A representative experiment of three (**A**, **B**) independent biological replicates is shown. Scale bars, 100µm (**A**, **B**). Error bars depict mean ± standard error of the mean (SEM). *P* values were calculated by ANOVA (**A**), or two-sided Student's t-test (**B**).

Remarkably, brain slice pre-conditioning with 231 BrT1-derived exosomes also enhanced colonization by 231 parental cells (Fig. 4a), which have limited ability to generate brain metastases[38, 91]. Brain slice pre-treatment with 231 BrT1-derived exosomes induced a five-fold and over two-fold increase in colonizing 231 parental cell number compared to PBS or 231 parental exosome pre-treatment, respectively (Fig. 4a).

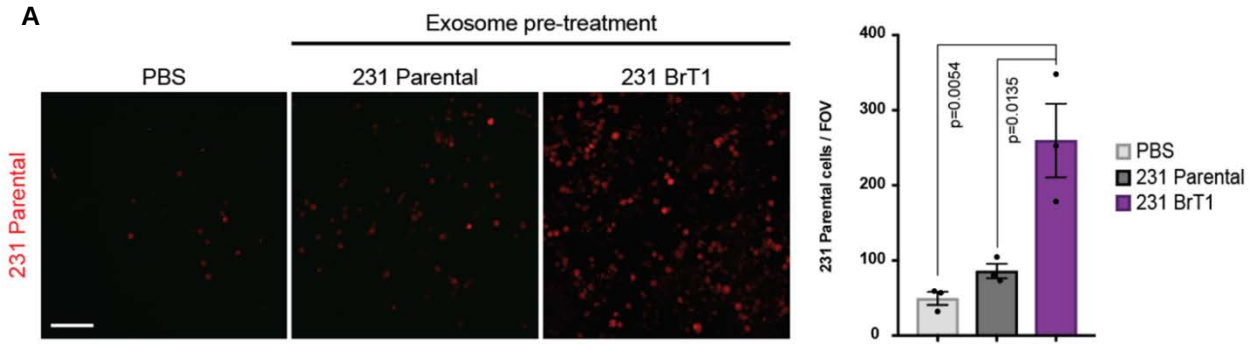

Figure 4. Exosomes from brain metastatic cells promote cancer cell growth and brain colonization by tumor cells without brain metastatic ability. A, Left, representative fluorescence images of 231 parental mCherry^{+} cells growing on top of brain slices pre-treated with exosomes or PBS. Right, quantification of 231 parental mCherry^{+} cell number. The number of cells per FOV are averages ± SEM, from *n* = 3 individual brain slices, scoring two fields per slice. A representative experiment of three independent biological replicates is shown. Scale bar, 100µm. Error bars depict mean ± SEM. *P* values were calculated by ANOVA.

Overall, pre-conditioning brain slices with brain metastatic cell-derived exosomes supported tumor colonization independent of cell-intrinsic brain metastatic potential, suggesting that exosome-mediated brain microenvironment remodeling supports metastatic cell proliferation and invasion.

ECs and microglia are the main brain cells that uptake exosomes

Since our findings suggest a role for tumor exosomes in reshaping the brain microenvironment to support metastatic colonization, we sought to identify resident cells within the brain interacting with this class of EVs and that could therefore be mediating this effect. The *ex vivo* model offered more control over exosome dose administration allowing the study of the main cellular players interacting with tumor exosomes once they reached the brain microenvironment, bypassing any restrictions imposed by the BBB. This was relevant given that our previous data suggested that brain metastatic tumor exosomes interacted with brain endothelial cells and induced vascular leakage *in vivo*, disrupting the BBB and thus allowing for the entry into the brain parenchyma of further exosomes, tumor-secreted factors and cells from blood circulation. We treated brain slices with 5 µg of fluorescently-labelled 231 BrT1-derived exosomes and examined exosome uptake by the major stromal cell types within the brain, namely endothelial cells, microglia, astrocytes and neurons, *via* immunofluorescence, at 24 hours post-treatment (Fig. 5a, b). Interestingly, exosomes still co-localized primarily with $CD31^+$ and $Glut1^+$ endothelial cells in this model but were also uptaken by $Iba1^+$ microglia, including perivascular ones, and, to much lower extent, by $GFAP^+$ astrocytes and $NeuN^+$ neurons (Fig. 5b, c).

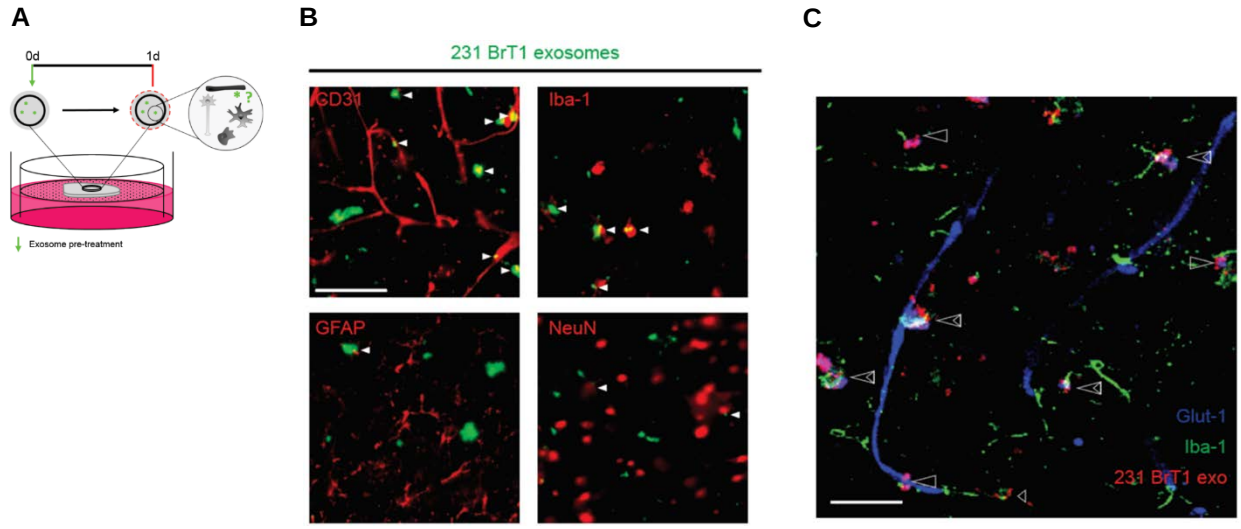

Figure 5. Exosome uptake by brain cells in the *ex vivo* 3D brain slice assay. A, Schematic of the brain slice model setup for the study of exosome interaction with brain microenvironment resident cells. **B**, Representative images of fluorescently-labelled 231 BrT1 exosomes (green) and brain endothelial cells (BrECs, CD31$^+$), microglia (Iba1$^+$), astrocytes (GFAP$^+$), or neurons (NeuN$^+$) (all in red). White arrows indicate co-localization of exosomes and the indicated cell type. **C**, Representative confocal microscopy image of Glut1$^+$ BrECs (blue, long arrows) and Iba1$^+$ microglia (green, short arrows) interacting with fluorescently-labelled BrT1 exosomes (red). Double arrows depict joint interaction of BrECs and microglia with exosomes. One of three independent biological replicates is shown for **B** and **C**. Scale bars, 100µm (**B**) and 50µm (**C**).

These data are consistent with our previous work highlighting the relevance of endothelial cells in tumor exosomal-mediated effects, where we demonstrated that BrECs are the cell type predominantly interacting with tumor cell-derived exosomes *in vivo* (Chapter III, Fig. 3 and Fig. 4a). These observations support the *ex vivo* model as a reliable representation of the *in vivo* scenario [56] and offer a very useful and reproducible platform to study the role of tumor exosomes in brain metastatic colonization.

CHAPTER V

CEMIP, a tumor exosome protein with functions in brain metastasis

Specific aims

Given our data suggesting that brain metastatic exosomes generate a pro-metastatic environment in the brain that facilitates tissue colonization, likely through their effects on vascular niche cells, and our published findings showing that exosomes play central functions in recipient cells and alter their phenotype [17, 56, 57], we set out to identify specific proteins in brain metastatic exosomes that could account for the observed effect in brain metastatic colonization.

The specific aims for this chapter are as follows:

a. identify candidate exosomal proteins specific for brain metastasis

b. evaluate the potential association between expression of candidate exosomal proteins and BrM using *in vivo* models of metastasis and the optimized *ex vivo* model

c. describe the effects and characterize the mechanisms of candidate exosomal proteins in exosomal preconditioning of the brain microenvironment *in vivo* and *ex vivo*

Proteomic analysis identifies exosomal CEMIP as a brain metastatic protein

We previously showed that tumor exosomes package specific proteins critical for the metastatic process at target organs [17, 57] and that integrins are abundantly packaged in tumor exosomes that promote lung and liver metastasis [56]. Surprisingly, brain metastatic exosomes packaged few integrins and at low levels [56], albeit ones whose cellular expression had previously been associated with BrM: α2, α3, β3 and β1 integrins [44, 92]. Thus, exosomal molecules other than integrins may support BrM. Quantitative mass spectrometry comparison of exosome proteomes from brain-tropic 231 BrT1 and BrT2 to those of 231 parental, lung-tropic (LuT1 and LuT2 [4173]) and bone-tropic BoT1 MDA-MB-231 cells revealed that only twenty proteins were differentially expressed in brain tropic exosomes when compared to exosomes from parental cells (Fig. 1a). Among these, CEMIP or KIAA1199 [93], emerged as a prominent exosomal protein in both brain metastatic models, with low or undetectable expression in exosomes from lung and bone metastatic models, suggesting a specific association with BrM potential. Of the brain metastatic cell models, CEMIP expression was highest in BrT1, the model that also displayed more consistent and higher brain metastatic ability *in vivo*. Therefore, we chose to further explore the role of CEMIP in BrM using the BrT1 model.

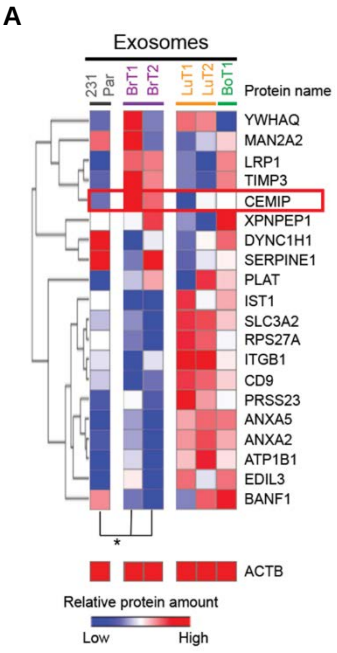

Figure 1. Differentially expressed proteins in exosomes of brain metastatic origin. A, Heatmap of 20 differentially expressed exosomal proteins and β-Actin (ACTB) based on the quantitative mass spectrometry label-free quantification (LFQ) values (technical triplicates, *FDR - false discovery rate < 0.05 by ANOVA). Hierarchical clustering (one minus the sample Spearman's rank of correlation between observations) was performed on protein expression levels. Heatmap depicting differentially expressed proteins in BrT-derived exosomes displays average of three independent exosome sample replicates.

CEMIP is involved in hyaluronic acid depolymerization [94], intracellular calcium regulation [95] and Wnt signaling [96], playing multiple roles in cancer progression [97], inflammation [98], and interestingly, in normal brain physiology [99]. Western blot quantification of exosomal CEMIP confirmed high abundance in brain metastatic cell-derived exosomes compared to parental and non-brain metastatic cell-derived exosomes (Fig. 2a). Interestingly, CEMIP was enriched ten-fold in 231 BrT1 exosomes relative to 231 BrT1 cells, suggesting selective packaging in exosomes (Fig. 2a). Moreover, CEMIP was abundant in exosomes from additional orthotopic brain metastatic models: MDA-MB-231-HM breast and N2LA-BR lung cancer (Fig. 2b), further supporting the association of exosomal CEMIP with BrM potential.

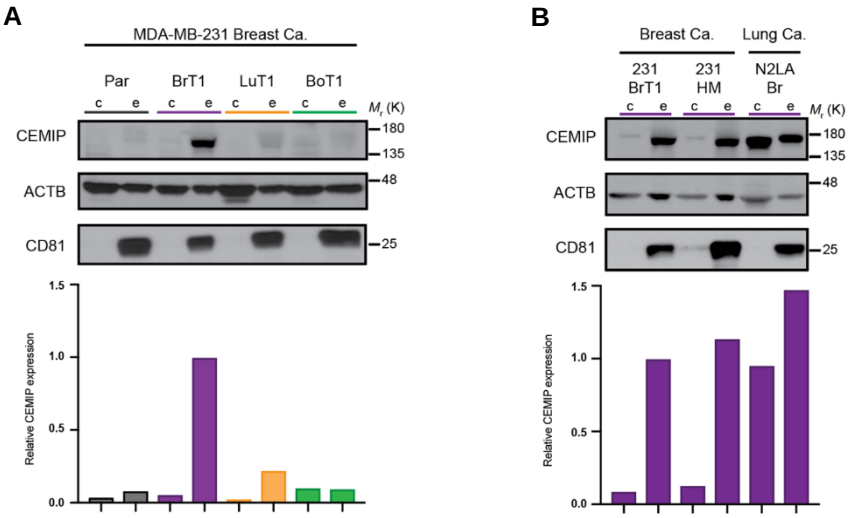

Figure 2. CEMIP expression is increased in exosomes from brain metastatic cell models. A, Top, CEMIP, ACTB (loading control), and CD81 (exosomal marker) immunoblot in cells and exosomes from organ-specific metastasis models. Bottom, densitometry quantification of CEMIP. **B**, Top, CEMIP, ACTB (loading control), and CD81 (exosomal marker) immunoblot in cells and exosomes from human cancer cell brain metastasis models. Bottom, densitometry quantification of CEMIP. Densitometry graphs show CEMIP expression normalized to CEMIP expression in BrT1 exosomes, and CEMIP expression was normalized to ACTB for each sample (**A**, **B**). A representative experiment of four (**A**) or three (**B**) independent biological replicates is shown.

At the cellular level, CEMIP expression was found to be the highest in the cell membrane (Fig. 3a), in agreement with previous reports [100], whereas at the secreted level it was patently found to be associated with tumor vesicles as opposed to being in the secreted-factor soluble fraction (Fig. 3b).

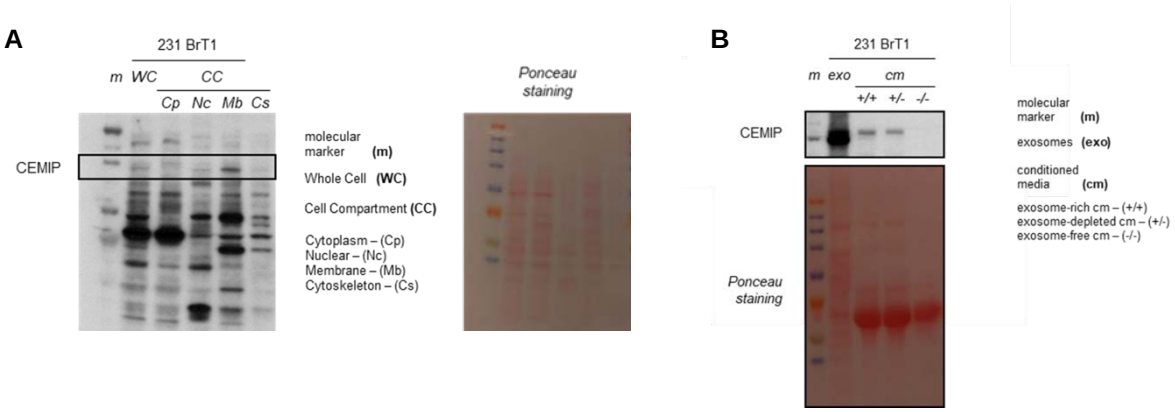

Figure 3. Characterization of cellular and secreted CEMIP expression in 231 BrT1 cells. A, Left, CEMIP, immunoblot of distinct subcellular compartments of 231 BrT1 cells. Right, Membrane Ponceau staining. **B**, Top, CEMIP, immunoblot of 231 BrT1 exosomes and 231 BrT1 exosome-rich cell conditioned media (cm) (+/+, before ultracentrifugation), exosome-depleted cm (+/-, after one round of ultracentrifugation for 70 minutes), and exosome-free cm (-/-, after one round of ultracentrifugation for 16h). Bottom, Membrane Ponceau staining.

To further investigate CEMIP specific association with extracellular vesicle (EV) fractions containing exosomes, we applied the 231 BrT1 EV pellet obtained from ultracentrifugation onto an iodixanol/Optiprep density gradient and quantified CEMIP expression in fractions positive for exosomal and small EV markers Syntenin-1, CD81, and HSP70 (fractions 6-9). CEMIP was detected in fractions 5-9 (Fig. 4a), with the highest CEMIP expression in the exosome-containing fraction 7, corresponding to a density of 1.10 g/mL. This indicates that CEMIP expression is specifically associated with small EVs, that include exosomes and their subpopulations (exosome large, exosome small vesicles and exomere particles) [70], as opposed to non-EV protein aggregates or microvesicles.

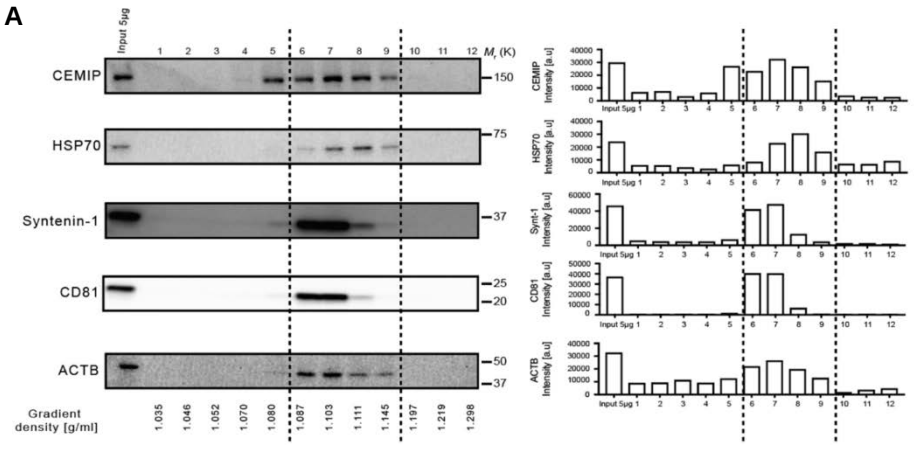

Figure 4. CEMIP expression is increased in exosomes from brain metastatic cell models. A, Left, immunoblot of CEMIP, small EV and exosomal markers (HSP70, Syntenin-1 and CD81) and ACTB in fractions obtained by OptiPrep™ density gradient ultracentrifugation of BrT1 exosomes. Right, densitometry quantification of protein expression in the initial exosome population (*Input*) and across fractions with different density, given in arbitrary units [a.u.]. Small EV and exosome-containing fractions are shown between dashed lines. A representative experiment of four independent biological replicates is shown.

Taken together, our data identify CEMIP as a protein enriched in exosomes from brain metastatic cancer cells.

CEMIP mediates brain metastasis and cancer cell vascular co-option

To determine whether CEMIP is required for exosome-mediated brain colonization, we targeted *CEMIP* in brain metastatic 231 BrT1 cancer cells using CRISPR/Cas9 (Fig. 5a). Western blot confirmed a significant reduction in CEMIP expression in two 231 BrT1 single cell clones with complex *CEMIP* indels (Fig. 5a), KO1 and KO2, and their exosomes, compared to control BrT1 cells (WT) and exosomes (Fig. 5b). CEMIP targeting was confirmed by immunoblot analysis with additional CEMIP antibodies, further supporting specific identification of CEMIP at the correct molecular weight in CEMIP-high 231 BrT1 brain metastatic cell-derived exosomes and reduction of expression at the exosomal protein level (Fig. 5c). Transmission electron microscopy (Fig. 5d) and nanoparticle tracking analysis (Exosome size; Fig. 5e) revealed that CEMIP targeting did not affect exosome morphology or size. In addition, protein levels (BCA protein assay; Fig. 5e) and expression of CD81, Syntenin-1 (Fig. 5b), and additional exosome/EV marker proteins (Fig. 5f) remained largely unaltered in 231 BrT1 CEMIP KO-derived exosomes, suggesting CEMIP loss does not alter exosomal protein packaging.

A

chromosome	target site start coordinate	target site end coordinate	gRNA	cutting efficiency score	cutting specificity score	strand	offtargets sum	offtargets summary	annotation	gRNA label
chr15	80929027	80929049	GGAGCCGTCGTCATACGGGA	62	1	-	0	2:0|3:0	CEMIP_ENST00000220244.7_exon_20_of_29,CEMIP_ENST00000356249.9_exon_21_of_30,CEMIP_ENST00000394685.7_exon_21_of_30	gRNA_1__58
chr15	80929135	80929157	GCGGCTTGGACCATAGCGGA	61	1	+	0	2:0|3:0	CEMIP_ENST00000220244.7_exon_20_of_29,CEMIP_ENST00000356249.9_exon_21_of_30,CEMIP_ENST00000394685.7_exon_21_of_30	gRNA_1__59
chr15	80922038	80922060	CGTACCAACGGGCCCCTCCG	56	1	+	0	2:0|3:0	CEMIP_ENST00000220244.7_exon_16_of_29,CEMIP_ENST00000356249.9_exon_17_of_30,CEMIP_ENST00000394685.7_exon_17_of_30	gRNA_1__57

Sample Id	Gene Name	Exon	Alleles	Flanking Sequence	Comments
KO1	CEMIP	16		TTTTTCACCACGTACCAACGGGCCCCTCCGTGGGAATGTA	Complex Indel
KO2	CEMIP	20		TGGGGCCCTGGCGGCTTGGACCATAGCGGAAGGACCCTCC	Complex Indel

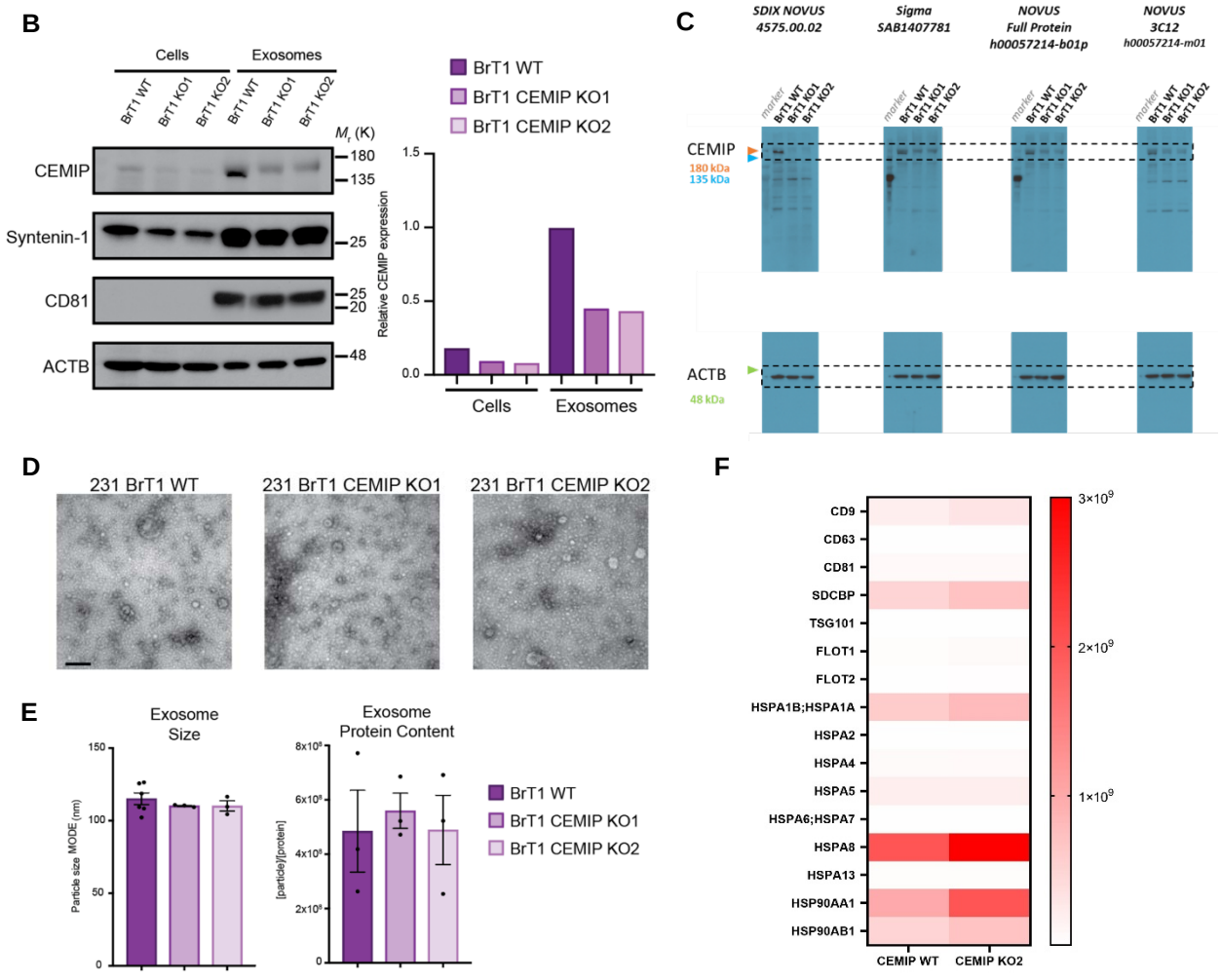

Figure 5. Generation and characterization of 231 BrT1 CEMIP KO cancer cell models. A, Construct information for human *CEMIP* gRNA used for CRISPR/Cas9 knockout of *CEMIP* in human 231 BrT1 cancer cells and sequencing information of selected clones. **B**, Left, immunoblot of CEMIP expression in cell and exosomal protein extracts from BrT1 WT and BrT1 CEMIP knockout (KO1 and KO2) cells. Immunoblotting for exosomal markers (Syntenin-1 and CD81) and ACTB is shown below. Right, densitometry quantification of CEMIP normalized to CEMIP expression in BrT1 WT exosomes. CEMIP expression was normalized to ACTB expression for each sample. **C**, Immunoblot analysis of CEMIP expression in exosomes derived from 231 BrT1 CEMIP WT, KO1 and KO2 cancer cells with a panel of anti-CEMIP/KIAA1199 commercial antibodies. ACTB is shown below. **D**, Transmission electron microscopy (TEM) of BrT1 WT and BrT1

CEMIP-KO1 and -KO2 exosomes. **E**, Size distribution and protein content analysis of BrT1 WT and BrT1 CEMIP-KO1 and -KO2 exosomes. Exosome size (mode, nm) and number were evaluated by NanoSight particle tracking. Protein content per exosome ([particle]/[protein]) was assessed by factoring in the protein concentration. **F**, Estimated abundance of exosomal and extracellular vesicle marker proteins evaluated by qualitative mass spectrometry analysis of 231 BrT1 CEMIP WT and KO2 cancer cell-derived exosomes. One of three independent biological replicates is shown (**B - E**). Scale bar, 200nm (**D**). Error bars depict mean ± SEM. *P* values were calculated by ANOVA (**E**).

We next investigated the functional role of CEMIP in BrM. Although the overall cancer cell number on the surface of *ex vivo* brain slices was not significantly impacted by CEMIP loss (Fig. 6a), 231 BrT1 CEMIP KO and WT cell morphology was distinct (Fig. 6b, white arrows). Consistent with previous reports [38, 44, 91], brain metastatic 231 BrT1 cells presented a spindle-like morphology and when invading, consistently associated with and spread along brain endothelial cells (BrECs) (Fig. 6c – right and left panels, full white arrows), a process known as vascular co-option [101]. Interestingly, 231 BrT1 CEMIP KO cells were rounder, lost spindle-like morphology (Fig. 6b, white arrows) and displayed significantly impaired ability to associate with brain vasculature, with a 50% reduction in both co-opting and invading cancer cells compared to 231 BrT1 CEMIP WT cells (Fig. 6b, d). Despite diminished brain colonizing ability *ex vivo*, CEMIP ablation did not affect *in vitro* proliferation or invasion (Fig. 6e, f) suggesting that CEMIP's role in BrM is dependent on the brain microenvironment. Collectively, these results indicate that CEMIP loss reduces the ability of brain metastatic cells to interact with brain vasculature and successfully invade the brain.

Whereas the above illustrated that CEMIP promotes vascular co-option, invasion, and subsequently colonization, the data were confined to brain slices and thus bypassed critical steps of the metastatic cascade. Therefore, we used experimental metastasis assays to investigate whether CEMIP mediates BrM *in vivo*. Loss of cellular CEMIP led to a significant reduction in BrM four weeks following intracardiac injection of 231 BrT1 cells (Fig. 7a). Histology revealed a 70% decrease in brain metastatic foci generated by 231 BrT1 CEMIP KO *versus* CEMIP WT cells (Fig. 7b, c – left graph) and a metastatic burden reduction in both CEMIP KO models relative to CEMIP WT, especially in KO1

(Fig. 7c – right graph). However, we observed no significant differences in individual lesion size between CEMIP WT and CEMIP KO cells, suggesting that CEMIP is required during early steps of metastatic colonization. Accordingly, we found no significant difference in tumor outgrowth after intracranial injection upon CEMIP loss (Fig. 7d), or in primary tumor growth after mammary fat pad injection (Fig. 7e).

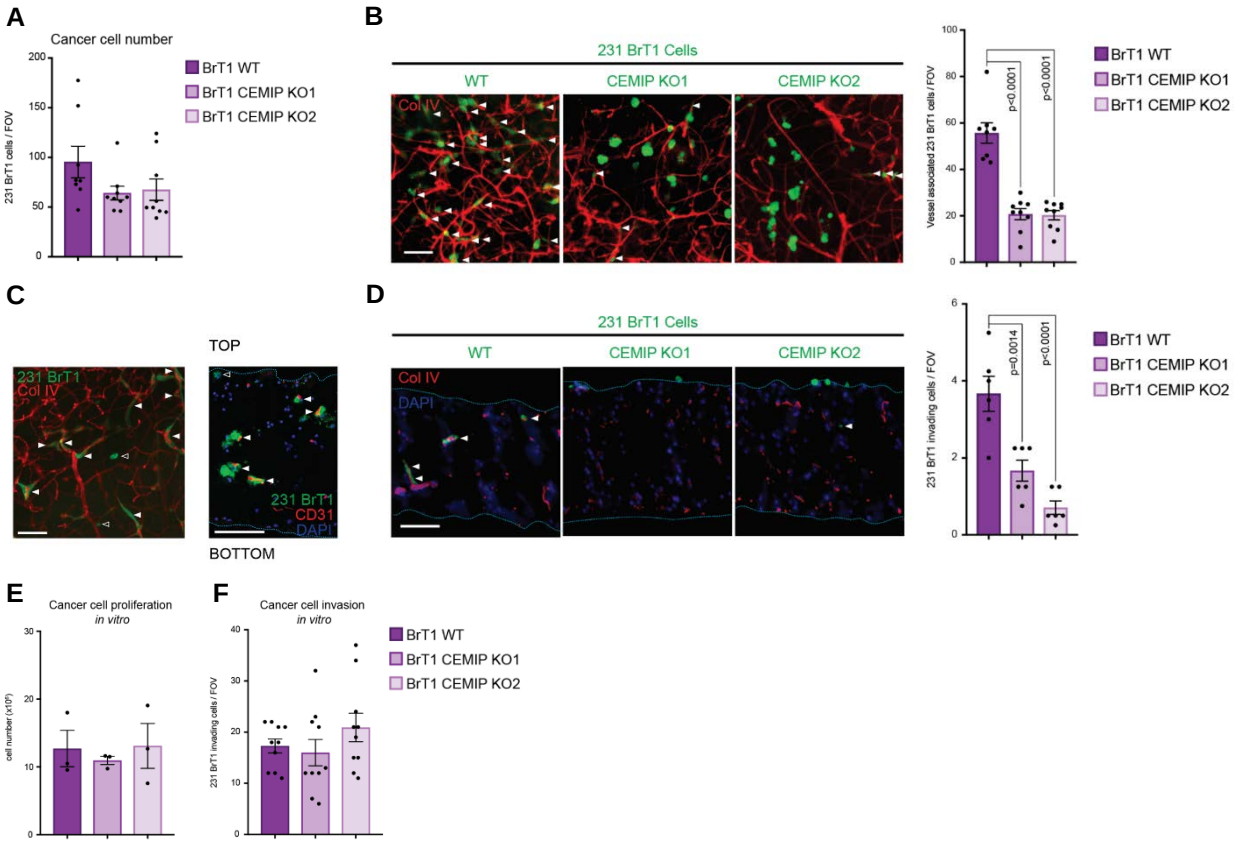

Figure 6. Tumor CEMIP promotes cancer cell vascular co-option and invasion. A, Quantification of BrT1 WT and 231 BrT1 CEMIP-KO1 and -KO2 GFP⁺ cell number on top of brain slices. **B**, Left, representative fluorescence microscopy images of vessel association of GFP-expressing BrT1 wild-type (WT, control cells with WT CEMIP expression) or GFP-expressing BrT1 CEMIP knockout (KO1 and KO2) cells growing on top of brain slices. Brain vasculature is shown by Col IV⁺ staining (red, all fluorescent images in Fig. 6b and d). Cells with spindle-like morphology and spread along vasculature (white arrows) were considered vessel-associated. Right, quantification of vessel-associated cancer cell number. **C**, Left, representative fluorescence microscopy image of BrT1 GFP⁺ cells growing on top of the brain slice. Right, representative fluorescence microscopy image of BrT1 GFP⁺ cells invading the brain slice in transversal section. **D**, Left, representative fluorescence microscopy images of BrT1 WT, BrT1 CEMIP-KO1, and CEMIP-KO2 GFP⁺ cells invading brain slices. Cancer cells were considered invasive when migrating inwards past the top cell layer of the brain slice (white arrows). Dotted blue lines delineate the top and

bottom limits of the slice. Right, quantification of invading cancer cell number. **E**, Quantification of proliferation of BrT1 WT and BrT1 CEMIP-KO1 and -KO2 cells *in vitro* over three days. **F**, Quantification of transwell Matrigel invasion of BrT1 WT and BrT1 CEMIP-KO1 and -KO2 cells *in vitro* over 24 hours. The number of cells per FOV are averages ± SEM, from *n* = 8, 9, 9 (**A**), *n* = 8, 9, 9 (**B**), or *n* = 6 (**D**) individual brain slices, scoring two fields per slice; and the number of invading cells per FOV are averages ± SEM, from *n* = 3 individual transwell cultures (**F**), scoring a representative field per transwell membrane. One of three (**A**, **B**, **D**) independent biological replicates is shown. Graphs depicting in vitro proliferation and invasion (**E**, **F**) display three independent biological replicates. Immunofluorescence brain slice images (**C**) are representative of three independent biological replicates. Brain slice sections are stained with DAPI, shown in blue (**D**). Scale bars, 100µm (**B** - **D**). Error bars depict mean ± SEM. *P* values were calculated by ANOVA (**A**, **B**, **D** - **F**).

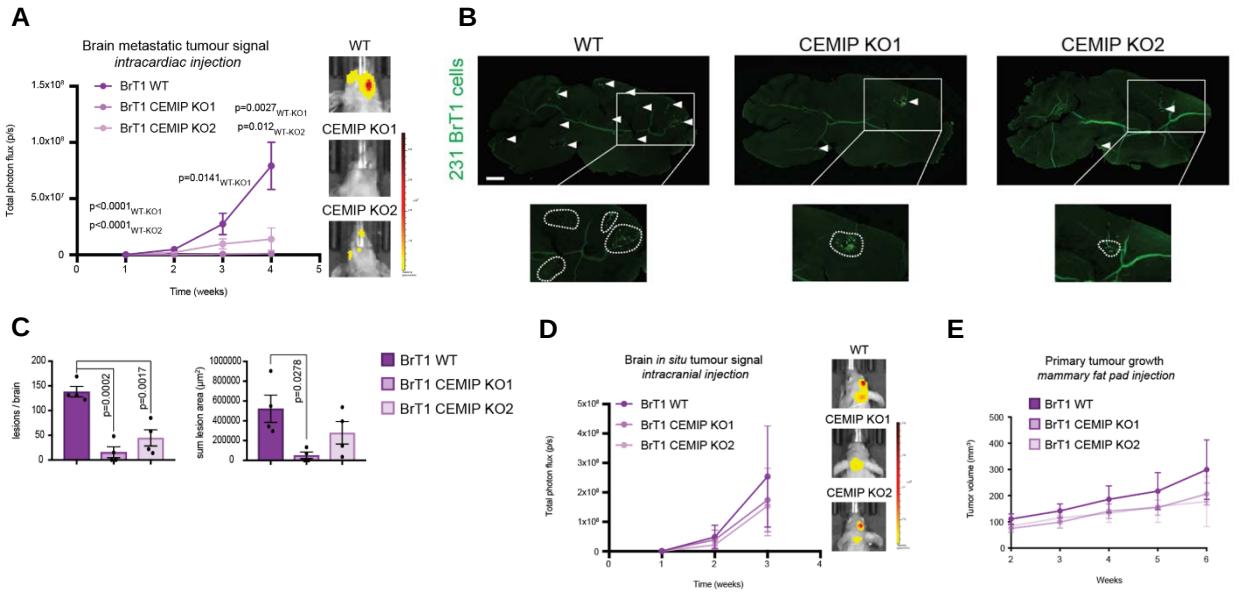

Figure 7. Tumor CEMIP drives brain metastasis *in vivo*. **A**, Quantification of brain metastasis in mice intracardiacally injected with BrT1 WT or CEMIP-KO cells by analysis of cranial bioluminescence signal (Total photon flux – photons/ second (p/s)) in mice over 4 weeks post-intracardiac injection of GFP-labelled BrT1 WT or BrT1 CEMIP-KO luciferase-positive cells and representative IVIS image of brain signal at week 4. **B**, Representative immunofluorescence images of whole brain sagittal sections from mice with brain metastatic lesions after 4 weeks (green, white arrows). **C**, Quantification of the number of lesions per brain (left graph) and total brain metastatic lesion area (µm^2, right graph). The number of lesions and total metastatic area per brain represent averages ± SEM, scored from lesions in two sagittal brain sections from different brain areas per mouse, and *n* = 4, 5, 5 mice per group. **D**, Left, quantification of brain metastatic in situ growth in mice intracranially injected with BrT1 WT or BrT1 CEMIP-KO cells. Cranial bioluminescence signal (Total photon flux – photons/ second (p/s)) in mice over 3-weeks post-intracranial injection of GFP-labelled BrT1 WT or BrT1 CEMIP-KO luciferase-positive cells. Right, representative IVIS

image of brain signal at week 3. **E**, Quantification of primary tumor growth in mice injected with BrT1 WT or BrT1 CEMIP-KO cells. Scale bar, 1mm (**B**). Error bars depict mean ± SEM. *P* values were calculated by ANOVA (**A**, **C** - **E**). One representative experiment of two is shown (**A** - **C**), and one experiment with *n* = 5 mice per experimental group was performed for **D** and **E**.

Exosomal CEMIP promotes tumor cell colonization of the brain

To evaluate the relative contributions of exosomal and cellular CEMIP to BrM, we investigated whether exosomal CEMIP was sufficient to rescue brain colonization, invasion and vascular co-option by 231 BrT1 CEMIP KO cells. Brain slice pre-treatment with 231 BrT1 CEMIP WT-derived exosomes induced a four-fold and two-fold increase in colonizing 231 BrT1 CEMIP KO2 cell number compared to PBS and CEMIP KO exosome pre-treatment, respectively (Fig. 8a). More importantly, brain slice pre-treatment with 231 BrT1 CEMIP WT-derived exosomes restored 231 BrT1 CEMIP KO2 vascular co-option, and their characteristic spindle-like phenotype (Fig. 8b, white arrows). Whereas 231 BrT1 CEMIP WT-derived exosomes increased cancer cell vascular co-option over two-fold, pre-treatment with CEMIP KO1 or KO2 exosomes did not (Fig. 8b). Moreover, pre-treatment with 231 BrT1 CEMIP WT-derived exosomes increased 231 BrT1 CEMIP KO2 invasion by three-fold compared to PBS and CEMIP KO exosome pre-treatment (Fig. 8c). These results suggest that exosomal CEMIP supersedes cellular CEMIP in promoting adaptation to the brain microenvironment *via* vascular co-option, ultimately supporting successful invasion and metastatic colonization of the brain.

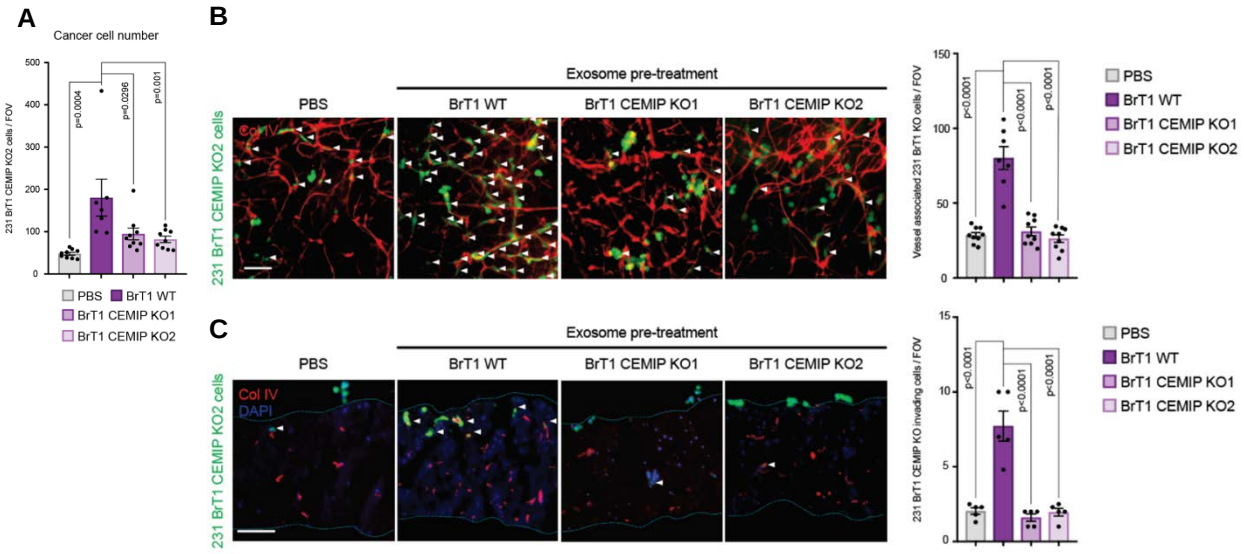

Figure 8. Exosomal CEMIP modulates the brain vascular niche to support vascular co-option and invasion. A, Quantification of BrT1 KO2 GFP+ cells on top of brain slices pre-treated with exosomes or PBS. **B**, Left, representative fluorescence microscopy images of vessel association of BrT1 CEMIP-KO2 GFP^+ cells growing on top of brain slices pre-treated with exosomes or PBS. White arrows indicate vasculature-associated cancer cells. Right, quantification of vessel-associated cancer cell number. **C**, Left, representative fluorescence microscopy images of BrT1 CEMIP-KO2 GFP^+ cells invading (white arrows) brain slices pre-treated with exosomes or PBS. Dotted blue lines delineate the top and bottom limits of the brain slice. Right, quantification of invading cancer cell number. Brain vasculature is shown by Col IV+ staining (red, all fluorescent images in Fig. 8b and c). Brain slice sections are stained with DAPI, shown in blue (**C**). Scale bar, 100µm (**B**, **C**). The number of cells per FOV are averages ± SEM, from *n* = 9, 7, 9, 9 (**A**, **B**), or *n* = 5 (**C**) individual brain slices, scoring two fields per slice. One of three (**A** - **C**) independent biological replicates is shown. Error bars depict mean ± SEM. *P* values were calculated by ANOVA (**A** - **C**).

To determine if exosomal CEMIP affects BrM *in vivo*, we evaluated if pre-treatment of mice with 10µg of 231 BrT1 CEMIP WT or CEMIP KO-derived exosomes every other day intravenously for three weeks prior to intracardiac injection of 231 BrT1 GFP-luciferase$^+$ cells enhanced BrM in a CEMIP-dependent manner. This approach mimics the systemic release of a tumor exosomes in a physiological manner equivalent to a growing primary tumor during pre-metastatic phase [17]. Pre-treatment with 231 BrT1 CEMIP WT-derived exosomes significantly boosted BrM compared to CEMIP KO1 and KO2 exosome pre-

treatments at week one and two post-injection (Fig. 9a), ultimately normalizing over time since emerging CEMIP$^+$ WT cells produce CEMIP$^+$ exosomes. Quantification of brain lesions revealed an increase in metastatic foci number and metastatic burden in CEMIP WT exosome pre-treated mice compared to PBS and one of the CEMIP KO exosome pre-treated groups (Fig. 9b).

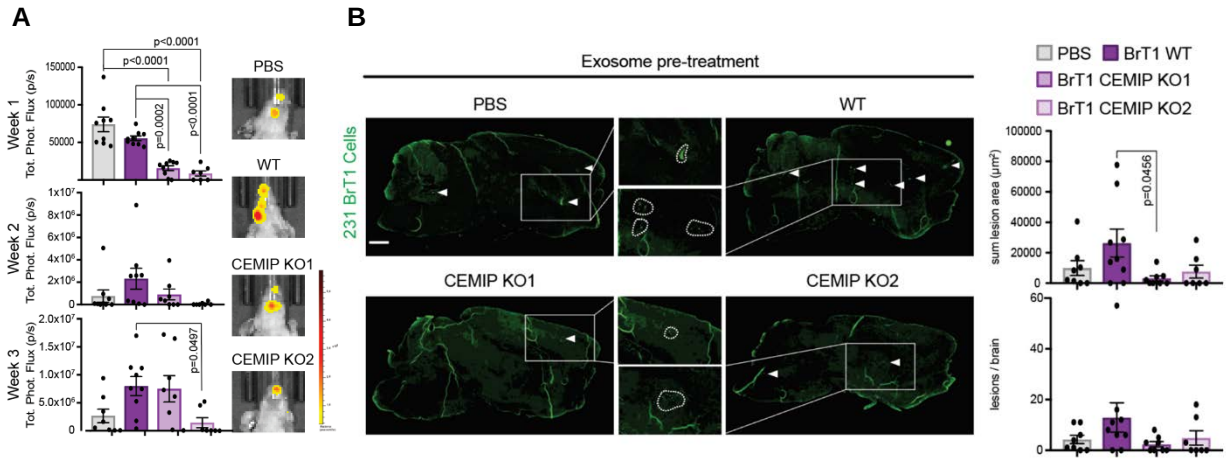

Figure 9. Exosomal CEMIP supports brain metastasis *in vivo*. A, Quantification of brain metastasis in mice pre-educated with exosomes or PBS by analysis of cranial bioluminescence signal (Total photon flux – photons/ second (p/s)) in mice educated for 3 weeks with exosomes or PBS, followed by intracardiac injection of GFP-labelled BrT1 luciferase-positive cells, and representative IVIS image of brain signals at week 3 post-cell injection. **B**, Left, representative immunofluorescence images of whole brain sagittal sections from mice showing GFP+ brain metastases (green, white arrows), 3 weeks post-cell injection. Right, quantification of total brain metastatic lesion area (µm^2, upper graph) and number of lesions per brain (lower graph), representing averages ± SEM scored from lesions in two sagittal brain sections representative of different brain areas per mouse, with *n* = 9, 9, 9, 7 mice per group. Scale bar, 1mm (**B**). Error bars depict mean ± SEM. *P* values were calculated by ANOVA (**A**, **B**). One representative experiment of two is shown (**A**, **B**).

Collectively, these data support a pro-metastatic role of exosomal CEMIP *in vivo* during the early stages of colonization and demonstrate that exosomal CEMIP promotes BrM *in vivo*. These results are in accordance with our *ex vivo* observations, which revealed the role of exosomal CEMIP upon the brain vascular niche in facilitating tumor cell vascular co-option.

CHAPTER VI

Exosomal CEMIP-dependent mechanisms underlying brain vascular niche reshaping

Specific aims

Our findings suggest that exosomal CEMIP drives brain metastasis and micrometastatic seeding through effects on endothelial cells and the brain vascular niche, facilitating cancer cell vascular co-option and invasion. Therefore, we set out to characterize the molecular mechanisms underlying the functions of exosomal CEMIP in brain metastatic colonization by determining their effects on endothelial cells and microglia, crucial components of the brain vascular niche.

The specific aims for this chapter are as follows:

a. characterize the function of CEMIP in the metastatic brain vascular niche

b. evaluate the effect of presence/absence of CEMIP for brain vascular niche remodeling

c. characterize the interaction and effects of brain metastatic exosomes and exosomal CEMIP on the gene expression of endothelial cells and microglia

d. identify the main pathways triggered by exosomal CEMIP in endothelial cells and microglia from the brain vascular niche

Exosomal CEMIP stimulates vascular remodeling

Since our findings suggest a critical role for tumor exosomes and exosomal CEMIP in reshaping of the brain vascular niche to allow successful metastatic colonization, we sought to characterize the vasculature of brain metastases formed by cancer cells lacking CEMIP. *In vivo*, in contrast to the surrounding normal brain tissue (empty white arrow), 231 BrT1 brain metastases had altered, morphologically heterogeneous vasculature with enlarged and dilated vessels (Fig. 1a, full white arrows), characteristic of metastatic lesions in the brain [102], while 231 BrT1 CEMIP KO metastatic lesions displayed significantly smaller vessel diameter, similar to the surrounding non-metastatic brain tissue (Fig. 1a). These findings support a functional role for tumor cell-derived CEMIP in the remodeling of brain vasculature.

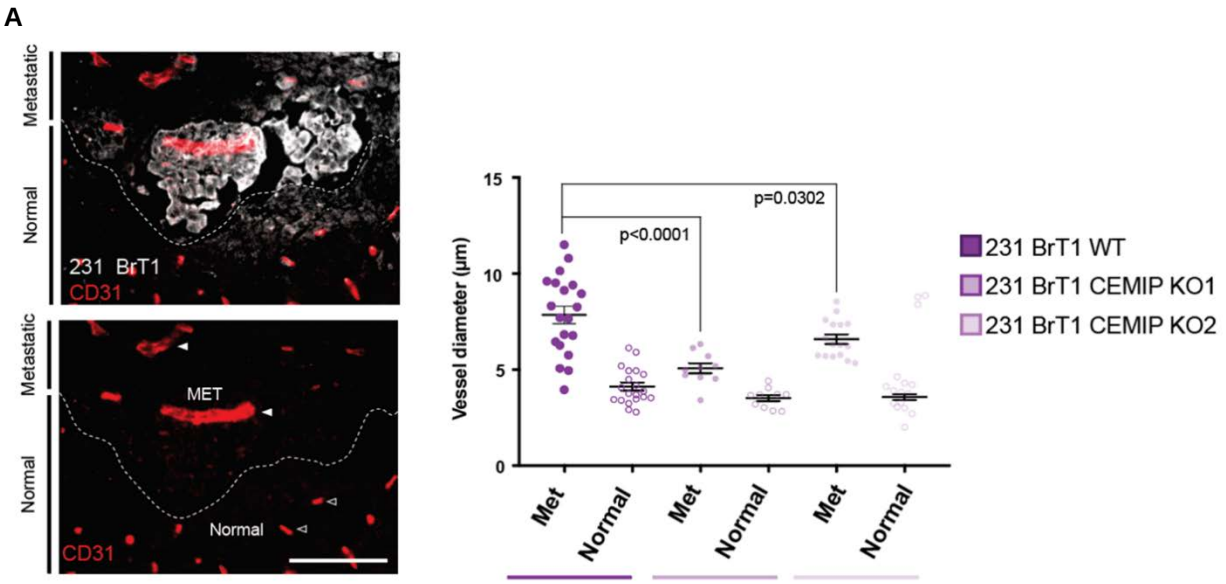

Figure 1. Tumoral CEMIP contributes to vascular remodeling *in vivo*. A, Left, representative fluorescence image of tumor vasculature (red) in BrT1 brain metastases (white). Right, quantification of metastatic tumor and normal vessel diameter in brains from mice injected intracardiacally with BrT1 WT, BrT1 CEMIP-KO1 or -KO2 cells. Individual vessel diameter was obtained from the average of three measurements along the extension of the vessel. Metastatic tumor and normal brain vascular diameters were scored in up to 5 individual metastatic lesions across two sagittal sections from different brain areas per individual presenting brain metastases, *n* = 4 mice were analyzed per group. Graph depicting tumor vasculature diameter displays the average of two independent biological replicates. Scale bar, 100µm. Error bars depict mean ± SEM. *P* values were calculated by ANOVA.

To determine whether exosomal CEMIP pre-conditioning led to vascular remodeling, we pre-treated murine BrEC *in vitro* with 10 µg of exosomes from CEMIP loss or gain of function models and, 24 hours later, evaluated vascular network formation in a 3D endothelial tube formation (ETF) assay (Fig. 2a). To test if high exosomal CEMIP levels were sufficient to support vascular network formation, we overexpressed CEMIP in 231 parental cells (231 parental CEMIP OE) and their exosomes (Fig. 2b). Pre-treatment with 231 parental CEMIP OE and 231 BrT1 CEMIP WT-derived exosomes promoted ETF, increasing the number and size of endothelial cell branches formed compared to 231 parental control and 231 BrT1 CEMIP KO exosomes (Fig. 2c, top graphs). Consistent with these metrics, pre-treatment with exosomal CEMIP also increased segment junction number and decreased isolated segment number (Fig. 2c, bottom graphs).

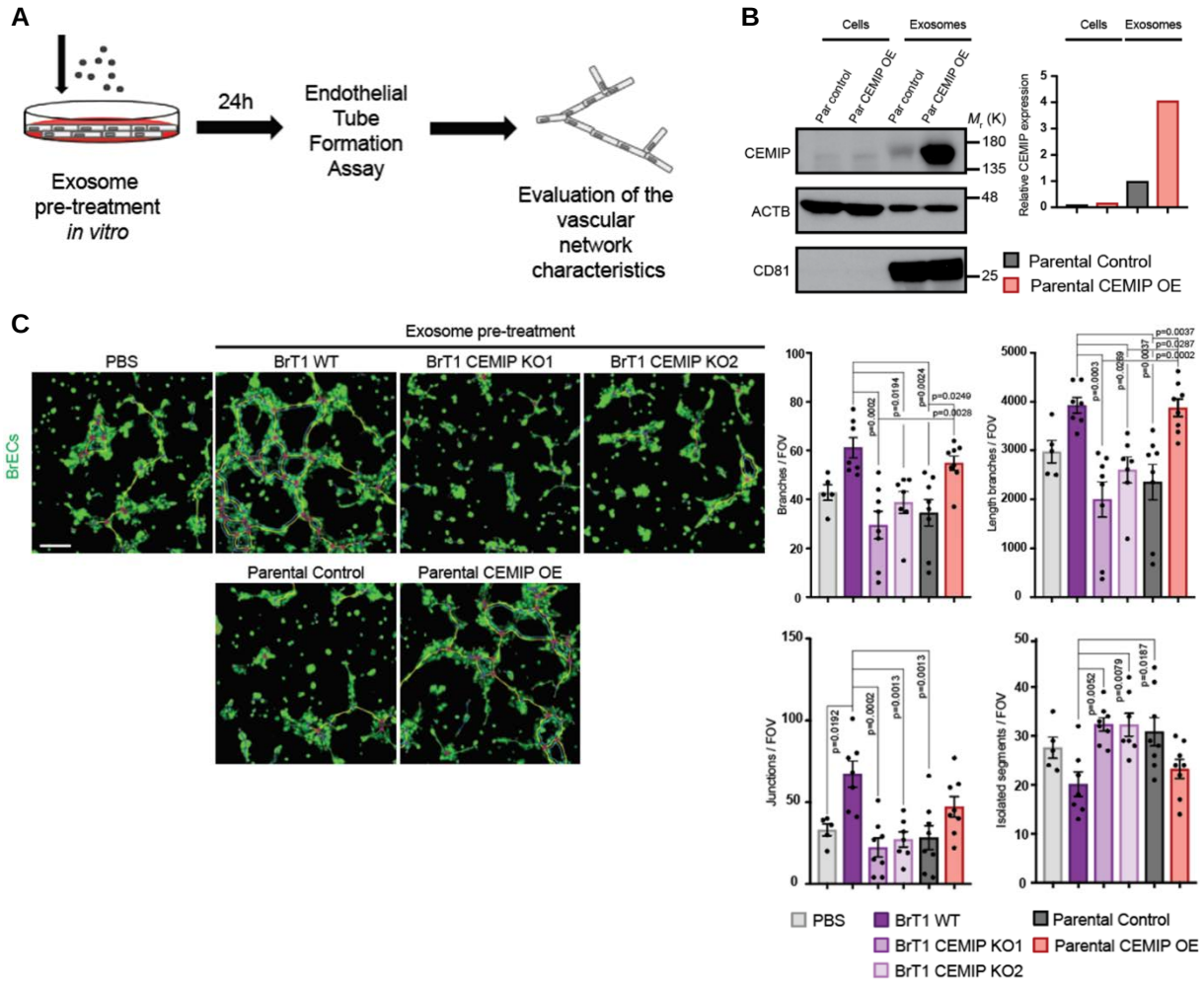

Figure 2. Exosomal CEMIP affects BrEC biology and induces vascular remodeling *in vitro*. A, Schematic of the ETF assay setup for studying exosome-dependent vascular network formation by BrECs. **B**, Left, immunoblot of CEMIP expression in cells and exosomes of 231 parental Control and 231 parental CEMIP overexpressing (OE) models generated. **C**, Left, representative images of calcein AM-loaded BrEC vascular networks (green) formed *in vitro* upon pre-treatment with exosomes or PBS. Vascular tree general topology is depicted by identification of the tree's master junctions (red) and master segments (yellow). Right, quantification of vascular network branch number (top left graph), length (top right graph), junction (bottom left graph) and isolated segment number (bottom right graph). The branch number, length of branches, number of junctions and isolated segments per FOV are averages ± SEM, from *n* = 5, 7, 8, 7, 8, 8 individual µ-slide wells (**C**), scoring a representative field per well. A representative experiment is shown from three independent biological replicates (**B**, **C**). Scale bar, 100µm (**C**). Error bars depict mean ± SEM. *P* values were calculated by ANOVA (**C**).

Exosomal CEMIP induces a pro-inflammatory vascular niche that supports metastasis

To dissect the molecular changes elicited by exosomal CEMIP during brain vascular niche remodeling, we analyzed the gene expression profiles of brain cells uptaking tumor exosomes, endothelial cells and microglia, the latter often observed in close contact with the brain vasculature (Chapter IV, Fig. 5c, double white arrow) and known to play critical roles during vascular remodeling and dysfunction [103]. We isolated exosome-positive BrEC ($CD45^-$ $CD31^+$) and microglia ($CD45^+$ $CD11b^{low}$ $CD49d^{low}$) from brain slices pre-conditioned with 5 µg of fluorescently-labelled exosomes from either 231 BrT1 CEMIP WT or 231 BrT1 CEMIP KO cells and analyzed gene expression changes by RNA sequencing (Fig. 3a). We observed no difference between the uptake of fluorescently-labelled 231 BrT1 CEMIP WT or 231 BrT1 CEMIP KO exosomes (Fig. 3b), indicating that ensuing gene expression differences are not due to differential binding or uptake of exosomes. Correspondingly, when analyzing the adhesion of exosomes to brain endothelial cells, identified as the major cell type in the brain interacting with this class of tumor EVs (Fig. 3c), we observed no difference between the adhesion of exosomes isolated from 231 BrT1 CEMIP WT and CEMIP KO cells to $CD31^+$ endothelial cells as evaluated by immunofluorescence analysis (Fig. 3d).

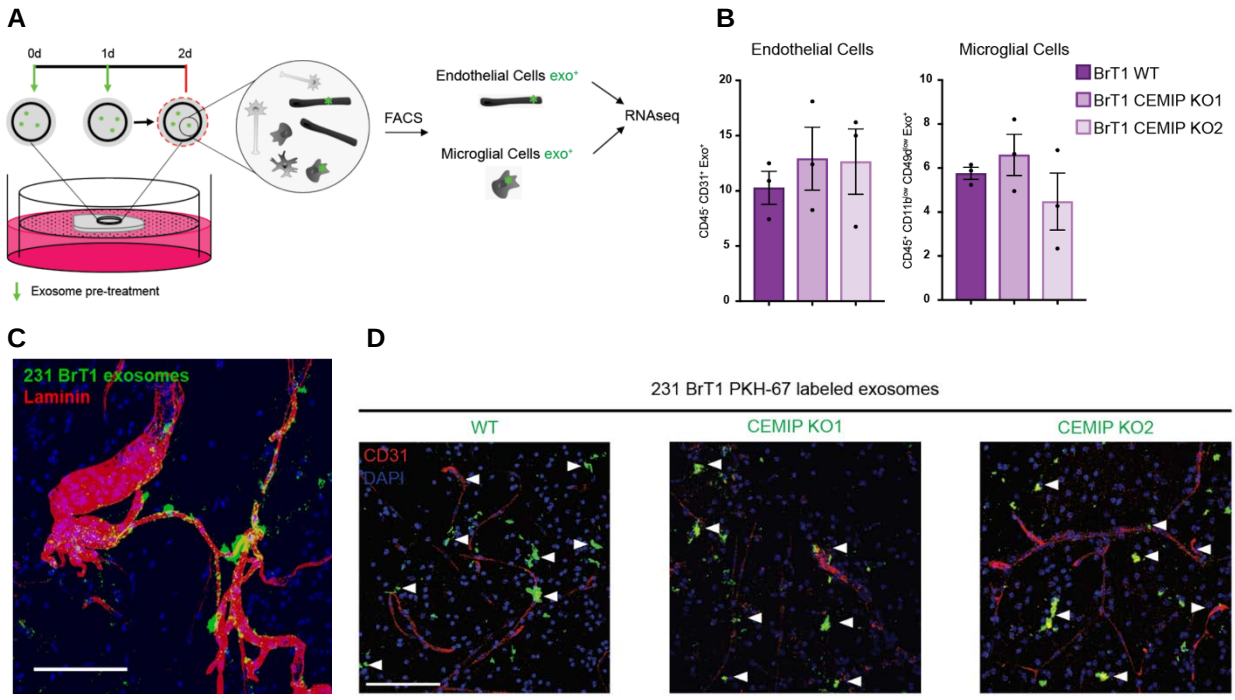

Figure 3. Isolation of brain vascular niche cells interacting with tumor exosomes and characterization of exosomal CEMIP-dependent uptake. A, Schematic of the brain slice model setup for studying exosome-induced gene expression changes in stromal cells of the brain. Brain slices were pre-treated with BrT1 WT, BrT1 CEMIP-KO1 or -KO2 cell-derived fluorescently-labelled exosomes. **B**, Flow cytometry analysis of exosome uptake. Percentage of exosome-positive (Exo^+) endothelial ($CD45^-$ $CD31^+$) and microglial ($CD45^+$ $CD11b^{low}$ $CD49d^{low}$) cells in brain slices is shown. **C**, Representative confocal image of the prevalent interaction between fluorescently-labelled BrT1 tumor exosomes (green) and vessels ($Laminin^+$, red) in the brain slice. **D**, Representative confocal images of the adhesion of fluorescently-labelled BrT1 WT, BrT1 CEMIP-KO1 or -KO2 exosomes to endothelial cells ($CD31^+$) in the brain slice. Arrows indicate co-localization of exosomes (green) with endothelial cells (red). Graphs depicting endothelial and microglial cell exosome uptake (**B**) display the average of three independent biological replicates. Immunofluorescence confocal images of the interaction and BrEC exosome uptake in the brain slice (**C**, **D**) are representative of three independent biological replicates. Scale bars, 100µm (**C**) and 75µm (**D**). Error bars depict mean ± SEM. *P* values were calculated by ANOVA (**B**).

Analysis of gene expression changes induced by brain metastatic-derived exosomes in both endothelial cells and microglia (Fig. 4a) suggested activation of several signaling pathways related to inflammation and cancer metastasis. To identify genes modulated by exosomal CEMIP, we first focused on genes significantly altered by pre-treatment with

231 BrT1 CEMIP WT-derived exosomes compared to the PBS control and then on the genes that showed significant and concordant difference in expression when compared to pre-treatment with both 231 BrT1 CEMIP KO exosomes. Pre-treatment with 231 BrT1-derived exosomes changed the expression levels of 286 endothelial cell genes and 193 microglial genes (Fig. 4a), with a higher proportion of CEMIP-dependent changes in BrEC *versus* microglia (119 versus 25 genes, respectively; Fig. 4b, c).

Gene ontology analysis of genes with altered expression upon CEMIP^{+} exosome treatment identified blood vessel morphogenesis and lymphangiogenesis as the second and third most significantly affected processes in BrECs (Fig. 5a), while inflammatory responses were the top most significantly affected biological process in exosome-positive microglia (Fig. 5a). Ingenuity Pathway Analysis (IPA) identified 14 pathways significantly affected by exosomal CEMIP in BrEC, half of which were inositol-related pathways, which CEMIP impacts through intracellular calcium release [95, 104] (Fig. 5b). CEMIP-dependent calcium signaling governs numerous cellular processes relevant for vascular remodeling and angiogenesis, such as cell migration and Wnt signaling [96, 105], suggesting these gene expression changes may underlie the exosome-dependent vascular phenotypes we observed. Other CEMIP-dependent pathways were osteoarthritis (*Tcf7l1, Acvrl1, P2rx7, Prkab2* and *Sp1*), an inflammatory condition modulated by CEMIP as well as gap junction signaling (*Gja1, Npr2. Adcy4* and *Sp1*), and several adhesion molecules (e.g. *Efnb2, Nedd9, Itgb3, Acvrl1, Farp1, Synm, Sema6d, Ocln,* etc.), with roles in vascular remodeling and endothelial cell-cell contacts (Fig. 4b and Fig. 5b). In microglia, IPA identified 69 exosomal CEMIP-dependent pathways, related to inflammation, immune regulation through cell adhesion, diapedesis (*Ccl5, Cxcl10, Cxcl1, Tnf and Tnfrsf1b*), and neuroinflammation (*Ccl5, Cxcl10, Ptgs2, Syk and Tnf*) (Fig. 4b and Fig. 5b).

A

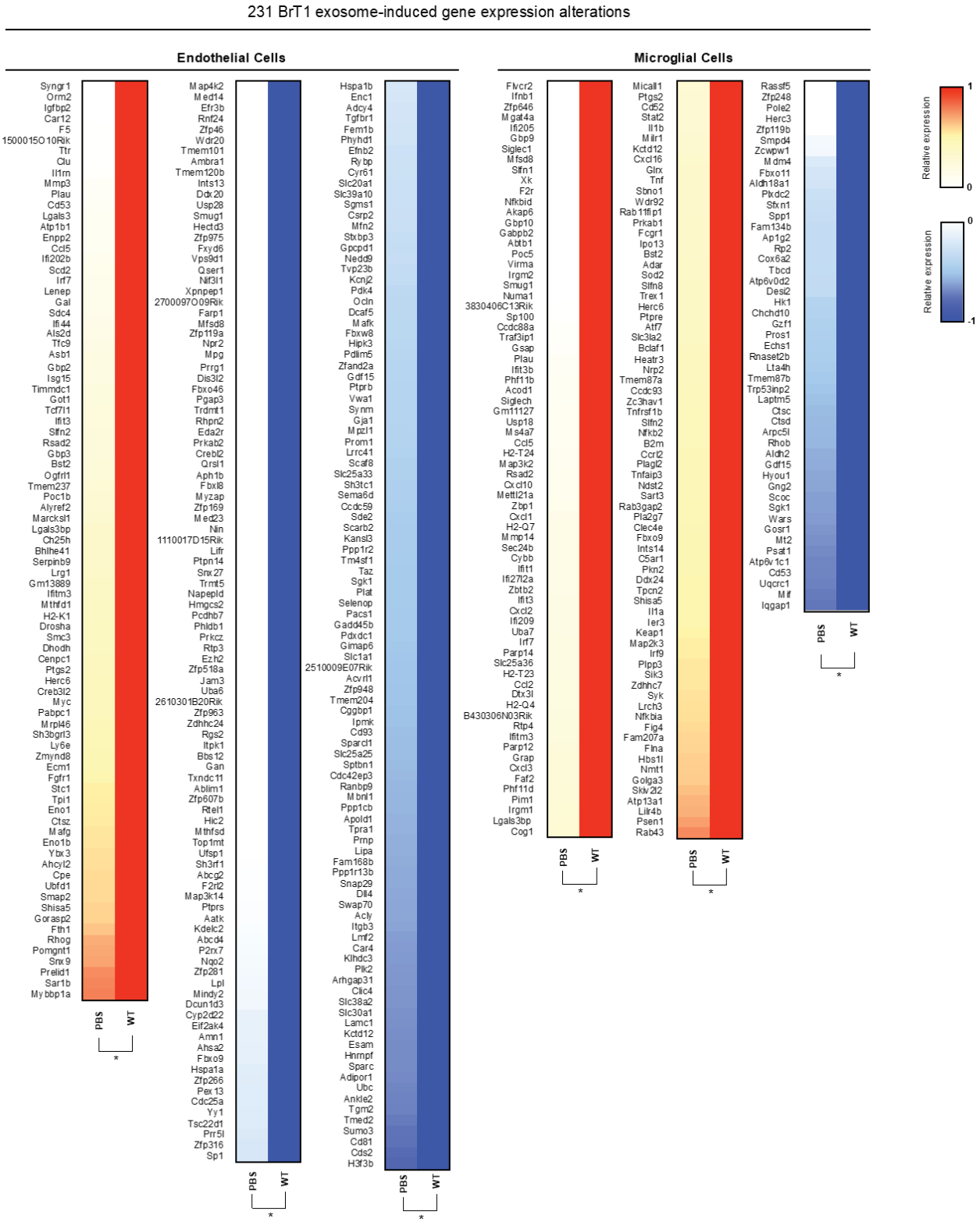
231 BrT1 exosome-induced gene expression alterations
Endothelial Cells
Microglial Cells
Relative expression
1
0
Relative expression
0
-1
PBS
WT
*

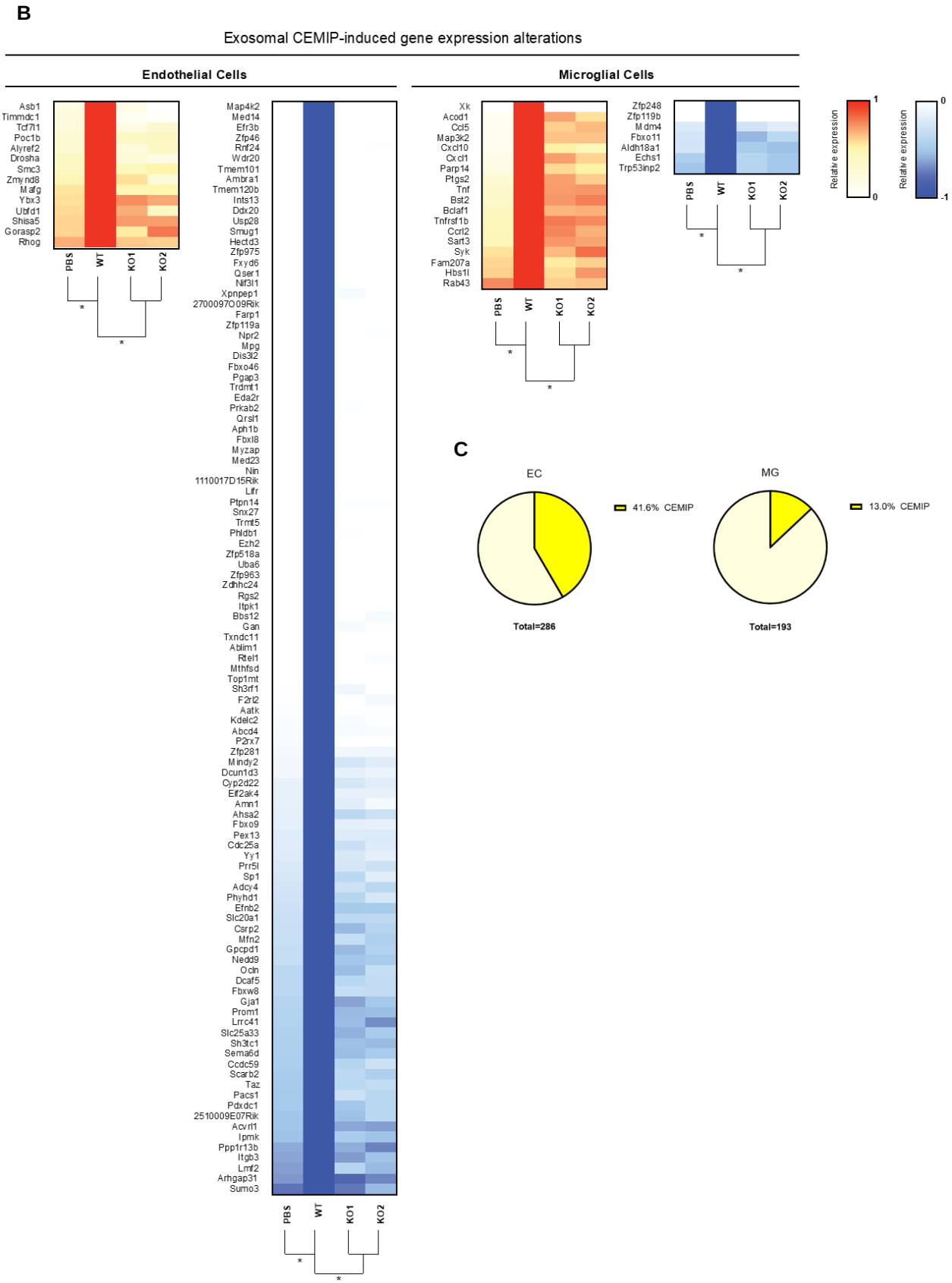
B
Exosomal CEMIP-induced gene expression alterations
Endothelial Cells
Microglial Cells
Asb1
Timmdc1
Tcf7l1
Poc1b
Alyref2
Drosha
Smc3
Zmynd8
Mafg
Ybx3
Ubfd1
Shisa5
Gorasp2
Rhog
PBS
WT
KO1
KO2
Map4k2
Med14
Efr3b
Zfp46
Rnf24
Wdr20
Tmem101
Ambra1
Tmem120b
Ints13
Ddx20
Usp28
Smug1
Hectd3
Zfp975
Fxyd6
Qser1
Nlf3l1
Xpnpep1
2700097O09Rik
Farp1
Zfp119a
Npr2
Mpg
Dis3l2
Fbxo46
Pgap3
Trdmt1
Eda2r
Prkab2
Qrsl1
Aph1b
Fbxl8
Myzap
Med23
Nin
1110017D15Rik
Lifr
Ptpn14
Snx27
Trmt5
Phldb1
Ezh2
Zfp518a
Uba6
Zfp963
Zdhhc24
Rgs2
Itpk1
Bbs12
Gan
Txndc11
Ablim1
Rtel1
Mthfsd
Top1mt
Sh3rf1
F2rl2
Aatk
Kdelc2
Abcd4
P2rx7
Zfp281
Mindy2
Dcun1d3
Cyp2d22
Eif2ak4
Amn1
Ahsa2
Fbxo9
Pex13
Cdc25a
Yy1
Prr5l
Sp1
Adcy4
Phyhd1
Efnb2
Slc20a1
Csrp2
Mfn2
Gpcpd1
Nedd9
Ocln
Dcaf5
Fbxw8
Gja1
Prom1
Lrrc41
Slc25a33
Sh3tc1
Sema6d
Ccdc59
Scarb2
Taz
Pacs1
Pdxdc1
2510009E07Rik
Acvrl1
Ipmk
Ppp1r13b
Itgb3
Lmf2
Arhgap31
Sumo3
Xk
Acod1
Ccl5
Map3k2
Cxcl10
Cxcl1
Parp14
Ptgs2
Tnf
Bst2
Bclaf1
Tnfrsf1b
Ccrl2
Sart3
Syk
Fam207a
Hbs1l
Rab43
Zfp248
Zfp119b
Mdm4
Fbxo11
Aldh18a1
Echs1
Trp53inp2
Relative expression
1
0
-1
C
EC
41.6% CEMIP
Total=286
MG
13.0% CEMIP
Total=193

Figure 4. Gene expression alterations induced in BrECs and microglia by brain metastatic exosomes and exosomal CEMIP. A, Heatmap of significant genes differentially expressed in brain endothelial and microglial cells following 231 BrT1 exosome treatment. The relative color scheme is based on the fold-change between the expression values of the PBS condition relative to the WT for each gene. The gene list is ordered from the largest to smallest fold difference, first for upregulated (white-red) and then for downregulated (white-blue) genes. High/Low expression is represented by red and blue, respectively. **B**, Heatmap of significant genes differentially expressed in brain endothelial and microglial cells following exosomal CEMIP treatment. The relative color scheme is based on the fold-change between the expression values of each condition relative to WT for each gene. The gene list is ordered from the largest to smallest fold difference, first for upregulated (white-red) and then for downregulated (white-blue) genes. High/Low expression is represented by red and blue, respectively. **C**, Pie chart depicting the percentage of CEMIP-dependent differentially expressed genes within all genes affected by 231 BrT1 brain metastatic exosome treatment in BrECs and microglia. Data used to generate the heatmaps of differentially expressed genes in FACS-isolated BrECs and microglia from exosome-treated brain slices (**A**, **B**) display average of three independent biological replicates. Student's t-test was used as statistical test (**A**, **B**).

A

GeneSet Analysis:
Gene Ontology – Top 3 Biological Processes – EC – exosomal CEMIP specific

Rank	GO Acc. and Desc.	p-value
1	GO:0010628	3.12E-04
	positive regulation of gene expression	
2	GO:0048514	3.83E-04
	blood vessel morphogenesis	
3	GO:0001946	1.12E-03
	lymphangiogenesis	

GeneSet Analysis:
Gene Ontology – Top 3 Biological Processes – MG – exosomal CEMIP specific

Rank	GO Acc. and Desc.	p-value
1	GO:0006954	1.16E-06
	inflammatory response	
2	GO:0031622	4.56E-06
	positive regulation of fever generation	
3	GO:0006952	1.43E-04
	defense response	

B

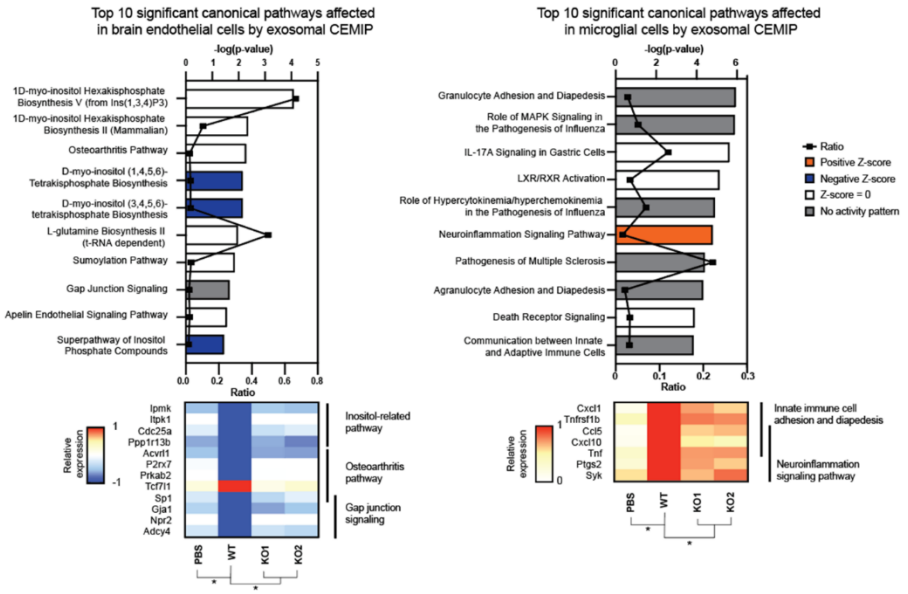

Figure 5. Gene ontology and IPA canonical pathways triggered by exosomal CEMIP in BrECs and microglia. A, Top 3 significant biological processes affected by exosomal CEMIP in BrECs and microglia identified by GeneSet gene ontology analysis. **B**, Highest ranked significant canonical pathways altered upon exosomal CEMIP treatment defined by IPA analysis. Top, pathways affected by exosomal CEMIP in BrECs (left) and microglia (right) isolated from exosome-treated brain slices. Z-score indicates activation (orange) or inhibition (blue), and ratio indicates number of genes from the CEMIP list that map to a pathway divided by the total number of genes that map to that same pathway. Associated *P* value of the Fisher's exact test is displayed in black. Bottom, heatmap of differentially expressed genes involved in selected pathways. The average of three independent biological replicates is displayed. *P* values were calculated by Fisher's exact test (chart) and two-sided Student's t-test (heatmap) (**B**).

Taken together, these data demonstrate that exosomal CEMIP affects molecular pathways in BrEC and microglia implicated in BrM that may underlie reshaping of the brain vascular niche and pre-metastatic niche formation, therefore accounting for the pro-metastatic effects supporting brain metastatic colonization.

CHAPTER VII

CEMIP as a biomarker of brain metastasis

Specific aims

Given the functions described for exosomal CEMIP in BrM using human cancer cell models and a combination of distinct *in vivo*, *ex vivo*, and *in vitro* models, we decided to investigate the correlation between CEMIP protein levels in tissues and exosomes collected from cancer patients with brain metastases.

The specific aims for this chapter are as follows:

a. characterize CEMIP expression in primary tumors and metastatic tumors from different organ sites

b. evaluate the association between CEMIP expression and BrM in cancer patients

c. investigate if CEMIP expression can predict the risk of BrM development and progression in cancer patients

d. characterize CEMIP expression in exosomes from viable metastatic tumor tissues from cancer patients

CEMIP expression is increased in brain metastasis patients

To evaluate a possible association between CEMIP and BrM in humans we first characterized CEMIP expression by immunohistochemistry in tissue microarrays from over 300 samples of primary tumors (PTs) and metastatic tumors (MTs) from breast and lung cancer patients with metastases in the brain, metastases in other organs (e.g. bone, colon, heart, kidney, liver, lung, pleura, skin or stomach) or no metastases. Analysis of brain MTs revealed that CEMIP expression was markedly increased in tumor tissue compared to surrounding brain stroma (Fig. 1a), and specificity of high-CEMIP staining in brain metastatic tumors was further supported by inclusion and analysis of immunohistochemistry staining controls and CEMIP staining in normal brain tissue. Interestingly, CEMIP expression within the tumor tissue was not completely homogeneous, presenting foci of higher expression (Fig. 1b). These foci could be comprised of tumor necrotic areas and associated-immune infiltrates, based on the analysis of the cell and nuclei morphology in the H&E panel. Based on staining intensity, brain MTs were categorized into low (staining score 0-2) or high (staining score >2-4) CEMIP expression (Fig. 1c).

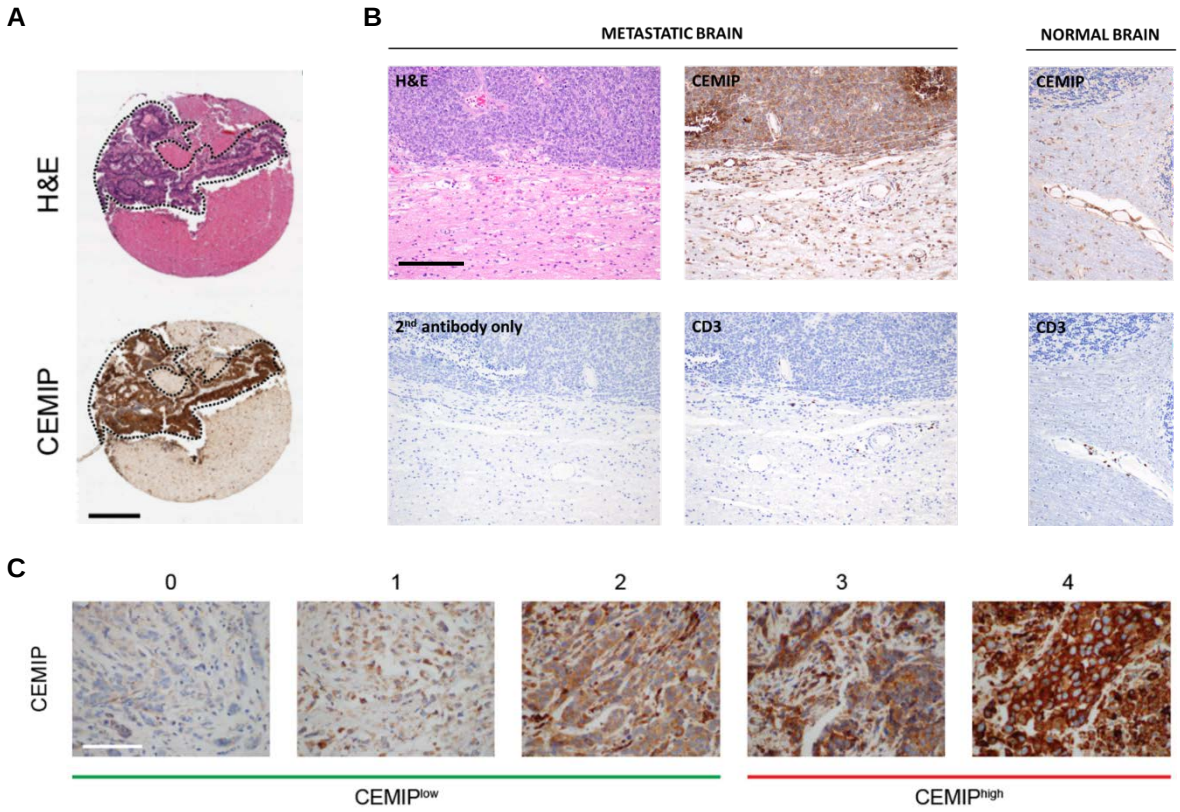

Figure 1. Characterization of CEMIP expression in patient tissue samples by IHC. A, Representative image of a lung cancer brain metastatic tumor patient sample analyzed by H&E (top) and CEMIP immunohistochemistry (bottom). The metastatic tumor is outlined by the black dashed line. **B**, Analysis of CEMIP immunostaining and antibody control stains (no primary antibody control and CD3 antibody control) in patient brain metastatic tissue and normal human brain. **C**, Representative immunohistochemistry images illustrating CEMIP expression for each scoring category in patient tumor samples. Samples with no (0) or low (1 and 2) CEMIP staining were considered $CEMIP^{low}$ (green). Samples displaying high expression (3 and 4) were considered $CEMIP^{high}$ (red). Scale bars, 300µm (**A**), 100µm (**B**) and 50µm (**C**). Immunohistochemistry score represents the average intensity in tumor cores analyzed (1 – 3 per sample) on a scale from 0 to 4 (**C**).

Interestingly, analysis of CEMIP expression in PTs revealed that patients with BrM had significantly higher CEMIP expression ($CEMIP^{high}$ sample percentage: 32.4 for PTs Brain MET versus 12.0 and 13.5 for PTs Non-Brain MET and No MET, respectively; Fig. 2a) than PTs from patients with metastasis to organ sites other than the brain, or without metastasis, indicating PT CEMIP expression levels correlated with BrM but not with non-brain metastasis (Fig. 2b). Moreover, analysis of brain MTs showed significantly higher CEMIP expression compared to MTs from other organs (Fig. 2a). Consistently, more than 40% of brain MTs analyzed were $CEMIP^{high}$, whereas of all non-brain MTs only 7% were $CEMIP^{high}$ (Fig. 2a).

A

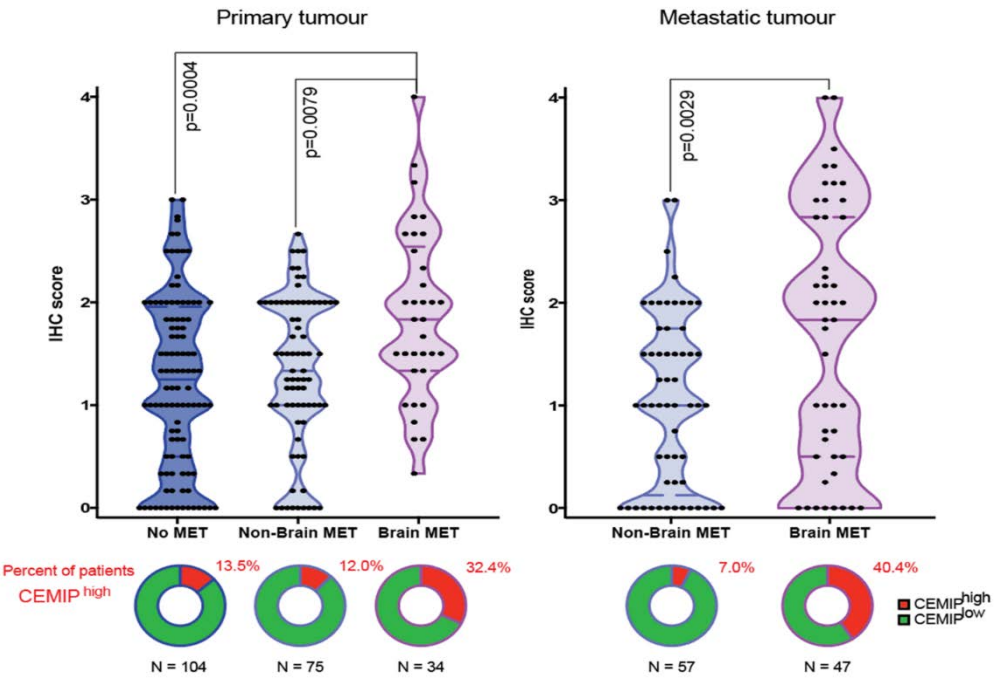

B

		METASTASIS		
			Non-Brain	Brain
CEMIP Expression	Spearman r	0.1598	0.0757	0.2956
	Significance (2-tailed)	* 0.0196	ns 0.3137	*** 0.0004
	Sample size	213	179	138

Figure 2. CEMIP expression is increased in tumors of brain metastasis patients and correlates with BrM. A, Top, quantification of CEMIP expression by immunohistochemistry in primary tumor (left) and metastatic tumor (right) from patients with or without brain metastasis. Bottom, percentage of CEMIP^{high} cases and information on total number of samples evaluated in each group. PT (Minimum: 0.00, 0.00, 0.33; Maximum: 3.00, 2.67, 4.00; and Median: 1.25, 1.33, 1.83), and MET (Minimum: 0, 0; Maximum: 3, 4; and Median: 1.00, 1.83). **B**, Correlation of CEMIP expression in primary tumor samples and metastatic status of patients (any metastasis, non-brain metastasis and brain metastasis). Human data consists of *n*=317 total unique tumor samples (213 primary and 104 metastatic) from 278 breast and lung cancer patients (**A**, **B**). Dashed line across violin plots depicts quartiles and full line depicts median (**A**). *P* values were calculated by ANOVA and two-sided Student's t-test (**A**). **P*<0.05; ***P*<0.01; ****P*<0.001 by Spearman r correlation test (**B**).

CEMIP predicts brain metastasis progression and survival

For patients that developed brain metastases, importantly, high PT CEMIP expression correlated with a shorter latency period for metastasis (Fig. 3a). Moreover, patients with CEMIP^{high} brain MTs had significantly poorer survival compared to patients with CEMIP^{low} brain MTs (Fig. 3b).

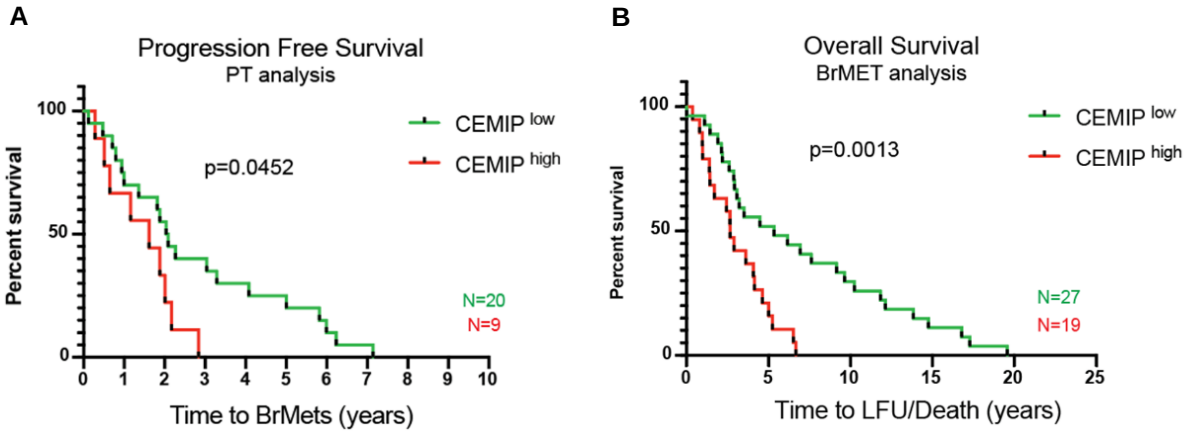

Figure 3. CEMIP tissue expression is a prognostic biomarker of BrM in patients. A, Progression-free survival Kaplan-Meier curve for brain metastasis patients depicting time to brain metastasis based on primary tumor CEMIP expression, low (green) or high expression (red). **B**, Kaplan-Meier survival curve for brain metastasis patients depicting time to last follow up (LFU) or death from time of primary tumor diagnosis based on low (green) or high (red) CEMIP expression in brain metastatic tumor. *P* values were calculated by Log-rank (Mantel-Cox) test (**A**, **B**).

CEMIP is represented in exosomes from viable brain metastatic tumor human samples

Similar to PTs and MTs of patients with brain metastases, CEMIP expression, measured by immunohistochemistry, was higher in cultured brain MT cells (Fig. 4a) whose exosomes also expressed high CEMIP by western blot (Chapter V, Fig. 2b). Evaluation of CEMIP expression in exosomes collected from 24-hour cultures of viable human brain MTs, as well as bone MTs, another common site of metastasis, revealed CEMIP in all human brain MT exosomes examined; but only in one of three bone MT-derived exosomes from lung cancer patients (Fig. 4b, top). Western blot analysis of exosomal CEMIP from surgically resected early stage human NSCLC PTs revealed variable

expression across patients, indicating exosomal CEMIP can be detected in PT-derived samples even at early stages and could therefore inform brain metastatic risk (Fig. 4b, bottom).

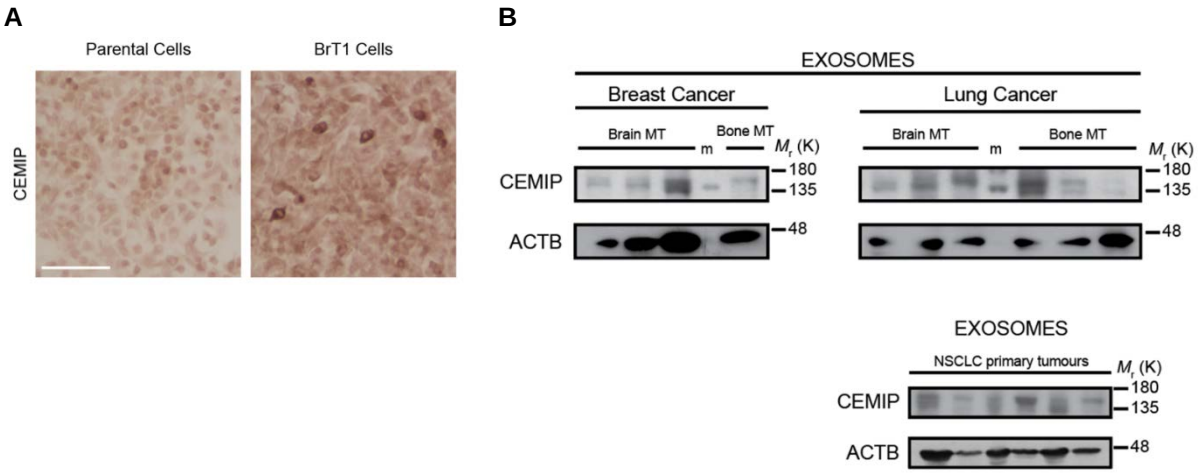

Figure 4. High CEMIP expression found in tumor tissues of BrM patients is reflected at the exosomal level. **A**, Representative image of CEMIP expression in 231 parental and BrT1 cells *in vitro* by immunohistochemistry. **B**, Top, immunoblot of CEMIP expression in exosomes collected from culture of human brain and bone metastatic tissue explants resected from patients (molecular weight marker indicated by "m"). Bottom, immunoblot of CEMIP expression in exosomes collected from culture of human non-small cell lung cancer primary tumor tissue resected from patients. ACTB was used as a loading control in immunoblots. IHC images (**A**) and immunoblots (**B**) are representative of one experiment. Scale bar, 100µm (**A**).

Collectively, our patient data demonstrated that CEMIP is expressed by brain MTs and their exosomes and that high CEMIP expression in PTs is associated with shorter latency to brain metastasis and poor patient survival, constituting a promising BrM biomarker and potential therapeutic target.

CHAPTER VIII

Discussion

Despite increased research interest in the molecular mechanisms driving BrM, there have been few advances in the early diagnosis and therapeutic targeting of this disease. The role of tumor-derived exosomes, emerging players in the interaction between tumor cells and the host microenvironment, remains widely unexplored in the brain metastatic process. Hence, gaining insight into the mechanisms of BrM and the specific contribution of tumor-derived exosomes to this process may open new avenues of investigation with potential clinical applications.

Biodistribution and vascular interaction of brain metastatic exosomes in the brain

In this work, using “sibling” breast cancer cell models with different metastatic tropisms (brain, lung, bone) that share a common cell of origin (parental), we observed that exosomes of brain metastatic cell origin localized more to the brain, in comparison to exosomes from parental, lung and bone metastatic cells. The brain metastatic exosomes also displayed a particular pattern of biodistribution, which is consistent with the vascular endings of major posterior cerebral arteries.

In our work demonstrating that tumor exosomal integrins determined exosome organ distribution and organotropic metastasis, we showed that exosomes from models with distinct metastatic organ specificity prevalently localized to the same organs as their cell of origin but we were only able to identify the exosomal protein signature responsible for this distribution for lung and liver metastatic tropisms [56]. Whereas laminin-binding and RGD/fibronectin-binding integrins determined lung and liver exosome biodistribution, respectively, and were abundant in the exosomes of these models, brain metastatic exosomes packaged few integrins and at low levels, although they were integrins previously associated with BrM: α2, α3, β3 and β1 integrins [44, 92]. These integrins are mainly involved in binding to collagen, but are also known interact with additional ECM molecules such as thrombospondin, tenascin, and others [106, 107]. Given the relevance of integrins determining exosome organ distribution and taking in consideration the complexity and systemic nature of organ communication *in vivo*, one possible explanation for this observation could be that exosome localization to the brain occurs as a direct consequence of lack of laminin and fibronectin-binding integrins that drive exosomes to

interact with ECM of other organs and as a result be uptaken there rather than the brain. Other possibilities are that the integrins on brain metastatic exosomes, α2, α3, β1 and β3, despite being present at low levels, drive brain tumor exosomes to interact with some of the matrix components of the brain vasculature, or that other proteins packaged at higher levels in BrM exosomes, such as LRP1 and TIMP3, mediate this process. Development of new tools and models of exosome-tagging for *in vivo* tracking, such as coupling of protein tags/ fluorescent markers to canonical exosome membrane proteins or other exosome fluorescent-tagging systems, would allow for better *in vivo* study of brain metastatic tumor exosome brain localization and cellular uptake. These tracking systems could be coupled with the development of better BrM models capable of reproducibly giving rise to brain metastasis following orthotopic implantation and therefore able to recapitulate the full disease progression, allowing for further exploration of the pro-metastatic effects of brain metastatic exosomes. These approaches would also grant the ability to evaluate the potential role for CEMIP in these processes. Although our finding that CEMIP loss did not affect exosome uptake by endothelial cells in brain slices, suggests CEMIP may not be essential for BrM exosome uptake by brain endothelial cells *in vivo*, some aspects of *in vivo* interaction with endothelial cells such as access to the intra-luminal vascular space or contact with other elements in blood circulation warrant further examination.

Furthermore, in addition to the abovementioned differences in tumor exosomal membrane proteins that dictate their organ tropism, differences in the ECM and vasculature within each organ can contribute to the biodistribution pattern of tumor exosomes within the brain [108]. The pattern of brain metastatic exosome association with specific endings of the cerebral vascular trees suggests that not all vasculature within the brain is equal across different areas, as supported by the presence of distinct ECM molecules or cell receptors in the vasculature of different organs [108] and in different areas of the same organ [109, 110]. Thus, additional characterization of intra-brain vascular heterogeneity could contribute to a better understanding of exosome uptake and distinct outcomes in different regions of the brain, such as cell uptake, vascular leakiness and metastasis.

Our results also highlighted how different cell types are responsible for tumor cell uptake in each organ and first described the *in vivo* interaction of brain metastatic exosomes with endothelial cells in the brain, in support of more recent findings demonstrating extracellular vesicles interact with endothelial cells [111, 112] and blood vessel-associated microglia in brain metastases and primary brain tumors [113, 114]. Additional approaches to immunofluorescence characterization of the interaction of tumor exosomes with the major brain cell types should be implemented, such as quantitative PCR for different brain cell-specific markers in exosome positive sorted brain cells or single-cell RNA sequencing cell profiling of exosome-positive sorted brain cells from *ex vivo* slices treated with fluorescently-labeled exosomes. These approaches would carry improvements regarding the quantitative aspect of the analysis while providing a more widespread and deeper characterization of the different cell types described in the brain, thus allowing for possible identification of new contributing cellular players in the interaction with tumor exosomes and more knowledge on subpopulations of the current ones described here. Given the known complexity and multi-cellular nature of the BBB and perivascular-associated cells, the presence of a newly described brain lymphatic system [115], and recent acknowledgement of distinct immune and glial cell subpopulations in the brain responsible for discrete functions [81] warrants main focus of future efforts in the characterization of the cells known to compose the brain vascular niche.

Exosomes in Brain Metastasis

Tumor-derived exosomal miRNA and proteins, often selectively packaged in exosomes, reprogram or educate target cells that uptake them towards a pro-metastatic and pro-inflammatory phenotype, generating pre-metastatic niches and supporting metastatic progression at distant sites [116]. The brain, an immunoprivileged site protected by the BBB, remains the least understood of potential metastatic sites, a challenge for disseminating tumor cells and cancer researchers alike.

While several studies had implicated extracellular vesicles in the growth of primary brain tumors, little else is known about the mechanisms through which primary tumor-derived exosomes promote brain pre-metastatic and metastatic niche formation and thus brain

metastasis. Thus, despite sharing the same microenvironment and equally poor prognosis, primary brain tumor-derived EV content and function in angiogenesis [117, 118], oncogene transfer [66] reprogramming of microglia and recruited macrophages towards tumor-supporting phenotypes [119, 120], astrocyte apoptosis and metabolic quiescence [121] have been extensively studied, while similar interactions during brain metastasis have yet to be explored.

A large proportion of studies on exosome/EV-mediated intercellular communication within the brain microenvironment has focused on the roles of non-coding RNA cargo. Early studies showed that miR-181c packaged in tumor-derived exosomes disrupts the BBB through downregulation of PDPK1, thus affecting actin localization and allowing breast cancer cell entry to the brain [111]. Moreover, tumor-derived microvesicles can suppress glucose uptake by stromal cells in brain PMNs through the transfer of miR-122 and inhibition of pyruvate kinase [122]. This increases glucose availability in PMNs, attracting tumor cells, thus favoring brain metastasis. Loss of the lncRNA XIST in breast cancer can also promote brain metastasis by increasing secretion of exosomal miRNA-503 by inducing M2 polarization of microglia [123]. Importantly, the brain microenvironment, specifically astrocytes, can also drive brain metastasis outgrowth, by inducing PTEN loss in brain metastatic breast cancer cells through transfer of exosomal miR-19a [114]. More recent studies explored the effects of brain metastatic melanoma EVs/exosome mRNA cargo on astrocytes, in which exosome treatment resulted in the upregulation of pro-inflammatory cytokines IL1a, CXCL-10, CXCL-1, 2, CCL-2, 3 and CCL-5 [124]. Finally, a new study proposed that brain metastatic breast cancer-derived EVs cross the BBB via transcytosis and are uptaken by perivascular astrocytes, but a mechanism for the role of these exosome-educated astrocytes in outgrowth of metastases was not proposed [112]. Overall, the discovery and description of the novel exosome-mediated functions in brain metastasis described above, is in accordance with our findings relative to the importance of the endothelial cells and glial cell populations and promotion of inflammatory niches in the brain for successful tumor colonization.

Additionally, since we are only now beginning to understand how tumor-derived EVs are involved in metastasis, there are still many outstanding issues awaiting further research in the scope general metastatic colonization. First, it is imperative to determine which

subpopulation of tumor cells gives rise to EVs that induce PMN formation. Second, a full characterization of secreted vesicles and their associated cargo is needed to understand how metabolic alterations affect PMN formation. Third, how long does EV-mediated education of recipient cells last? Can EV-mediated education be reverted? Can educated cells be further re-educated by exposure to new EV content? And, are these cells more or less sensitive to repeated EV exposure? Lastly, much emphasis is now placed on understanding how EVs form, adhere, fuse and educate recipient cells within PMNs, which is crucial to dissecting EV involvement at all stages of PMN formation.

Ex vivo modeling of brain metastatic colonization and pro-metastatic effects of brain metastatic exosomes

Tumor exosomes were also shown to promote BBB dysfunction [125], consistent with the vascular leakiness induced by brain metastatic exosomes we and others have observed [111]. Better understanding of the specific tumor exosomal mechanisms driving vascular permeability of the brain's tight vascular barrier will aid in the development of strategies focused on limiting this process during early steps of the metastatic process as a means to stop cancer cell extravasation to the brain, but also promoting it later in advanced metastatic disease as a way of inducing permeability in brain metastatic lesions for delivery of chemotherapeutic agents. In addition to the contribution of tumor exosomes in the recognized but not yet fully understood heterogeneous vascular permeability of brain metastases [126], their role in other vascular events remains to be elucidated. Namely, the role/effect of tumor exosomes on the permeability of specific brain areas presenting a distinct and more permissive BBB (such as the circumventricular organs of the brain and the blood-cerebrospinal fluid barrier associated to choroid plexus capillaries), and in triggering of other intra-vascular insults linked to vascular dysfunction and BrM, such as thrombus formation in the brain and induction of platelet aggregation need to be examined.

Furthermore, we show that pre-conditioning the brain microenvironment with exosomes from brain metastatic tumor cells generates a supportive niche for tumor cell outgrowth and invasion during brain colonization. Notably, this brain pre-metastatic niche was specific for pre-conditioning with exosomes from brain metastatic tumor cells and not

recapitulated by pre-conditioning with exosomes from lung or bone metastatic tumor cells. Additionally, exosomes from brain metastatic tumor cells also supported colonization by parental metastatic tumor cells, which have low intrinsic potential to generate BrM, further highlighting the pivotal role of tumor-derived exosomes in promoting favorable niches for organ specific metastasis [56, 57, 116].

CEMIP functions and exosomal CEMIP role in brain metastasis

Using an unbiased and quantitative approach of proteomic analysis we identified CEMIP as a protein specifically enriched in exosomes from brain metastatic tumor cells. CEMIP was first described in non-syndromic familial deafness [93], and more recently has been implicated in brain biological processes related to memory, likely due to roles in synaptic formation [99] [127] [93]. This suggests important functions for CEMIP in the normal and pathological brain. While cellular expression of CEMIP has been previously associated with hyaluronic acid depolymerization [94, 128, 129], intracellular calcium regulation [95], cancer progression [96, 97, 100, 130-136] and inflammatory diseases [98, 128, 137], our study is the first to reveal a role for exosomal CEMIP in brain metastasis. Our findings are consistent with CEMIP roles in brain biology and with the work of others showing links between CEMIP and the brain, an organ with relatively high endogenous CEMIP expression under normal physiological conditions [93, 99, 138]. Besides the aforementioned physiological functions for CEMIP, which are more relevant and active in earlier steps of development, CEMIP appears to not be critical during adulthood and is only expressed in inflammatory and oncological settings of disease. Accordingly, our findings suggest that the pro-metastatic colonization outcome is a result of exosomal CEMIP inducing a pro-inflammatory state in the brain vascular niche.

A very interesting observation arising from our study was the particularly increased expression of CEMIP in exosomes of brain metastatic cells over other secreted fractions or cellular compartments. This remark, similar to what was observed for the presence of particular integrin heterodimers in exosomes of lung metastatic cells, underlines the existence of mechanisms of selective exosomal packaging. The mechanisms regulating selective cargo packaging into exosomes and extracellular vesicles remain largely

unexplored and subject of great interest in the field [56, 139]. While they will certainly depend on the overall expression level of a molecule there is evidence that cell-extrinsic factors and conditions can determine differential packaging [140] by affecting the subcellular localization or availability of a given molecule. Regarding CEMIP, one can hypothesize that its packaging in exosomes might be the result of passive loading into these vesicles during EV biogenesis given its location at the cell membrane and known functions in the endoplasmic reticulum, two cell compartments involved in exosome biology. Alternatively, CEMIP packaging could be due to shuttling *via* interaction/binding to exosome structural proteins, such as HSPA5 [95]. Analysis of known CEMIP protein interactors and development of new tools for the study of CEMIP protein-protein interaction with other partners, such as proximity-dependent labeling approaches (e.g. BioID [141]), can shed light onto the mechanism of CEMIP selective exosomal packaging. Furthermore, and given the recent discovery that exosomes are comprised by a heterogeneous population of particles [70], CEMIP association with distinct exosome size subpopulations and position relative to the exosomal membrane (inside exosome membrane, transmembrane, or outside membrane) should be better characterized, as these can impact entry through the size-limiting BBB and affect exosome binding properties and uptake. Lastly, investigation into the mechanisms underlying CEMIP regulation at the genetic level (i.e. gene copy number amplifications, overexpression, epigenetic dysregulation, etc.) in brain metastatic cancer cells and characterization of possible post-translational modifications (such as glycosylation pattern, which can impact interaction with other molecular partners and inherent binding properties) should contribute to advance our understanding of this molecule and how to manipulate its expression and functions.

Our work demonstrates also that CEMIP targeting in a cancer cell model of brain metastasis impairs brain metastatic ability *in vivo* and *ex vivo*. However, despite previously reported effects of CEMIP on the proliferation and migration of breast cancer tumor cells [132], we did not observe any CEMIP-dependent changes in proliferation or invasion *in vitro*. We demonstrate that CEMIP targeting impairs brain metastatic ability *in vivo* but not *in vivo* orthotopic primary tumor growth of brain tropic 231 BrT1 cells. These findings underscore that CEMIP functions described here are exerted upon the brain

microenvironment. Furthermore, they also indicate that different thresholds of CEMIP may regulate distinct processes and that reduction of its high expression in the brain metastatic model to levels approaching the parental model is insufficient to impact these basic cellular functions outside the brain microenvironment context, either *in vitro* or *in vivo*.

In vivo, the impaired brain metastatic ability due to CEMIP targeting resulted mainly from a reduced number of brain metastatic colonies formed in an experimental brain metastatic setting. In contrast, *in situ* brain outgrowth was not significantly affected upon direct implantation of metastatic cells within the brain, suggesting CEMIP is most critical in the early phases of brain colonization. Remarkably, exosomal CEMIP pre-conditioning enhanced brain metastatic colonization, restoring the ability of CEMIP-depleted cells to associate with brain vasculature.

Tumor exosomal CEMIP-induced reshaping of the brain vascular niche

In addition to identifying CEMIP as a key effector protein in promoting brain metastatic colonization, we showed that exosomal CEMIP pre-conditioning enhances brain metastatic colonization *in vivo* and *ex vivo*. Remarkably, exosomal CEMIP was also sufficient to restore the ability of CEMIP-depleted cells to associate with the brain vasculature. Two observations specifically hinted towards a functional role for exosomal CEMIP in re-shaping the brain vascular niche. First, pre-conditioning with CEMIP^{high} brain metastatic-derived exosomes promoted the interaction between tumor and brain endothelial cells. This was accompanied by increased vessel-associated invasion of tumor cells. Second, the vessel caliber size in brain metastatic tumors that were developed by 231 BrT1 CEMIP KO cells was significantly smaller compared to the enlarged vasculature that is typical of brain metastatic tumors that are derived from the 231 BrT1 tumor cell model, which recapitulate the abnormal vasculature classically observed in brain metastasis patients. Moreover, we show that brain endothelial cell interaction with tumor-derived exosomes leads to loss of vascular integrity, consistent with another recent report [111]. We also showed that vascular remodeling is induced in a CEMIP-dependent fashion.

Brain metastatic cancer cells often display angiocentric growth in the brain, taking advantage of the close association with pre-existing host brain vasculature [35, 38, 44, 91]. Brain metastases in patients and pre-clinical models traditionally present extremely altered vessel morphology with tortuous shape and enlarged lumen vessel size compared to normal brain vascular architecture [44]. The typical angiogenic strategy of brain metastatic tumors [41], usually referred to as non-sprouting or intussusceptive angiogenesis (IA), differs from the standard process of angiogenesis that requires formation of new blood vessels by sprouting and is commonly observed in primary tumors and metastases outside the central nervous system. Instead, IA relies on the formation of intravascular structures that lead to morphological remodeling in existing blood vessels. In particular, these changes involve distinct alterations in the branch angle of bifurcating vessels and cause duplication of existing vessels or even vascular pruning [142] [143]. IA remodels and expands the size and complexity of a capillary bed into developing vascular trees [40]. Ultimately, this aberrant form of vascular morphogenesis allows for vessel growth, while also inducing perturbations in vascular function and promoting pathological features such as aberrant vessel topology, with enlarged vessels and altered vascular permeability associated with alterations in mural cell coverage. The mechanisms regulating IA during brain metastasis formation are still largely unexplored [43]; however, it is thought that it results from the combined action of diverse tumor secreted factors, which allow for the incorporation and growth of the host vasculature into the developing metastases [144].

Our work showing exosomal CEMIP promotes vascular network formation and triggers a pro-inflammatory gene signature in the brain provides mechanistic insight into IA-dependent mechanisms of brain metastasis. The formation of larger vascular branches by BrEC *in vitro* results from exosomal CEMIP-stimulation of endothelial cell branching and cell junction, implying alterations in cell adhesive and migratory properties. This latter observation is supported by identification of vessel morphogenesis among the top biological processes specifically affected by exosomal CEMIP in BrECs *ex vivo* and the reduction in caliber of the metastatic vasculature of CEMIP-depleted brain metastatic cancer cells *in vivo*.

Furthermore, Notch signaling inhibition in existing vascular beds has been shown to potently stimulate IA [145], as opposed to the sprouting angiogenesis observed at the level of developing vessels, a process that involved downregulation of *ephrin B2*. Interestingly, we also found *ephrin B2* downregulated in BrECs upon exosomal CEMIP treatment. The overlap between these molecular mechanisms known to be associated with IA and the gene expression changes induced by exosomal CEMIP in the brain microenvironment suggest that CEMIP may be a key morphogenetic remodeling agent in IA associated with brain metastasis. Of notable importance, exosomal CEMIP upregulated genes in microglia consistent with a pro-inflammatory signature associated with pathological neuro-inflammation mediated brain IA [146]. Neuro-inflammation mediated-IA has been proposed to occur as a compensatory mechanism in response to impaired sprouting angiogenesis and is characterized by increased expression of cytokines such as *Cxcl-1*, *Cxcr4*, *Fgf2*, *IL-1α*, and *TNF-α* by immune cells in the brain microenvironment [146].

Exosomal CEMIP induced gene expression changes in brain endothelial cells associated with inositol signaling. CEMIP has previously been linked to inositol signaling [147] which are involved in the PI3K pathway, promotes migration and ultimately vascular remodeling via calcium-mediated cytoskeletal re-arrangement [95], cell junction disassembly and activation of Rho GTPases [148]. We also observed that exosomal CEMIP upregulated RhoG expression and affected the expression of other several cell junction and adhesion-related molecules. Interestingly, the osteoarthritis pathway, which is linked to vascular dysfunction and remodeling, ranked amongst the most significantly affected pathways both in exosomal CEMIP and brain metastatic exosome conditions. This suggests a critical role for CEMIP in the regulation of the number one ranked brain metastatic tumor exosome-stimulated pathway in the brain microenvironment and an inflammatory function for exosomal CEMIP in the brain vascular niche. In support of our own findings, recent reports have implicated CEMIP in rheumatoid arthritis [128, 137],[98], where it promoted endothelial cell migration and branching *in vitro* and stimulated vessel growth and enlargement *in vivo* [98].

Of all CEMIP-dependent pathways identified in either endothelial cells or microglia, osteoarthritis was the only one significantly modulated by exosomal CEMIP in both cell

types [149]. Microglia exhibited gene expression alterations in additional inflammatory pathways involved in rheumatoid arthritis, IL-17 signaling, neuroinflammation, immune cell adhesion and vascular transmigration. Microglia are commonly found in the vicinity of vessels and are known key players in brain microenvironment reshaping [150] and in brain metastasis [91, 151] [114, 152]. Our results agree with recent findings demonstrating that extracellular vesicles interact with microglia in primary brain tumors [113]. Strikingly, among the gene expression changes associated with exosomal CEMIP in microglia, we observed upregulation of pro-inflammatory *Tnf* , *Ptgs2*, and *Ccl/Cxcl* cytokines*,* all molecules that promote vascular dysfunction at the BBB level and, more critically, that support brain metastasis formation [153] [154, 155] [36, 125, 156-163]. Of note that while only exosomal CEMIP effect in brain vascular niche reshaping was addressed, CEMIP targeting strongly impaired vascular co-option but didn't completely abrogate brain metastasis or exosomal-induced growth advantages during brain colonization. Other molecules such as TIMP3 and LRP1, which had been found to be increased in brain metastatic exosomes, could account for some of these effects and be responsible for gene expression alterations verified in brain endothelial cells and microglia by tumor-derived exosomes that were not driven by exosomal CEMIP.

Exosomal CEMIP molecular mechanisms underlying brain vascular reshaping and pro-metastatic BrM functions

A more detailed characterization of the pathways downstream of exosomal CEMIP should provide additional information on the prospective involvement of the Wnt signaling pathway [96, 100, 130, 131] and intracellular calcium release [95, 100] for vascular niche reshaping and pre-metastatic niche formation in the brain. In particular, the specific genes affected by exosomal CEMIP that are pivotal for the observed changes in vascular co-option remains to be identified. Their identification should be followed by targeting of these molecules (e.g. function-blocking antibodies, small peptide inhibitors, chemical inhibitors, etc.) and evaluation of their impact in pre-metastatic brain vascular niche formation can be addressed using the *ex vivo* brain metastasis platform developed here. In addition to these, given the inflammatory nature of the pathways promoted by exosomal

CEMIP in the brain vascular niche and their importance for BrM, the specific links between PTEN/PI3K signaling pathway, and the expression of CEMIP and COX2, deserve further exploration.

Another mechanistic avenue that should be addressed in the context of CEMIP-mediated functions is to determine if the capability of CEMIP bind and depolymerize hyaluronic acid (HA), impacts the pro-metastatic BrM function described in this study. CEMIP achieves HA depolymerization through rapid vesicle endocytosis via cell membrane-associated clathrin-coated pits and activation of the endocytic pathway [94]. Hyaluronic acid is an anionic nonsulfated glycosaminoglycan whose size can span from just a couple of monomers to very large polymer forms of several million Daltons, and is one of the major components of the brain extracellular matrix. HA is involved in several biological functions such as wound repair, cell migration and angiogenesis and is an important molecule with recognized functions in primary brain tumor formation, mainly through receptors CD44, RHAMM and ICAM-1 in cancer cells [164]. While CEMIP binds and hydrolyzes high-molecular weight HA in a cell-dependent way, and the mechanism of depolymerization involves cell-dependent mechanisms, the capability of exosomal CEMIP to perform any of these functions still needs to be evaluated. Interestingly, HA polymer size has the ability to induce dramatically distinct cellular functions, with high molecular HA being a potent tumor suppressor [165] and low molecular HA a tumor-promoting molecule with pro-angiogenic and pro-inflammatory properties [166], the latter mainly by acting through TLR2/4 in immune and stromal cells. Exploration of HA-related functions of CEMIP with impact in BrM should be dissected out, mainly by addressing the capability of tumor exosomal CEMIP to bind and/or depolymerize high molecular HA and the possibility of exosomal CEMIP to act as a carrier of low molecular HA to the brain vascular niche.

CEMIP as a biomarker of brain metastasis in patients

Consistent with the association between CEMIP and BrM in tumor cell models, analysis of CEMIP expression in human metastases revealed that CEMIP expression is significantly increased in BrM and is associated with poor patient survival. The clinical relevance of CEMIP in BrM is underscored by the significantly increased CEMIP

expression found in human brain metastases, compared to adjacent brain stroma and non-brain metastatic lesions, more importantly, was secreted in exosomes from patient-derived brain metastatic live tumor tissue. Moreover, CEMIP expression at the primary tumor level specifically correlated with metastasis to brain but not other organs and was already elevated in primary tumors from patients that developed brain metastasis. Finally, higher CEMIP expression in the primary tumors from these patients was also significantly associated with rapid metastatic disease progression to the brain, suggesting that CEMIP may be a reliable biomarker of brain metastatic risk.

Additional characterization of CEMIP BrM prognostic value within specific tumor type patient cohorts (e.g. breast cancer *versus* lung cancer; non-small cell lung cancer *versus* small cell lung cancer, different breast cancer subtypes, etc.), as well as association with groups of patient presenting distinct clinical parameters (e.g. hormonal receptor status, response to specific therapy, smoking, presence of particular immune infiltrate subsets, etc.) should be performed. This analysis could yield new exciting data, in particular for breast cancer, given the relevance of hormonal receptor status for brain metastasis [167] and specifically in respect to the ErbB receptor family since CEMIP has been shown to affect EGFR signaling [168].

To bridge the gap between our findings using human cancer cell models in mice and patients it is required that new mouse cancer cell models to allow evaluation of CEMIP BrM function in immunocompetent mouse models are developed. In addition to further advance our understanding on the role of CEMIP for BrM and its influence on the immune compartment, mouse cancer cell models will allow combined use with CEMIP KO mouse models in immune-competent mice strains [127], thus providing pivotal information into the contribution of stromal CEMIP to the this process as well.

Lastly, due to the pro-tumoral inflammatory action of exosomal CEMIP upon the brain microenvironment, investigation of its function in primary brain tumor biology and other pathological conditions with strong inflammatory driving force, such as epilepsy, are warranted. In line with this claim, study of other CEMIP protein family members, such as the more recently identified CEMIP2, could lead to the disclosure of similar functions with implications for brain metastasis and other pathologies.

Future perspectives and concluding remarks

Overall, our findings identify a previously unknown role for CEMIP in brain metastasis, suggesting this molecule could serve as a novel prognostic biomarker and promising therapeutic target for brain metastasis. The organotypic brain slice model presented several advantages that facilitated the study of tumor exosome interaction with cells of the brain microenvironment and analysis of their pro-metastatic effects. As a result, new organotypic slice models are currently being established in the lab to explore tumor exosome functions in different organ microenvironments that present *in vivo* limitations. Regarding CEMIP, future studies will focus on exploring the potential of circulating tumor-derived exosomal CEMIP as a plasma-based biomarker to non-invasively screen patients for primary and recurrent brain metastases, or to stratify patients with higher risk of developing BrM. Further definition of tumor specific exosomal markers, in particular outer membrane proteins, should allow for improved isolation of tumor exosomes from circulating exosomes and better evaluation of exosomal CEMIP as a blood-based biomarker for BrM. Furthermore, following our studies in patients we have filled a provisional patent application for the use of an anti-CEMIP antibody as a method of detecting and inhibiting BrM. These antibodies, currently being generated and validated by our collaborators, are being developed not only with the purpose of binding and identifying CEMIP in circulating exosomes and tissues of patients, but also to block CEMIP's function. These antibodies will allow to test targeted therapies aimed at blocking this protein and the molecular pathways it alters in the brain vascular niche in pre-clinical models of brain metastasis. If successful in pre-clinical models, CEMIP-targeting antibodies could become not only a new treatment approach but a novel prophylactic treatment for patients at risk of BrM as well. CEMIP blocking-antibody therapies could be used as single agents or combined with therapies that target other exosomal CEMIP-induced BrM factors (such as COX2, a BrM mediator with a known inhibitor – NS-398, which has also been reported to affect CEMIP [169]), and these should be evaluated using *ex vivo* and *in vivo* BrM models. Alternatively, anti-CEMIP binding antibodies could also be potentially used in conjunction with drug-delivery systems, such as artificial nanoparticles, to direct chemotherapeutic agents to brain metastatic cells.

In sum, our work proposes a novel and previously undescribed function for exosomal CEMIP in the process of brain metastasis by promoting tumor cell colonization through remodeling of the brain vascular niche and induction of a pro-inflammatory milieu. Our results also support CEMIP's association with brain metastasis in patients and propose it as a determinant factor in metastatic disease progression to the brain with potential diagnostic and therapeutic value.

REFERENCES

1. Peinado, H., et al., *Pre-metastatic niches: organ-specific homes for metastases.* Nat Rev Cancer, 2017. **17**(5): p. 302-317.
2. Egeblad, M., E.S. Nakasone, and Z. Werb, *Tumors as organs: complex tissues that interface with the entire organism.* Dev Cell, 2010. **18**(6): p. 884-901.
3. Welch, D.R. and D.R. Hurst, *Defining the Hallmarks of Metastasis.* Cancer Res, 2019. **79**(12): p. 3011-3027.
4. Mehlen, P. and A. Puisieux, *Metastasis: a question of life or death.* Nat Rev Cancer, 2006. **6**(6): p. 449-58.
5. Quail, D.F. and J.A. Joyce, *Microenvironmental regulation of tumor progression and metastasis.* Nat Med, 2013. **19**(11): p. 1423-37.
6. Bissell, M.J. and M.A. Labarge, *Context, tissue plasticity, and cancer: are tumor stem cells also regulated by the microenvironment?* Cancer Cell, 2005. **7**(1): p. 17-23.
7. Weaver, V.M., et al., *The importance of the microenvironment in breast cancer progression: recapitulation of mammary tumorigenesis using a unique human mammary epithelial cell model and a three-dimensional culture assay.* Biochem Cell Biol, 1996. **74**(6): p. 833-51.
8. Landskron, G., et al., *Chronic inflammation and cytokines in the tumor microenvironment.* J Immunol Res, 2014. **2014**: p. 149185.
9. Paget, S., *The distribution of secondary growths in cancer of the breast. 1889.* Cancer Metastasis Rev, 1989. **8**(2): p. 98-101.
10. Ewing, J., *The Problems of Melanoma.* Br Med J, 1930. **2**(3646): p. 852-6.
11. Fidler, I.J., *L-asparaginase and metastasis.* Lancet, 1970. **1**(7650): p. 777-8.
12. Hart, I.R. and I.J. Fidler, *Role of organ selectivity in the determination of metastatic patterns of B16 melanoma.* Cancer Res, 1980. **40**(7): p. 2281-7.
13. Fidler, I.J., *The pathogenesis of cancer metastasis: the 'seed and soil' hypothesis revisited.* Nat Rev Cancer, 2003. **3**(6): p. 453-8.
14. Muller, A., et al., *Involvement of chemokine receptors in breast cancer metastasis.* Nature, 2001. **410**(6824): p. 50-6.
15. Chen, W., et al., *Organotropism: new insights into molecular mechanisms of breast cancer metastasis.* NPJ Precis Oncol, 2018. **2**(1): p. 4.
16. Weilbaecher, K.N., T.A. Guise, and L.K. McCauley, *Cancer to bone: a fatal attraction.* Nat Rev Cancer, 2011. **11**(6): p. 411-25.
17. Peinado, H., et al., *Melanoma exosomes educate bone marrow progenitor cells toward a pro-metastatic phenotype through MET.* Nat Med, 2012. **18**(6): p. 883-91.
18. Kaplan, R.N., et al., *VEGFR1-positive haematopoietic bone marrow progenitors initiate the pre-metastatic niche.* Nature, 2005. **438**(7069): p. 820-7.
19. Psaila, B. and D. Lyden, *The metastatic niche: adapting the foreign soil.* Nat Rev Cancer, 2009. **9**(4): p. 285-93.
20. Joyce, J.A. and J.W. Pollard, *Microenvironmental regulation of metastasis.* Nat Rev Cancer, 2009. **9**(4): p. 239-52.
21. Albrengues, J., et al., *Neutrophil extracellular traps produced during inflammation awaken dormant cancer cells in mice.* Science, 2018. **361**(6409).
22. Barnholtz-Sloan, J.S., et al., *Incidence proportions of brain metastases in patients diagnosed (1973 to 2001) in the Metropolitan Detroit Cancer Surveillance System.* J Clin Oncol, 2004. **22**(14): p. 2865-72.
23. Tabouret, E., et al., *Recent trends in epidemiology of brain metastases: an overview.* Anticancer Res, 2012. **32**(11): p. 4655-62.
24. Valiente, M., et al., *The Evolving Landscape of Brain Metastasis.* Trends Cancer, 2018. **4**(3): p. 176-196.

25. Achrol, A.S., et al., *Brain metastases.* Nat Rev Dis Primers, 2019. **5**(1): p. 5.
26. Nayak, L., E.Q. Lee, and P.Y. Wen, *Epidemiology of brain metastases.* Curr Oncol Rep, 2012. **14**(1): p. 48-54.
27. Percy, A.K., *Neoplasms of the central nervous system: epidemiologic considerations.* Neurology, 1970. **20**(4): p. 398-9.
28. Sperduto, P.W., et al., *Summary report on the graded prognostic assessment: an accurate and facile diagnosis-specific tool to estimate survival for patients with brain metastases.* J Clin Oncol, 2012. **30**(4): p. 419-25.
29. Martin, A.M., et al., *Brain Metastases in Newly Diagnosed Breast Cancer: A Population-Based Study.* JAMA Oncol, 2017. **3**(8): p. 1069-1077.
30. Yamanaka, R., *Medical management of brain metastases from lung cancer (Review).* Oncol Rep, 2009. **22**(6): p. 1269-76.
31. Toyokawa, G., et al., *Insights into brain metastasis in patients with ALK+ lung cancer: is the brain truly a sanctuary?* Cancer Metastasis Rev, 2015. **34**(4): p. 797-805.
32. Hall, W.A., et al., *Long-term survival with metastatic cancer to the brain.* Med Oncol, 2000. **17**(4): p. 279-86.
33. Shi, C.L., et al., *Monocyte chemoattractant protein-1 modulates invasion and apoptosis of PC-3M prostate cancer cells via regulating expression of VEGF, MMP9 and caspase-3.* Asian Pac J Cancer Prev, 2011. **12**(2): p. 555-9.
34. Chambers, A.F., A.C. Groom, and I.C. MacDonald, *Dissemination and growth of cancer cells in metastatic sites.* Nat Rev Cancer, 2002. **2**(8): p. 563-72.
35. Kienast, Y., et al., *Real-time imaging reveals the single steps of brain metastasis formation.* Nat Med, 2010. **16**(1): p. 116-22.
36. Bos, P.D., et al., *Genes that mediate breast cancer metastasis to the brain.* Nature, 2009. **459**(7249): p. 1005-9.
37. Malladi, S., et al., *Metastatic Latency and Immune Evasion through Autocrine Inhibition of WNT.* Cell, 2016. **165**(1): p. 45-60.
38. Valiente, M., et al., *Serpins promote cancer cell survival and vascular co-option in brain metastasis.* Cell, 2014. **156**(5): p. 1002-16.
39. Holash, J., et al., *Vessel cooption, regression, and growth in tumors mediated by angiopoietins and VEGF.* Science, 1999. **284**(5422): p. 1994-8.
40. Mentzer, S.J. and M.A. Konerding, *Intussusceptive angiogenesis: expansion and remodeling of microvascular networks.* Angiogenesis, 2014. **17**(3): p. 499-509.
41. Bugyik, E., et al., *Lack of angiogenesis in experimental brain metastases.* J Neuropathol Exp Neurol, 2011. **70**(11): p. 979-91.
42. Paku, S., et al., *A new mechanism for pillar formation during tumor-induced intussusceptive angiogenesis: inverse sprouting.* Am J Pathol, 2011. **179**(3): p. 1573-85.
43. Burri, P.H., R. Hlushchuk, and V. Djonov, *Intussusceptive angiogenesis: its emergence, its characteristics, and its significance.* Dev Dyn, 2004. **231**(3): p. 474-88.
44. Carbonell, W.S., et al., *The vascular basement membrane as "soil" in brain metastasis.* PLoS One, 2009. **4**(6): p. e5857.
45. Louie, E., et al., *Neurotrophin-3 modulates breast cancer cells and the microenvironment to promote the growth of breast cancer brain metastasis.* Oncogene, 2013. **32**(35): p. 4064-77.
46. You, H., S. Baluszek, and B. Kaminska, *Immune Microenvironment of Brain Metastases-Are Microglia and Other Brain Macrophages Little Helpers?* Front Immunol, 2019. **10**: p. 1941.
47. Chen, E.I., et al., *Adaptation of energy metabolism in breast cancer brain metastases.* Cancer Res, 2007. **67**(4): p. 1472-86.

48. Siam, L., et al., *The metastatic infiltration at the metastasis/brain parenchyma-interface is very heterogeneous and has a significant impact on survival in a prospective study.* Oncotarget, 2015. **6**(30): p. 29254-67.
49. van Niel, G., G. D'Angelo, and G. Raposo, *Shedding light on the cell biology of extracellular vesicles.* Nat Rev Mol Cell Biol, 2018. **19**(4): p. 213-228.
50. Wolf, P., *The nature and significance of platelet products in human plasma.* Br J Haematol, 1967. **13**(3): p. 269-88.
51. Trams, E.G., et al., *Exfoliation of membrane ecto-enzymes in the form of micro-vesicles.* Biochim Biophys Acta, 1981. **645**(1): p. 63-70.
52. Harding, C., J. Heuser, and P. Stahl, *Endocytosis and intracellular processing of transferrin and colloidal gold-transferrin in rat reticulocytes: demonstration of a pathway for receptor shedding.* Eur J Cell Biol, 1984. **35**(2): p. 256-63.
53. Johnstone, R.M., A. Bianchini, and K. Teng, *Reticulocyte maturation and exosome release: transferrin receptor containing exosomes shows multiple plasma membrane functions.* Blood, 1989. **74**(5): p. 1844-51.
54. Johnstone, R.M., *Revisiting the road to the discovery of exosomes.* Blood Cells Mol Dis, 2005. **34**(3): p. 214-9.
55. Raposo, G., et al., *B lymphocytes secrete antigen-presenting vesicles.* J Exp Med, 1996. **183**(3): p. 1161-72.
56. Hoshino, A., et al., *Tumour exosome integrins determine organotropic metastasis.* Nature, 2015. **527**(7578): p. 329-35.
57. Costa-Silva, B., et al., *Pancreatic cancer exosomes initiate pre-metastatic niche formation in the liver.* Nat Cell Biol, 2015. **17**(6): p. 816-26.
58. Wortzel, I., et al., *Exosome-Mediated Metastasis: Communication from a Distance.* Dev Cell, 2019. **49**(3): p. 347-360.
59. Becker, A., et al., *Extracellular Vesicles in Cancer: Cell-to-Cell Mediators of Metastasis.* Cancer Cell, 2016. **30**(6): p. 836-848.
60. Figueroa, J.M., et al., *Detection of wild-type EGFR amplification and EGFRvIII mutation in CSF-derived extracellular vesicles of glioblastoma patients.* Neuro Oncol, 2017. **19**(11): p. 1494-1502.
61. Zomer, A., et al., *In Vivo imaging reveals extracellular vesicle-mediated phenocopying of metastatic behavior.* Cell, 2015. **161**(5): p. 1046-1057.
62. Janowska-Wieczorek, A., et al., *Microvesicles derived from activated platelets induce metastasis and angiogenesis in lung cancer.* Int J Cancer, 2005. **113**(5): p. 752-60.
63. Janowska-Wieczorek, A., et al., *Enhancing effect of platelet-derived microvesicles on the invasive potential of breast cancer cells.* Transfusion, 2006. **46**(7): p. 1199-209.
64. Peinado, H., S. Lavotshkin, and D. Lyden, *The secreted factors responsible for pre-metastatic niche formation: old sayings and new thoughts.* Semin Cancer Biol, 2011. **21**(2): p. 139-46.
65. Ratajczak, J., et al., *Membrane-derived microvesicles: important and underappreciated mediators of cell-to-cell communication.* Leukemia, 2006. **20**(9): p. 1487-95.
66. Skog, J., et al., *Glioblastoma microvesicles transport RNA and proteins that promote tumour growth and provide diagnostic biomarkers.* Nat Cell Biol, 2008. **10**(12): p. 1470-6.
67. Valadi, H., et al., *Exosome-mediated transfer of mRNAs and microRNAs is a novel mechanism of genetic exchange between cells.* Nat Cell Biol, 2007. **9**(6): p. 654-9.
68. Liu, Y., et al., *Tumor Exosomal RNAs Promote Lung Pre-metastatic Niche Formation by Activating Alveolar Epithelial TLR3 to Recruit Neutrophils.* Cancer Cell, 2016. **30**(2): p. 243-256.
69. Zhou, W., et al., *Cancer-secreted miR-105 destroys vascular endothelial barriers to promote metastasis.* Cancer Cell, 2014. **25**(4): p. 501-15.

70. Zhang, H., et al., *Identification of distinct nanoparticles and subsets of extracellular vesicles by asymmetric flow field-flow fractionation.* Nat Cell Biol, 2018. **20**(3): p. 332-343.
71. Polleux, F. and A. Ghosh, *The slice overlay assay: a versatile tool to study the influence of extracellular signals on neuronal development.* Sci STKE, 2002. **2002**(136): p. pl9.
72. Rappsilber, J., M. Mann, and Y. Ishihama, *Protocol for micro-purification, enrichment, pre-fractionation and storage of peptides for proteomics using StageTips.* Nat Protoc, 2007. **2**(8): p. 1896-906.
73. Cox, J., et al., *Andromeda: a peptide search engine integrated into the MaxQuant environment.* J Proteome Res, 2011. **10**(4): p. 1794-805.
74. Freitas, D., et al., *Different isolation approaches lead to diverse glycosylated extracellular vesicle populations.* J Extracell Vesicles, 2019. **8**(1): p. 1621131.
75. Wapnir, I.L., et al., *The inverse relationship between microvessel counts and tumor volume in breast cancer.* Breast J, 2001. **7**(3): p. 184-8.
76. Campeau, E., et al., *A versatile viral system for expression and depletion of proteins in mammalian cells.* PLoS One, 2009. **4**(8): p. e6529.
77. Dull, T., et al., *A third-generation lentivirus vector with a conditional packaging system.* J Virol, 1998. **72**(11): p. 8463-71.
78. Lis, R., et al., *Conversion of adult endothelium to immunocompetent haematopoietic stem cells.* Nature, 2017. **545**(7655): p. 439-445.
79. Butler, J.M., et al., *Endothelial cells are essential for the self-renewal and repopulation of Notch-dependent hematopoietic stem cells.* Cell Stem Cell, 2010. **6**(3): p. 251-64.
80. Seandel, M., et al., *Generation of a functional and durable vascular niche by the adenoviral E4ORF1 gene.* Proc Natl Acad Sci U S A, 2008. **105**(49): p. 19288-93.
81. Bowman, R.L., et al., *Macrophage Ontogeny Underlies Differences in Tumor-Specific Education in Brain Malignancies.* Cell Rep, 2016. **17**(9): p. 2445-2459.
82. Bolger, A.M., M. Lohse, and B. Usadel, *Trimmomatic: a flexible trimmer for Illumina sequence data.* Bioinformatics, 2014. **30**(15): p. 2114-20.
83. Patro, R., et al., *Salmon provides fast and bias-aware quantification of transcript expression.* Nat Methods, 2017. **14**(4): p. 417-419.
84. Love, M.I., W. Huber, and S. Anders, *Moderated estimation of fold change and dispersion for RNA-seq data with DESeq2.* Genome Biol, 2014. **15**(12): p. 550.
85. Zerbino, D.R., et al., *Ensembl 2018.* Nucleic Acids Res, 2018. **46**(D1): p. D754-D761.
86. Yoneda, T., et al., *A bone-seeking clone exhibits different biological properties from the MDA-MB-231 parental human breast cancer cells and a brain-seeking clone in vivo and in vitro.* J Bone Miner Res, 2001. **16**(8): p. 1486-95.
87. Kang, Y., et al., *A multigenic program mediating breast cancer metastasis to bone.* Cancer Cell, 2003. **3**(6): p. 537-49.
88. Gupta, G.P., et al., *Identifying site-specific metastasis genes and functions.* Cold Spring Harb Symp Quant Biol, 2005. **70**: p. 149-58.
89. Minn, A.J., et al., *Genes that mediate breast cancer metastasis to lung.* Nature, 2005. **436**(7050): p. 518-24.
90. Lowery, F.J. and D. Yu, *Brain metastasis: Unique challenges and open opportunities.* Biochim Biophys Acta Rev Cancer, 2017. **1867**(1): p. 49-57.
91. Lorger, M. and B. Felding-Habermann, *Capturing changes in the brain microenvironment during initial steps of breast cancer brain metastasis.* Am J Pathol, 2010. **176**(6): p. 2958-71.
92. Lorger, M., et al., *Activation of tumor cell integrin alphavbeta3 controls angiogenesis and metastatic growth in the brain.* Proc Natl Acad Sci U S A, 2009. **106**(26): p. 10666-71.

93. Abe, S., S. Usami, and Y. Nakamura, *Mutations in the gene encoding KIAA1199 protein, an inner-ear protein expressed in Deiters' cells and the fibrocytes, as the cause of nonsyndromic hearing loss.* J Hum Genet, 2003. **48**(11): p. 564-70.
94. Yoshida, H., et al., *KIAA1199, a deafness gene of unknown function, is a new hyaluronan binding protein involved in hyaluronan depolymerization.* Proc Natl Acad Sci U S A, 2013. **110**(14): p. 5612-7.
95. Evensen, N.A., et al., *Unraveling the role of KIAA1199, a novel endoplasmic reticulum protein, in cancer cell migration.* J Natl Cancer Inst, 2013. **105**(18): p. 1402-16.
96. Birkenkamp-Demtroder, K., et al., *Repression of KIAA1199 attenuates Wnt-signalling and decreases the proliferation of colon cancer cells.* Br J Cancer, 2011. **105**(4): p. 552-61.
97. Zhang, Y., S. Jia, and W.G. Jiang, *KIAA1199 and its biological role in human cancer and cancer cells (review).* Oncol Rep, 2014. **31**(4): p. 1503-8.
98. Yang, X., et al., *KIAA1199 as a potential diagnostic biomarker of rheumatoid arthritis related to angiogenesis.* Arthritis Res Ther, 2015. **17**: p. 140.
99. Yoshino, Y., et al., *Distribution and function of hyaluronan binding protein involved in hyaluronan depolymerization (HYBID, KIAA1199) in the mouse central nervous system.* Neuroscience, 2017. **347**: p. 1-10.
100. Tiwari, A., et al., *Early insights into the function of KIAA1199, a markedly overexpressed protein in human colorectal tumors.* PLoS One, 2013. **8**(7): p. e69473.
101. Winkler, F., *Hostile takeover: how tumours hijack pre-existing vascular environments to thrive.* J Pathol, 2017. **242**(3): p. 267-272.
102. Fidler, I.J., *The role of the organ microenvironment in brain metastasis.* Semin Cancer Biol, 2011. **21**(2): p. 107-12.
103. Arnold, T. and C. Betsholtz, *The importance of microglia in the development of the vasculature in the central nervous system.* Vasc Cell, 2013. **5**(1): p. 4.
104. Tran, Q.K., K. Ohashi, and H. Watanabe, *Calcium signalling in endothelial cells.* Cardiovasc Res, 2000. **48**(1): p. 13-22.
105. Liebner, S., et al., *Wnt/beta-catenin signaling controls development of the blood-brain barrier.* J Cell Biol, 2008. **183**(3): p. 409-17.
106. Barczyk, M., S. Carracedo, and D. Gullberg, *Integrins.* Cell Tissue Res, 2010. **339**(1): p. 269-80.
107. Kechagia, J.Z., J. Ivaska, and P. Roca-Cusachs, *Integrins as biomechanical sensors of the microenvironment.* Nat Rev Mol Cell Biol, 2019. **20**(8): p. 457-473.
108. Nolan, D.J., et al., *Molecular signatures of tissue-specific microvascular endothelial cell heterogeneity in organ maintenance and regeneration.* Dev Cell, 2013. **26**(2): p. 204-19.
109. Crouch, E.E. and F. Doetsch, *FACS isolation of endothelial cells and pericytes from mouse brain microregions.* Nat Protoc, 2018. **13**(4): p. 738-751.
110. Crouch, E.E., et al., *Regional and stage-specific effects of prospectively purified vascular cells on the adult V-SVZ neural stem cell lineage.* J Neurosci, 2015. **35**(11): p. 4528-39.
111. Tominaga, N., et al., *Brain metastatic cancer cells release microRNA-181c-containing extracellular vesicles capable of destructing blood-brain barrier.* Nat Commun, 2015. **6**: p. 6716.
112. Morad, G., et al., *Tumor-Derived Extracellular Vesicles Breach the Intact Blood-Brain Barrier via Transcytosis.* ACS Nano, 2019. **13**(12): p. 13853-13865.
113. van der Vos, K.E., et al., *Directly visualized glioblastoma-derived extracellular vesicles transfer RNA to microglia/macrophages in the brain.* Neuro Oncol, 2016. **18**(1): p. 58-69.
114. Zhang, L., et al., *Microenvironment-induced PTEN loss by exosomal microRNA primes brain metastasis outgrowth.* Nature, 2015. **527**(7576): p. 100-4.
115. Jessen, N.A., et al., *The Glymphatic System: A Beginner's Guide.* Neurochem Res, 2015. **40**(12): p. 2583-99.

116. Peinado, H., et al., *Pre-metastatic niches: organ-specific homes for metastases.* Nat Rev Cancer, 2017.
117. Kucharzewska, P., et al., *Exosomes reflect the hypoxic status of glioma cells and mediate hypoxia-dependent activation of vascular cells during tumor development.* Proc Natl Acad Sci U S A, 2013. **110**(18): p. 7312-7.
118. Giusti, I., et al., *From glioblastoma to endothelial cells through extracellular vesicles: messages for angiogenesis.* Tumour Biol, 2016. **37**(9): p. 12743-12753.
119. de Vrij, J., et al., *Glioblastoma-derived extracellular vesicles modify the phenotype of monocytic cells.* Int J Cancer, 2015. **137**(7): p. 1630-42.
120. Abels, E.R., et al., *Glioblastoma-Associated Microglia Reprogramming Is Mediated by Functional Transfer of Extracellular miR-21.* Cell Rep, 2019. **28**(12): p. 3105-3119 e7.
121. Morad, G. and M.A. Moses, *Brainwashed by extracellular vesicles: the role of extracellular vesicles in primary and metastatic brain tumour microenvironment.* J Extracell Vesicles, 2019. **8**(1): p. 1627164.
122. Fong, M.Y., et al., *Breast-cancer-secreted miR-122 reprograms glucose metabolism in premetastatic niche to promote metastasis.* Nat Cell Biol, 2015. **17**(2): p. 183-94.
123. Xing, F., et al., *Loss of XIST in Breast Cancer Activates MSN-c-Met and Reprograms Microglia via Exosomal miRNA to Promote Brain Metastasis.* Cancer Res, 2018. **78**(15): p. 4316-4330.
124. Gener Lahav, T., et al., *Melanoma-derived extracellular vesicles instigate proinflammatory signaling in the metastatic microenvironment.* Int J Cancer, 2019. **145**(9): p. 2521-2534.
125. Doron, H., T. Pukrop, and N. Erez, *A Blazing Landscape: Neuroinflammation Shapes Brain Metastasis.* Cancer Res, 2019. **79**(3): p. 423-436.
126. Lockman, P.R., et al., *Heterogeneous blood-tumor barrier permeability determines drug efficacy in experimental brain metastases of breast cancer.* Clin Cancer Res, 2010. **16**(23): p. 5664-78.
127. Yoshino, Y., et al., *Targeted deletion of HYBID (hyaluronan binding protein involved in hyaluronan depolymerization/ KIAA1199/CEMIP) decreases dendritic spine density in the dentate gyrus through hyaluronan accumulation.* Biochem Biophys Res Commun, 2018. **503**(3): p. 1934-1940.
128. Nagaoka, A., et al., *Regulation of Hyaluronan (HA) Metabolism Mediated by HYBID (Hyaluronan-binding Protein Involved in HA Depolymerization, KIAA1199) and HA Synthases in Growth Factor-stimulated Fibroblasts.* J Biol Chem, 2015. **290**(52): p. 30910-23.
129. Yoshida, H., et al., *N-Terminal signal sequence is required for cellular trafficking and hyaluronan-depolymerization of KIAA1199.* FEBS Lett, 2014. **588**(1): p. 111-6.
130. Matsuzaki, S., et al., *Clinicopathologic significance of KIAA1199 overexpression in human gastric cancer.* Ann Surg Oncol, 2009. **16**(7): p. 2042-51.
131. Jia, S., et al., *KIAA1199 promotes migration and invasion by Wnt/beta-catenin pathway and MMPs mediated EMT progression and serves as a poor prognosis marker in gastric cancer.* PLoS One, 2017. **12**(4): p. e0175058.
132. Jami, M.S., et al., *Functional proteomic analysis reveals the involvement of KIAA1199 in breast cancer growth, motility and invasiveness.* BMC Cancer, 2014. **14**: p. 194.
133. Evensen, N.A., et al., *Hypoxia promotes colon cancer dissemination through up-regulation of cell migration-inducing protein (CEMIP).* Oncotarget, 2015. **6**(24): p. 20723-39.
134. Koga, A., et al., *KIAA1199/CEMIP/HYBID overexpression predicts poor prognosis in pancreatic ductal adenocarcinoma.* Pancreatology, 2017. **17**(1): p. 115-122.
135. Kohi, S., et al., *KIAA1199 is induced by inflammation and enhances malignant phenotype in pancreatic cancer.* Oncotarget, 2017. **8**(10): p. 17156-17163.
136. Suh, H.N., et al., *Identification of KIAA1199 as a Biomarker for Pancreatic Intraepithelial Neoplasia.* Sci Rep, 2016. **6**: p. 38273.

137. Shimizu, H., et al., *Hyaluronan-Binding Protein Involved in Hyaluronan Depolymerization Is Up-Regulated and Involved in Hyaluronan Degradation in Human Osteoarthritic Cartilage.* Am J Pathol, 2018. **188**(9): p. 2109-2119.
138. Terashima, M., et al., *KIAA1199 interacts with glycogen phosphorylase kinase beta-subunit (PHKB) to promote glycogen breakdown and cancer cell survival.* Oncotarget, 2014. **5**(16): p. 7040-50.
139. Rodrigues, G., H. Zhang, and D. Lyden, *Tumour vesicular micromachinery uncovered.* Nat Cell Biol, 2019. **21**(7): p. 795-797.
140. Kowal, J., et al., *Proteomic comparison defines novel markers to characterize heterogeneous populations of extracellular vesicle subtypes.* Proc Natl Acad Sci U S A, 2016. **113**(8): p. E968-77.
141. Li, P., et al., *BioID: A Proximity-Dependent Labeling Approach in Proteomics Study.* Methods Mol Biol, 2019. **1871**: p. 143-151.
142. Gianni-Barrera, R., et al., *To sprout or to split? VEGF, Notch and vascular morphogenesis.* Biochem Soc Trans, 2011. **39**(6): p. 1644-8.
143. Patan, S., *TIE1 and TIE2 receptor tyrosine kinases inversely regulate embryonic angiogenesis by the mechanism of intussusceptive microvascular growth.* Microvasc Res, 1998. **56**(1): p. 1-21.
144. Qian, C.N., et al., *Revisiting tumor angiogenesis: vessel co-option, vessel remodeling, and cancer cell-derived vasculature formation.* Chin J Cancer, 2016. **35**: p. 10.
145. Dimova, I., et al., *Inhibition of Notch signaling induces extensive intussusceptive neo-angiogenesis by recruitment of mononuclear cells.* Angiogenesis, 2013. **16**(4): p. 921-37.
146. Giacomini, A., et al., *Brain angioarchitecture and intussusceptive microvascular growth in a murine model of Krabbe disease.* Angiogenesis, 2015. **18**(4): p. 499-510.
147. Prole, D.L. and C.W. Taylor, *Inositol 1,4,5-trisphosphate receptors and their protein partners as signalling hubs.* J Physiol, 2016. **594**(11): p. 2849-66.
148. Sun, M.Y., M. Geyer, and Y.A. Komarova, *IP3 receptor signaling and endothelial barrier function.* Cell Mol Life Sci, 2017. **74**(22): p. 4189-4207.
149. Rodrigues, G., et al., *Tumour exosomal CEMIP protein promotes cancer cell colonization in brain metastasis.* Nat Cell Biol, 2019. **21**(11): p. 1403-1412.
150. Frost, J.L. and D.P. Schafer, *Microglia: Architects of the Developing Nervous System.* Trends Cell Biol, 2016. **26**(8): p. 587-97.
151. Sevenich, L., et al., *Analysis of tumour- and stroma-supplied proteolytic networks reveals a brain-metastasis-promoting role for cathepsin S.* Nat Cell Biol, 2014. **16**(9): p. 876-88.
152. Fitzgerald, D.P., et al., *Reactive glia are recruited by highly proliferative brain metastases of breast cancer and promote tumor cell colonization.* Clin Exp Metastasis, 2008. **25**(7): p. 799-810.
153. Maddahi, A., et al., *The role of tumor necrosis factor-alpha and TNF-alpha receptors in cerebral arteries following cerebral ischemia in rat.* J Neuroinflammation, 2011. **8**: p. 107.
154. Hu, J., et al., *Inhibition of cerebral vascular inflammation by brain endothelium-targeted oligodeoxynucleotide complex.* Neuroscience, 2016. **329**: p. 30-42.
155. O'Carroll, S.J., et al., *Pro-inflammatory TNFalpha and IL-1beta differentially regulate the inflammatory phenotype of brain microvascular endothelial cells.* J Neuroinflammation, 2015. **12**: p. 131.
156. He, B.P., et al., *Differential reactions of microglia to brain metastasis of lung cancer.* Mol Med, 2006. **12**(7-8): p. 161-70.
157. Rippaus, N., et al., *Metastatic site-specific polarization of macrophages in intracranial breast cancer metastases.* Oncotarget, 2016. **7**(27): p. 41473-41487.
158. Xing, F., et al., *miR-509 suppresses brain metastasis of breast cancer cells by modulating RhoC and TNF-alpha.* Oncogene, 2015. **34**(37): p. 4890-900.

159. Jassam, S.A., et al., *TNF-alpha enhancement of CD62E mediates adhesion of non-small cell lung cancer cells to brain endothelium via CD15 in lung-brain metastasis.* Neuro Oncol, 2016. **18**(5): p. 679-90.
160. Li, M. and R.M. Ransohoff, *The roles of chemokine CXCL12 in embryonic and brain tumor angiogenesis.* Semin Cancer Biol, 2009. **19**(2): p. 111-5.
161. Brandenburg, S., et al., *Resident microglia rather than peripheral macrophages promote vascularization in brain tumors and are source of alternative pro-angiogenic factors.* Acta Neuropathol, 2016. **131**(3): p. 365-78.
162. Wu, K., et al., *Roles of the cyclooxygenase 2 matrix metalloproteinase 1 pathway in brain metastasis of breast cancer.* J Biol Chem, 2015. **290**(15): p. 9842-54.
163. Lee, K.Y., et al., *Human brain endothelial cell-derived COX-2 facilitates extravasation of breast cancer cells across the blood-brain barrier.* Anticancer Res, 2011. **31**(12): p. 4307-13.
164. Chen, J.E., et al., *Influence of Hyaluronic Acid Transitions in Tumor Microenvironment on Glioblastoma Malignancy and Invasive Behavior.* Front Mater, 2018. **5**.
165. Tian, X., et al., *High-molecular-mass hyaluronan mediates the cancer resistance of the naked mole rat.* Nature, 2013. **499**(7458): p. 346-9.
166. Petrey, A.C. and C.A. de la Motte, *Hyaluronan, a crucial regulator of inflammation.* Front Immunol, 2014. **5**: p. 101.
167. Darlix, A., et al., *Hormone receptors status: a strong determinant of the kinetics of brain metastases occurrence compared with HER2 status in breast cancer.* J Neurooncol, 2018. **138**(2): p. 369-382.
168. Shostak, K., et al., *NF-kappaB-induced KIAA1199 promotes survival through EGFR signalling.* Nat Commun, 2014. **5**: p. 5232.
169. Galamb, O., et al., *Reversal of gene expression changes in the colorectal normal-adenoma pathway by NS398 selective COX2 inhibitor.* Br J Cancer, 2010. **102**(4): p. 765-73.